



Flanders
State of
the Art

16_089_4
FH reports

Monitoring the morphodynamics of the Zwin inlet

Final report 2019-2022 period

DEPARTMENT
MOBILITY &
PUBLIC
WORKS

www.flandershydraulics.be

Monitoring the morphodynamics of the Zwin inlet

Final report 2019-2022 period

Montreuil, A-L.; Dan, S.; Houthuys, R.; Verwaest, T.

Legal notice

Flanders Hydraulics is of the opinion that the information and positions in this report are substantiated by the available data and knowledge at the time of writing.

The positions taken in this report are those of Flanders Hydraulics and do not reflect necessarily the opinion of the Government of Flanders or any of its institutions.

Flanders Hydraulics Research nor any person or company acting on behalf of Flanders Hydraulics is responsible for any loss or damage arising from the use of the information in this report.

Copyright and citation

© The Government of Flanders, Department of Mobility and Public Works, Flanders Hydraulics 2023
D/2023/3241/079

This publication should be cited as follows:

Montreuil, A-L.; Dan, S.; Houthuys, R.; Verwaest, T. (2023). Monitoring the morphodynamics of the Zwin inlet: Final report 2019-2022 period. Version 4.0. FH Reports, 16_089_4. Flanders Hydraulics: Antwerp.


Reproduction of and reference to this publication is authorised provided the source is acknowledged correctly.

Document identification

Customer:	Coastal Division MDK	Ref.:	WL2023R16_089_4
Keywords (3-5):	Entrance and inlet units; erosion/accretion; hydrodynamics; Zwin.		
Knowledge domains:	Coastal protection>Coastal protection against erosion>Morphodynamics soft coastal defence>Literature and desktop study, in-situ measurements		
Text (p.):	59	Appendices (p.):	7
Confidentiality:	<input checked="" type="checkbox"/> No	<input checked="" type="checkbox"/> Available online	

Author(s):	Montreuil, A-L.; Dan, S.; Houthuys, R.
------------	--

Control

	Name	Signature
Reviser(s):	Verwaest, T.	Getekend door: Toon Verwaest (Signatur) Getekend op: 2023-04-11 10:02:44 +02:0 Reden: Ik keur dit document goed <i>Toon Verwaest</i>
Project leader:	Dan, S.	Getekend door: Sebastian Dan (Signatur) Getekend op: 2023-05-04 08:47:19 +02:0 Reden: Ik keur dit document goed <i>Sebastian Dan</i> 

Approval

Head of Division:	Bellafkih, K.	Getekend door: Abdelkarim Bellafkih (Sig) Getekend op: 2023-04-11 09:05:35 +02:0 Reden: Ik keur dit document goed <i>Abdelkarim Bellafkih</i>
-------------------	---------------	--



Abstract

The Zwin tidal inlet and marshland system was nearly doubled in surface in 2019 when a large part of the Willem-Leopold polder was incorporated in the floodable area. The main channel connecting the marshlands to the sea is characterized by a complex 3D morphology with a main channel, sandy bedforms including banks and bars as well as secondary channels. Their presence and movements reflect active sediment transport in the system. The inlet is controlled by hydrodynamics (currents and water level), beach dynamics, tidal prism and sediment supply. This study reports the morpho- and hydrodynamics of the entire tidal channel part from before the opening of the dyke on 04/02/2019 to nearly 3 years after. The results indicate significant morphological changes in the entire channel system where the main channel has become deeper, wider and migrated eastward. Since the opening, the sediment balance is stable in the entrance inlet. In contrast, the inland inlet has lost a significant sediment volume. Short term dynamics in the middle of the entrance and inland inlet unit were studied during field campaigns under calm and energetic conditions. A regime of ebb-dominance is found in the center of the channel and to a lower degree at its east side, while the west side of the channel is flood-dominated. In general, the ebb phase lasts about two times the duration of the flood phase. Based on the tidal prism and cross-sectional area analysis, it is concluded that the expansion of the intertidal area in early 2019 meant a very significant increase of tidal prism, which almost quadrupled. The response in the main channel was rapid and strong. A recent sandbank was quickly cleared during the first year after the expansion. As a result, the channel cross-sectional area at the border of the entrance inlet and the inland inlet attained a new equilibrium around 450 m² at the Spring 2020 survey. This section was only reduced by about 10 m² at the Spring 2021 survey. The continued monitoring programme will help to fine tune the insights into the process-response of the Zwin inlet and to estimate the time scales of the expected sanding up in order to guide future management and interventions.

Contents

Abstract	III
Contents	IV
List of tables.....	VI
List of figures	VII
1 Project overview and objectives	1
2 Topo-bathymetric data acquisition and methodology.....	3
2.1. Survey timeline	3
2.2. Airborne LiDAR surveys	4
2.3. RTK-GPS profiles	4
2.4. Qboat surveys.....	5
3. Morphodynamics results.....	7
3.1 Large-scale dynamics – entrance and inland inlet (LiDAR).....	7
3.2 Entrance inlet	13
3.3 Inland inlet.....	15
4 Forcing factors	26
4.1 Marine conditions.....	26
5 Ad-hoc hydrodynamics measurements.....	30
5.1 Background.....	30
5.2 Results	31
5.2.1 Hydrodynamics and sediment characteristics.....	31
5.2.2 Water discharge	36
5.2.3 Inland inlet before and after the opening of the dyke	38
6 Tidal prism and stability of a tidal inlet	40
6.1 Context	40
6.2 Evolution of the tidal prism before and after the expansion	41
6.2.1 Method	41
6.2.2 Definition of partial areas.....	41
6.3 Results	43
6.3.1 Discussion	47
6.4 Evolution of the Cross-Sectional Area A of the Tidal Channel.....	48
6.4.1 Data and method.....	48
6.4.2 Results	48

6.5	Relation A/P	50
6.5.1	Method	50
6.5.2	Discussion	52
7	Discussion	53
8	Conclusions.....	57
9	References	58
	Appendix A: Ad-hoc campaigns.....	A1
	Appendix B: Estimation of water discharge	A6

List of tables

Table 1 – Overview of the data timeline from 2018 to 2022.	3
Table 2 – Summary of the characteristics of the Qboat surveys.....	5
Table 3 – Sediment volume in the Zwin inlet units before and after the dyke opening based on the LiDAR surveys. Area of the entrance inlet is around 446 700 m ² and of 107 550 m ² for the inland inlet.....	12
Table 4 – Definition of morphological indicators	15
Table 5 – Summary indicators of the cross-channel marker locations based on the RTK-GPS profiles. Reference spring HW (4.7 m TAW).....	15
Table 6 – Statistic summary of the Qboat DoDs.....	23
Table 7 – Description of the continuous measurement stations collected from Meetnet Vlaamse Banken.	26
Table 8 – Description of the past storm surges over the study period from 11/2018.....	26
Table 9 – Summary of meteo-marine conditions recorded from the stations during the ad-hoc measurements.	30
Table 10 – Statistic summary of the grain size for the three sediment samples collected near the Aquadopps during the ad-hoc measurements.	36
Table 11 – Overview of Lidar surveys used for the A-P analysis.	41
Table 12 – Tidal prism for the section in the north of zone 1 as a function of water level. The volumes are graphically depicted in Figure 19.....	44
Table 13 – Tidal prism for the section at the boundary of zones 1 and 2 as a function of water level. Results at water level +5 m in bold as this is used in the analysis below. The volumes are graphically depicted in Figure 20.	45
Table 14 – Altitudes in m TAW of lowest land surface point at some locations of the main tidal channel....	47
Table 15 – Cross-sectional areas for the profile across the tidal channel at the boundary of zone 1 and 2, with respect to water level +5 m TAW.	48
Table 16 – Cross-sectional area A and tidal prism P for the successive available surveys at the border of zone 1 and 2.	51
Table 17 – Summary statistics of water discharge across the channel, water level, current velocity and direction measured in the deep channel during the three ad-hoc campaigns.	A6

List of figures

Figure 1 – Morphological units of the Zwin tidal inlet (left). Zoom on the entrance and inland inlet (right)...	2
Figure 2 – Example of typical tracks of a Qboat survey.	6
Figure 3 – LiDAR DEMs from 2019 to 2022 (i.e. from 2.5 months to 2.8 years after opening of the dyke) and DoDs with ca. 1 year interval.....	9
Figure 4 – LiDAR DoDs between the T0 survey before the opening of the dyke (06/11/2018) and the recent surveys.....	10
Figure 5 – LiDAR DoD just after the opening of the dyke on 20/04/2019 and 23/02/2022.	11
Figure 6 – A) Cross-channel profiles from 11/2018 (pre-opening) to 02/2022; B) difference of consecutive surveys. Insert: location of the profile measurement. Benchmark is located in the west dune.	14
Figure 7 – Qboat DEMs of the inland inlet of the Zwin from 2019 to 2021.	18
Figure 8 – Qboat DoDs of the inland of the Zwin from 2019 to 2021.....	20
Figure 9 – Qboat DoDs of the inland of the Zwin based on a reference survey on 30/01/2019 (pre-opening dyke survey).....	22
Figure 10 – Extracted profiles from the Qboat DoDs.	25
Figure 11 – Time series of water level at Scheur, significant wave height, wave direction and wave period from the Zwin buoy. Blue vertical lines correspond to the LiDAR surveys, green lines to the Qboat surveys, yellow lines to the RTK-GPS profile surveys and red line to the opening of the dyke. Red stars indicate the storm events.....	28
Figure 12 – Wave distribution from the Zwin buoy for the period from 02/2019 to 03/2022. The coastline and the Zwin entrance channel are oriented WSW-ENE (70-250°) and NW-SE (145°-325°) respectively.....	29
Figure 13 – Time series of water level, depth-averaged current and direction for the Aquadopps and Scheur station, Roses of current velocity (m/s) from the 3 Aquadopps indicating the current direction going to. Black line corresponds to the main channel orientation (145°-325°) for the ad-hoc campaigns.	34
Figure 14 – Sketches of processes in the entrance and inland inlet based on the ad-hoc campaigns.	35
Figure 15 – Time series of 30 minutes averaged water level and estimated water discharge across the channel.	37
Figure 16 – Time series of water level and water discharge before (23/10/2018) and 1.8 years after the opening of the dyke (29/9/2020) (Aqua Vision, 2020). Note that the vertical discharge axis in the first subplot has reversed sign.	39
Figure 17 – Definition of partial areas that contribute to the tidal prism of the Zwin channel.....	42
Figure 18 – Principle of calculating the tidal prism in a zone, here shown on an arbitrary cross section.	43
Figure 19 – Evolution of the tidal prism at the entrance of the Zwin channel (at north border of zone 1) as a function of water level, and through time.	46
Figure 20 – Evolution of the tidal prism at the pile row in the Zwin channel (at boundary of zones 1 and 2) as a function of water level, and through time.	46
Figure 21 – Cross-sectional profiles, based on Lidar surveys, of the main tidal channel at the boundary of zones 1 and 2. For three surveys, the bed profile from the Qboat surveys has been added (for dates, see Table 11). Elevation in m TAW.	49

Figure 22 – Evolution of cross-sectional area of profile at boundary of zones 1 and 2 through time..... 50

Figure 23 – Cross-sectional area A versus tidal prism P for the successive available surveys at the border of zone 1 and 2. 51

Figure 24 – Summary sketch of the morphological changes and hydrodynamics under calm weather conditions on the Zwin inlet. Arrows indicate the direction of movement of morphology based on successive DEMs. Contour lines correspond to 5 m TAW..... 55

Figure 25 – Ad-hoc 1 – entrance inlet. 1

Figure 26 – Ad-hoc 2 – border between entrance inlet and inland inlet. 2

Figure 27 – Ad-hoc 3– entrance inlet. 3

Figure 28 – Ad-hoc 1 – meteo-marine parameters. 4

Figure 29 – Ad-hoc 2 – meteo-marine parameters. 4

Figure 30 – Ad-hoc 3 – meteo-marine parameters. 5

Figure 31 – Method of estimating water discharge. 7

1 Project overview and objectives

The Zwin is a unique nature reserve designated as Natura2000 site and situated at the border between Belgium and the Netherlands. It consists of a small tidal inlet connected to the North Sea through a tidal channel and terminates in a saltmarsh. The Zwin forms a tidal flood plain of 3 188 000 m², exhibiting a broad range of diverse and well-organized bedforms (e.g. coastal dunes, sand banks/bars, tidal flats and other landforms) (Figure 1). The Zwin tidal inlet system is composed of two morphological units. The entrance inlet unit consists of a tidal delta where waves and tides are important constituents of the water motion and sediment transport. In contrast, tidal currents prevail over waves in the inland inlet unit. It is characterized by a main channel undergoing a sequence of bifurcations resulting in a complex pattern of meanders. The inlet is flooded twice a day and the sea floods the inland area during high tide. The water volume in the inlet is variable, depending on the tidal phase and cycle (i.e. neap and spring). Also storm surge can further increase the volume of the water exchanged with the sea. The morphology of the tidal channel is controlled by hydrodynamic forcings (waves, tide), local relief and vegetation. In the past, the Zwin inlet was subject to continuous sediment deposition and siltation ranging from 3000 to 40 000 m³/year which was mainly caused by the tidal asymmetry (Houthuys et al., 2013). In order to tackle this, large scale intervention works took place in the Zwin from August 2016 to February 2019. These included excavation of the tidal area and coastal dunes, removal of Willem-Polder and opening of the dyke. More details are reported in Montreuil et al., 2021a. These interventions aimed to increase the tidal prism (volume of water that enters and leaves the Zwin inlet) by enabling more and faster seawater flow in and out of the channel in order to reduce the silting process. Specifically, the intention of the channel extension was to allow three times as much seawater to flow in and out by increasing the tidal prism up to 1 million m³ (ZTAR Newsletter, 2017).

To evaluate whether the interventions achieved the desired objectives and to gain knowledge about the morphological response of the area, it is crucial to monitor the situation of the Zwin system before and after completion of the management works. The monitoring program covers: (i) hydro-morphodynamics, (ii) ecological, (iii) fresh-salt ground water dynamics. In this final monitoring report, the results on the characteristics and changes of the hydro- and morphodynamics of the Zwin area over the period between the opening of the dyke (February 2019) and nearly 3 years and four months afterwards are presented. Morphological changes from the pre-opening situation to 8 months, 1.9 years, and 2.8 years later are presented in Montreuil et al. (2021a), Montreuil et al. (2021b) and Montreuil et al. (2022) respectively. Topographic and hydrodynamic data obtained during the study period were processed, analysed and integrated in order to understand the post-interventions evolution of the tidal inlet and hydro-morphodynamic interactions.

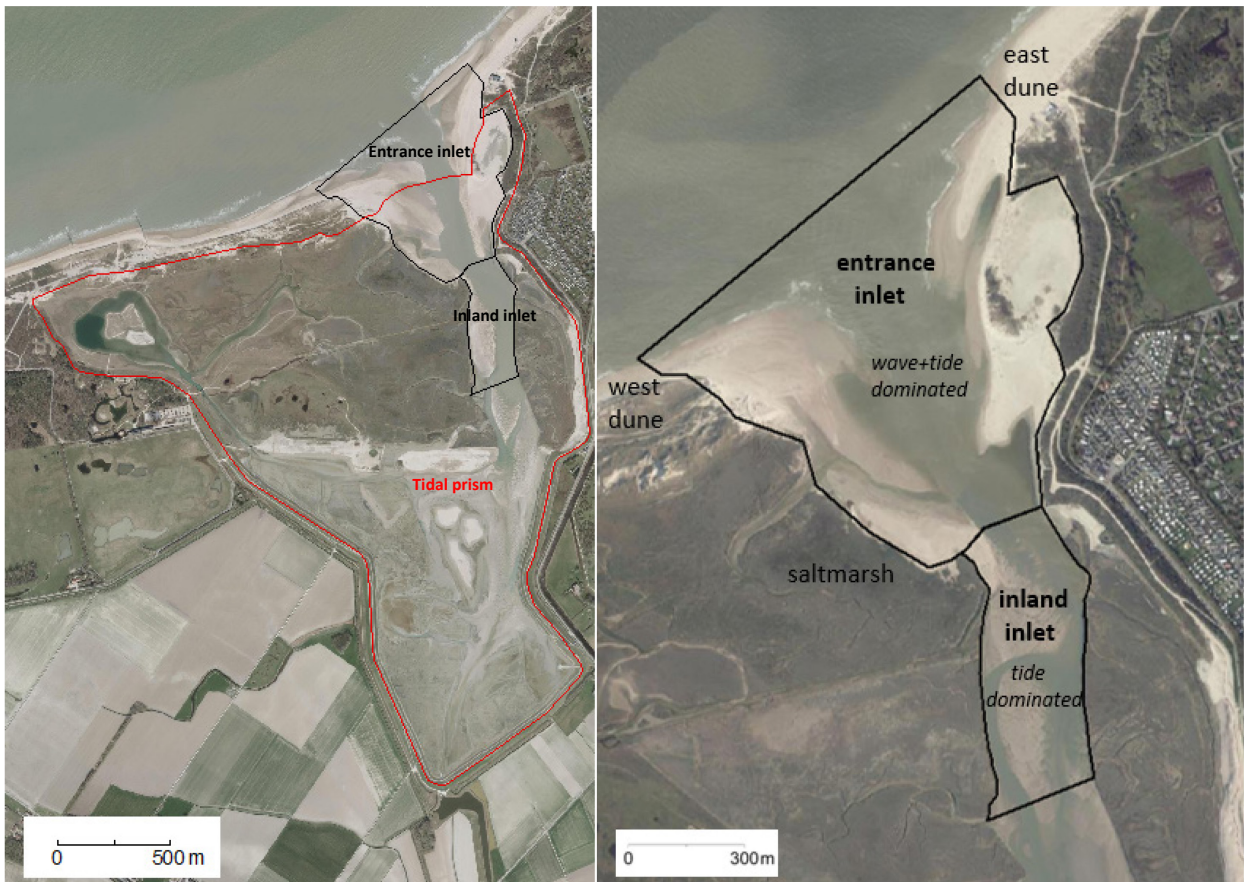


Figure 1 – Morphological units of the Zwin tidal inlet (left). Zoom on the entrance and inland inlet (right).

2 Topo-bathymetric data acquisition and methodology

Within the framework of this project, a large amount of data was gathered (Table 1). This data set consists of topographic and bathymetric surveys (airborne LiDAR, Qboat, and RTK-GPS profiles), hydrological and sediment measurements with several sources (Coastal Division, Aqua Vision and Flanders Hydraulics Research) and times of acquisition. For their usage, an updated data timeline and a coherent storage structure of the data set was applied to assess the morphodynamics of the Zwin inlet. The presented data timeline was used to analyze and interpret the morphological evolution of the study site, taking into account the information on wave climate and tidal action (forcing factors).

2.1. Survey timeline

The morphological change of the Zwin before, immediately after and a longer time after the opening of the dyke on 04/02/2019 was investigated at a large-scale based on airborne LiDAR surveys. Also, the behaviour of the entrance inlet and inland inlet was assessed using Real-time kinematic positioning (RTK-GPS) profiles and Qboat surveys respectively.

Table 1 – Overview of the data timeline from 2018 to 2022.

2018	06/11	LiDAR
2019	28/01	Lowering the old dyke
	30/01-1/02	Qboat flow and bathymetry
	04/02	Opening of the dyke
	06-07/03	Qboat flow and bathymetry
	20/04	LiDAR
	17-18/06	Qboat flow and bathymetry
	04/07	RTK-GPS cross-channel topography
	16-17/09	Qboat flow and bathymetry
	29/10	LiDAR
	11-12/12	Qboat flow and bathymetry
2020	28/02	LiDAR (post-storm)
	16/03	RTK-GPS cross-channel topography
	14/04	LiDAR

	03-04/06	Qboat flow and bathymetry
	29-30/09	Qboat flow and bathymetry
	30/09	RTK-GPS cross-channel topography
	28/10	Qboat flow and bathymetry
	18/11	LiDAR
	01-02/12	Qboat flow and bathymetry
2021	16/03	RTK-GPS cross-channel topography
	13-14/04	Qboat flow and bathymetry
	28/04	LiDAR
	24/06	RTK-GPS cross-channel topography
	24-25/06	Qboat flow and bathymetry
	08-09/09	Qboat flow and bathymetry
2022	23/02/2022	LiDAR

Note: surveys before 2019 are reported in Montreuil et al. (2021a).

2.2. Airborne LiDAR surveys

Airborne LiDAR surveys were commissioned along the entire coast by Coastal Division. They are usually performed at low tide. For each survey, the elevation point clouds (x, y, z) were used to generate a Triangulated Irregular Network (TIN) which was then converted to a Digital Elevation Model (DEM) with 2 m cell size. The cell size was chosen as a trade-off between the survey points spacing (density: > 1 point/m²) and the relatively large area covered. Consecutive DEMs of Difference (DoD) were calculated from the DEMs, by subtracting the elevations in each grid, on a cell-by-cell basis, in order to visualize the morphological changes after the opening of the dyke. The survey error (root-mean-square) is below +/-0.03 m.

LiDAR does not penetrate through water. Though the surveys are performed during low tide, ponds and lakes are present in the backwater areas. The TINs interpolate between the shores of these water areas and thus locally do not cover the real bed surface. Due to changing morphology and water levels from survey to survey, this may cause apparent change in the lowest areas of the Zwin.

2.3. RTK-GPS profiles

RTK-GPS profiles of the channel entrance were carried out by Coastal Division approximately every 6 months, while for 28/02 and 10/04/2020 additional profiles were extracted from LiDAR surveys. All the profiles extend from the coastal dunes at the west side of the Zwin to the backshore across the Dutch border. In general, the interval between measured points varies from less than 1 to 20 m. All profiles were interpolated with a 1 m interval for further analysis. The survey error (root-mean-square) is +/- 0.05 m.

2.4. Qboat surveys

Bathymetry of the inland inlet area was surveyed by Aqua Vision using a remotely-controlled Q-Boat 1800RP system equipped with ADCP and GPS devices. The advantage of such a system is the possibility to sound the bed surface in shallow zones. Bathymetric measurements were done with an interval of 3 to 6 months between January 2019 and June 2021 (Table 1 and Table 2). The reported error ranges from +/-2 cm in horizontal to +/-3 cm in vertical direction. A typical survey track is displayed in Figure 2. Regarding the post-processing, the point clouds (x ,y, z) were first converted to Lambert72 from ETRS89. Then, they were used to generate a TIN and then converted to a Qboat DEM with 0.1 m cell size (i.e. appropriate for the spacing between the survey points). Finally, consecutive Qboat DoDs were calculated from the Qboat DEMs, by subtracting the elevations in each grid, on a cell-by-cell basis.

Table 2 – Summary of the characteristics of the Qboat surveys.

Time	Total point clouds	Processed area (m ²)	Meteo-marine conditions
30/01-01/02/2019	157249	79899	SE, E low wind speed (<4 Bft) HW of 3.8 m TAW
06-07/03/2019	89065	49297	S, SW with medium to high wind speed (<7 Bft) Spring tide with HW of 4.4 m TAW Restricted survey coverage due to the occurrence of a storm
17-18/06/2019	214593	95076	NNW, NNE low wind speed Spring tide with HW of 4.5 m TAW
16-17/09/2019	215333	97814	N, NNW medium wind speed (4 Bft) Spring tide with HW around 4.6 m TAW
11-12/12/2019	249593	108512	SSW-S with calm wind speed (< 4 Bft) Spring tide with HW of 4.88 m TAW
03-04/06/2020	230454	111623	NNW with calm wind speed (< 4 Bft) Spring tide with HW of 4.50 m TAW
29-30/09/2020	260870	93850	SW with calm wind speed (2 Bft) Spring tide with HW of 4.5 m TAW
28-29/10/2020	279280	109267	SW with medium wind speed (5-6 Bft) Spring tide with HW of 4.8 m TAW
01-02/12/2020	256428	102284	NW, E with low wind speed (2-6 Bft) Spring tide with HW of 4.4 m TAW
14-15/04/2021	246969	103203	N with low wind speed (2-4 Bft) Spring tide with HW of 4.6 m TAW
24-25/06/2021 (Limited survey coverage)	89485	69673	N with low wind speed (2-3 Bft) Spring tide with HW of 4.5 m TAW
08-09/09/2021	189350	114042	E, S with low wind speed (1-3 Bft) Spring tide with HW of 5 m TAW

HW: high water

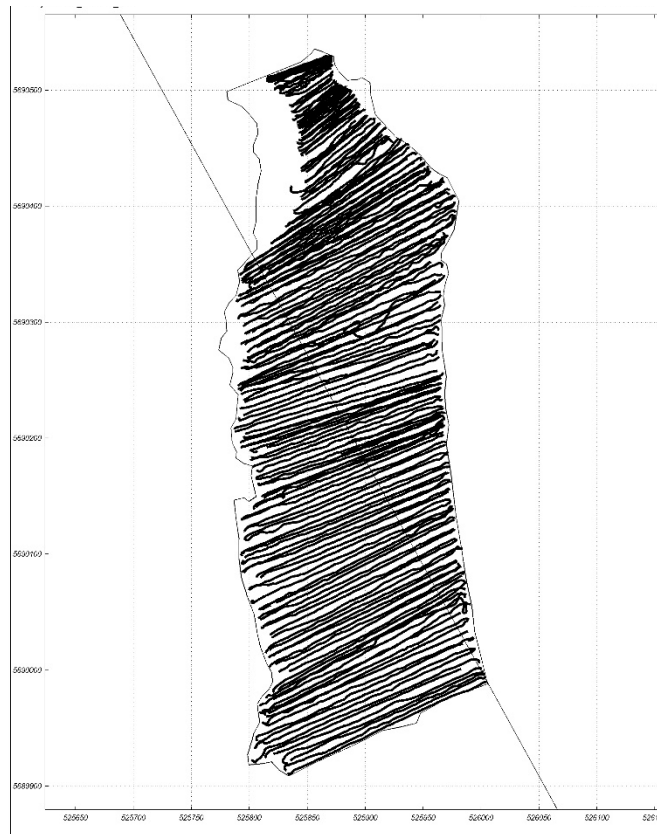


Figure 2 – Example of typical tracks of a Qboat survey.

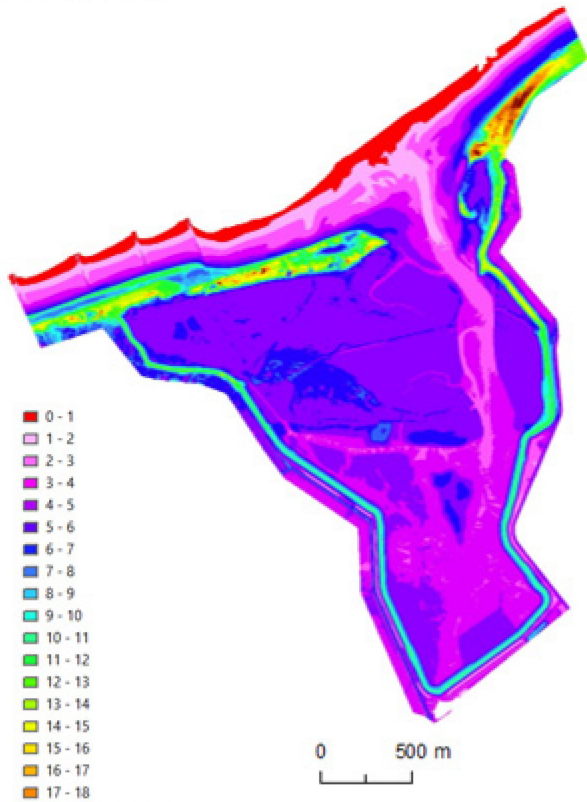
3. Morphodynamics results

3.1 Large-scale dynamics – entrance and inland inlet (LiDAR)

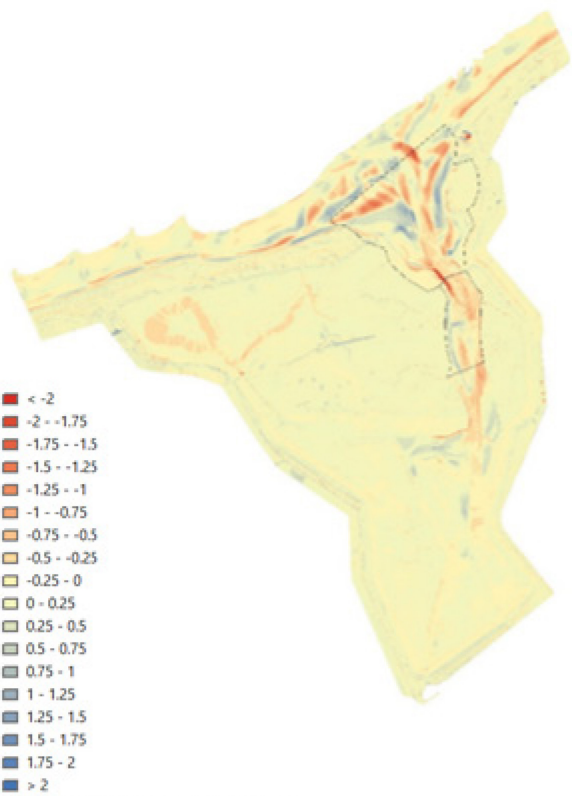
Based on the LiDAR surveys from before (06/11/2018) and after opening of the dyke, until February 2022, Figure 3 displays the elevation and the consecutive elevation differences of the entire Zwin inlet. The inlet is composed of a main channel exceeding 1.3 km in length from the seaward entrance to the most inland branches of the inlet (i.e. study area), and it intersects the beach plain backed by the Belgian and Dutch coastal dunes. The sand flat is characterized by dynamic sandy bedforms and rimmed by tidal flats backed by salt marshes above 4 m TAW at the west side of the inlet while an intertidal beach with dunes is present at the eastward side. In the entrance inlet unit, the main tidal channel is approximately 200 m wide and oriented 170-350° (SSE-NNW). Its bed elevation is around 1.2 m TAW in the seaward part while it is slightly shallower in the more landward part of the inlet (1.7 m TAW). Noteworthy, these elevation values have to be treated with caution due to the limitation of LiDAR to penetrate water. The Qboat surveys show depths between 0 and 1 m in the most seaward part of the surveyed area (see section 3.3). The sandy bedforms consisting of banks and bars as well as the presence of secondary channels give the channel a morphologically meandering and dynamic character. The inland inlet unit is characterized by a main channel oriented 140-320° in the seaward part of the unit while the landward part is 180-360°. It is characterized by a width below 100 m and an average bed elevation of 2 m TAW. The channel undergoes a sequence of bifurcations resulting in a complex pattern of small meandering channels and tidal flats. This leads to spatial variability of the width of the channel over time.

Significant morphological changes at the yearly scale exceeding 2 m in height occurred along the channel banks after the opening of the dyke (20/04/2019-10/04/2020, 10/04/2020-28/04/2021, 28/04/2021-23/02/2022), however in most of the area the changes remain below +/- 0.5 m. After 5.5 months (06/11/2018-20/04/2019), the inland inlet unit was subject to a decrease of sediment volume of -19 000 m³ which was equivalent to an average reduction in elevation of about 0.18 m (Table 3). Over this period, the sediment volume in the entrance inlet did not change so significantly. Between 20/04/2019-10/04/2020, the sediment loss in the entrance and inland inlet was -34 700 m³ and -26 260 m³ respectively which was greater than after 6 months of the opening of the dyke. Noteworthy, the period from 10/04/2020-28/04/2021 and from 28/04/2021-23/02/2022 was characterized by a sediment accretion in the entrance inlet of 15850 m³ and 51 430 m³ respectively whereas the inland inlet was still losing sand material. Therefore sediment loss occurred in the inlet area during during the 1.2 years after the opening of the dyke, while it was much lower over the last 2 years (2020-2022). The sand balance of the inlet area changed after this first period (2019 – 2020). An influencing factor is the sand supply from the coastal nourishments at Knokke and Cadzand. Sand supply is clearly observed with a large accretion of approximately 400 m long and 190 m wide at the west side of the entrance inland in the tidal area (Figure 3). Future LiDAR surveys will help to confirm the morphological trend of the inlet and especially whether the entrance inlet has reached an equilibrium. Future LiDAR surveys will help to confirm the morphological trend of the inlet and especially whether the entrance inlet has reached an equilibrium.

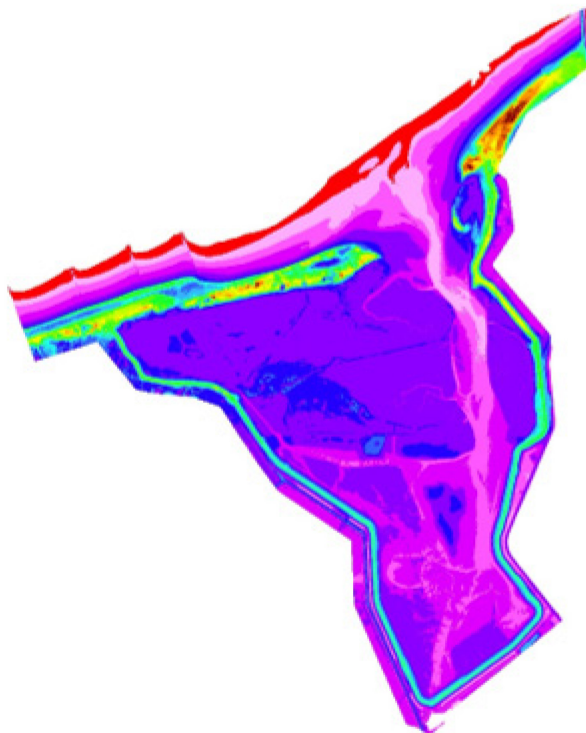
A) 20/04/2019



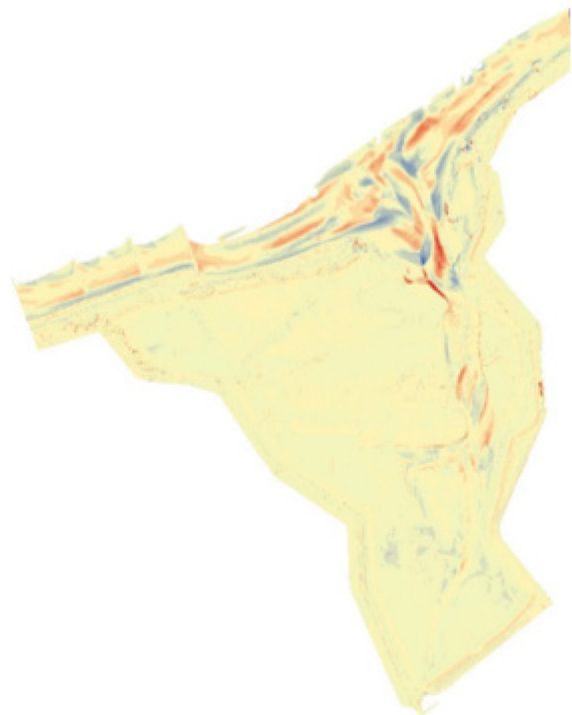
E) 20/04/2019 - 10/04/2020



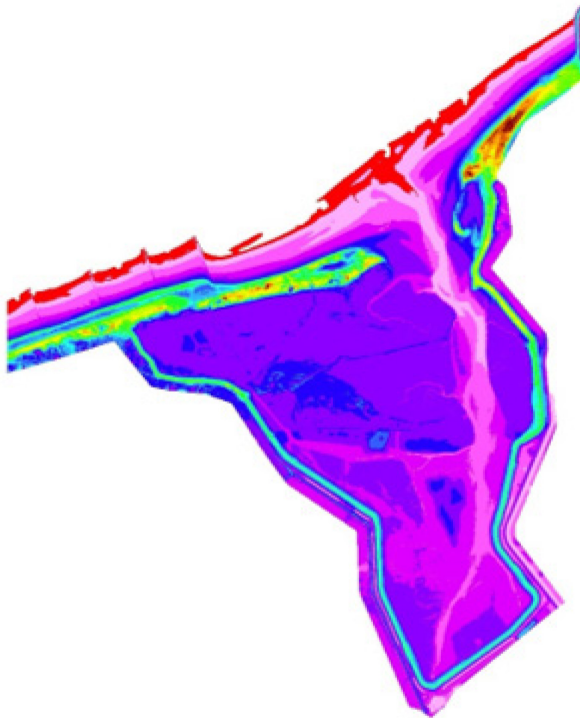
B) 10/04/2020



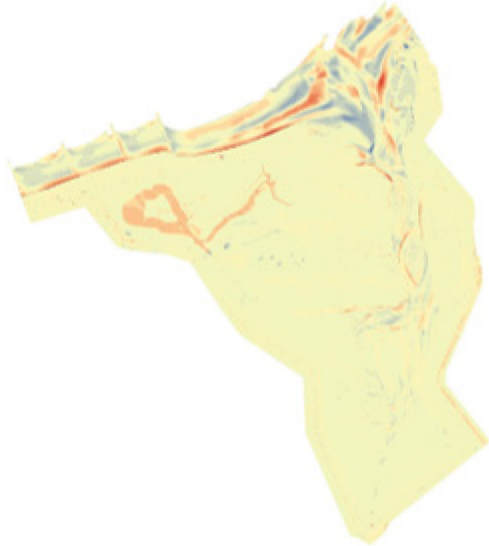
F) 10/04/2020 - 28/04/2021



C) 28/04/2021



G) 28/04/2021-23/02/2022



D) 23/02/2022

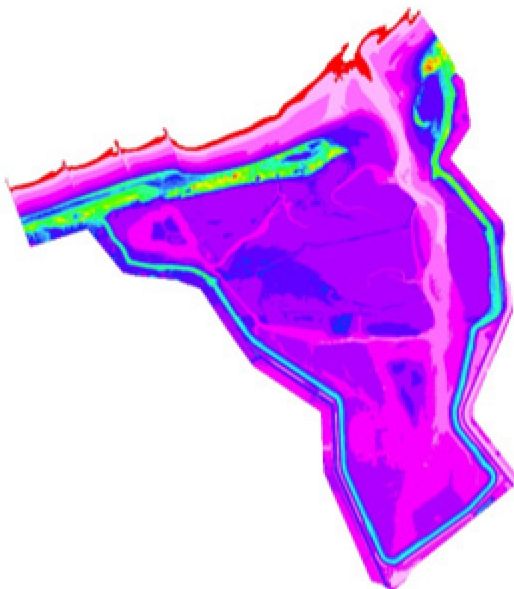
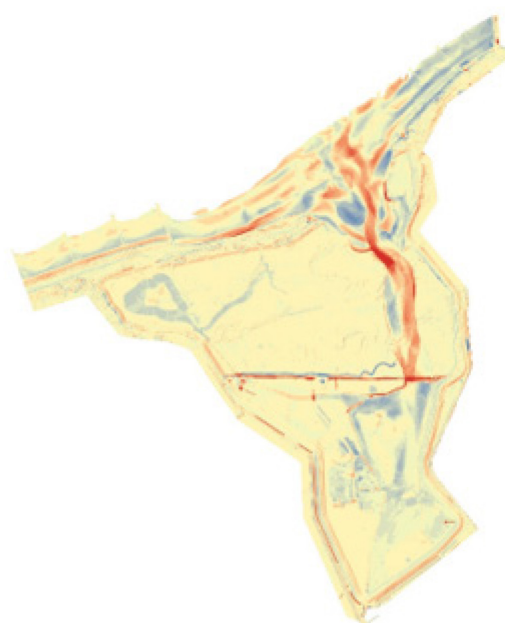
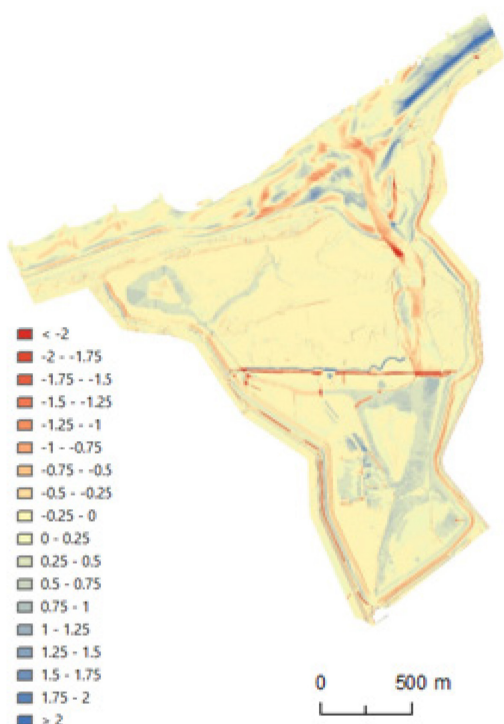


Figure 3 – LiDAR DEMs from 2019 to 2022 (i.e. from 2.5 months to 2.8 years after opening of the dyke) and DoDs with ca. 1 year interval.

A) 06/11/2018 - 20/04/2019

B) 06/11/2018 - 10/04/2020



C) 06/11/2018 - 28/04/2021

D) 06/11/2018 - 23/02/2022

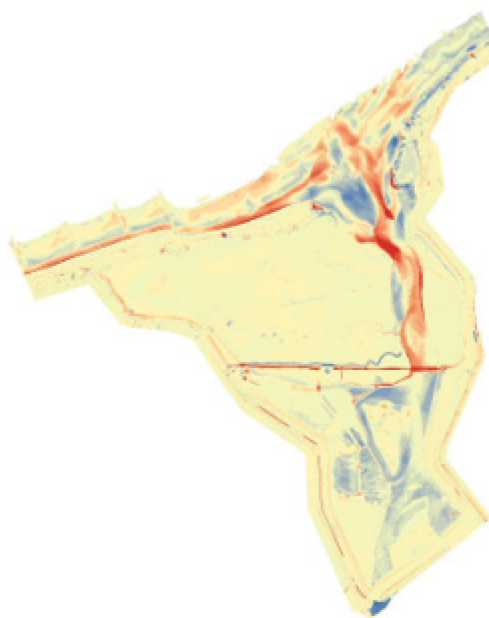
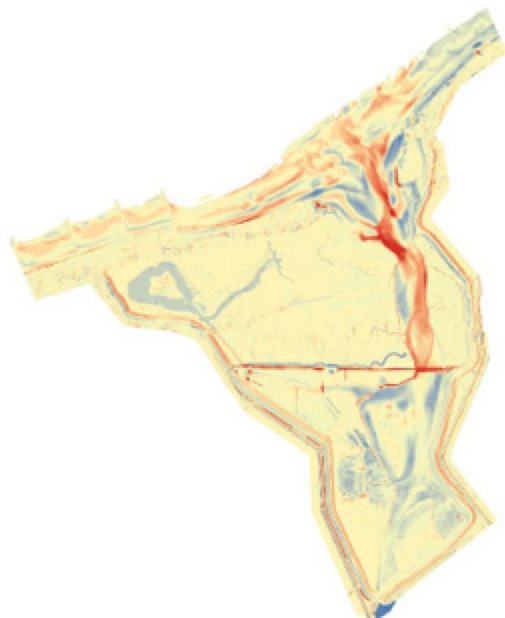


Figure 4 – LiDAR DoDs between the T0 survey before the opening of the dyke (06/11/2018) and the recent surveys.

Three years after the opening (06/11/2018-23/02/2022), the sediment loss in the inland inlet exceeded -46 890 m³. While the entrance inlet gained sand of 30 940 m³. Significant morphological changes occurred in the main channel which became deeper and wider. A clear eastward shift of the main channel is observed ranging from 4 to 45 m in 02/2022 compared to the pre-opening in 11/2018 based on the spring tide contours. The average migration rate is of 4 m/year. A westward channel migration at the border of the entrance inlet and the inland inlet (around 600 m from the seaward entrance) is observed. This coincides with a decrease of the height of the sand bank located on the westward edge. Also, a spatial dynamic variation is observed in the entrance inlet with alternating accretion and erosion zones parallel to the coast as well as on the edge of the salt marsh and dune line. This footprint is typical of alongshore migration of a three dimensional pattern of sandy bedforms which is probably related to the littoral drift. In the inland inlet, erosion dominantly along the east side of the channel suggests deepening associated with eastward migration. In contrast, the west side of the inland inlet is subject to a slight accretion along the edge of the salt marsh.

Figure 5 presents a DoD just after the opening of the dyke on 20/04/2019 and 23/02/2022. In general, similar evolution over this period of 2.8 years occurred compared to the pre-opening and 23/02/2002. The differences are related to the dynamics of the sand banks and secondary meanders of the channel.

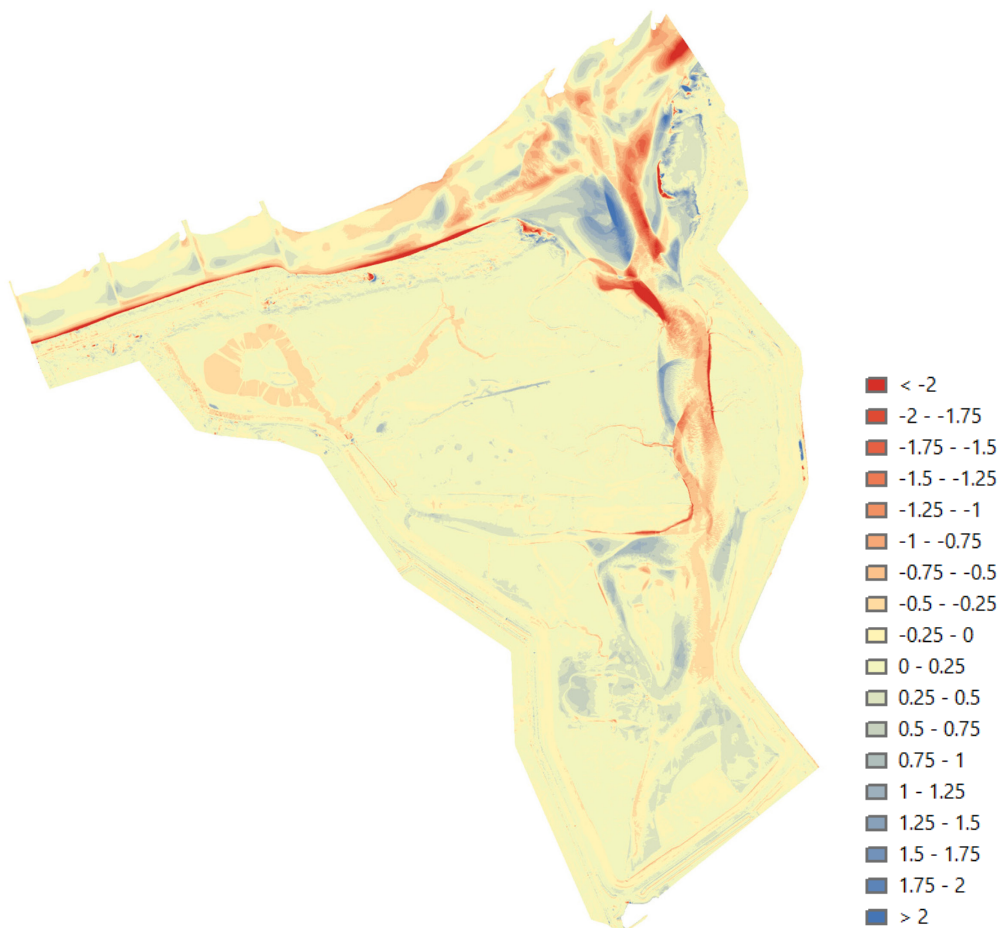


Figure 5 – LiDAR DoD just after the opening of the dyke on 20/04/2019 and 23/02/2022.

Table 3 presents the sediment volume change before and after the dyke opening. In summary, for the inland inlet first there was significant loss of sand but afterwards the sand balance stabilized, while for the entrance inlet first there was significant loss of sand and afterwards there was significant gain of sand (no stabilization of the sand balance).

Table 3 – Sediment volume in the Zwin inlet units before and after the dyke opening based on the LiDAR surveys.
Area of the entrance inlet is around 446 700 m² and of 107 550 m² for the inland inlet.

	Volume above 0 m TAW (m ³)	
	Entrance inlet	Inland inlet
	Volume (m ³)	Volume (m ³)
06/11/2018 (T0 survey, before the opening of the dyke)	174951	343850
23/02/2022 (2.83 years after the opening of the dyke)	1780445	296950
Difference	30940	-46890
Difference normalized	-0.08	-0.43
06/11/2018	1749510	343850
20/04/2019	1747870	324810
Difference	-1640	-19040
Difference normalized	0.00	-0.18
20/04/2019	1747870	324810
10/04/2020	1713170	298550
Difference	-34700	-26260
Difference normalized	-0.06	-0.24
10/04/2020	1713170	298550
28/04/2021	1729020	292390
Difference	15850	-6160
Difference normalized	0.04	-0.06
28/04/2021	1729020	292390
23/02/2022	1780445	296954
Difference	51428	4562
Difference normalized	0.12	0.04

Note: normalized to the covered area.

3.2 Entrance inlet

Cross-channel morphology of the entrance inlet was investigated based on the RTK-GPS profiles carried out from 11/2018 (pre-opening) to 02/2022. Previous cross-shore topographic profiles are presented in the progress report after the first year (Montreuil et al., 2020). Figure 5A shows the bed elevation as a function of distance from the origin of the profile and confirms the previous observations. The main channel has become deeper and moved eastward. It appears that the channel at the location of the cross-shore profiles has been stable between 30/09/2020 and 24/06/2021, and then further shifted eastward in 02/2022.

On 23/02/2022 survey, the lowest elevation of the channel was at 1.3 m TAW, while it was at 1.71 m TAW before the opening of the dyke (07/11/2018). The channel became thus 0.4 m deeper in its centre. A large difference of elevation up to 2.3 m occurred between 04/07/2019 and 16/03/2020 in the centre of the channel due to an eastward migration of the channel (Figure 5B), while the following periods were subject to lower elevation change (not exceeding 1.3 m). A slightly lower depth in the channel is observed for the most recent surveys. From 24/06/2021-23/02/2022, the channel migrated of 30 m eastward which was probably exacerbated by the presence of the westward sand bank. Morphological indicators were defined and extracted from the cross-shore channel profiles (Table 5). The channel width changed over time ranging from 322 m on 07/11/2018 to 358 m on 28/04/2021. During the last period (23/02/2022), it has decreased caused by the presence of the sand bank. This must be confirmed by the future surveys. Generally, the channel has become wider (average 40 m) since the opening.

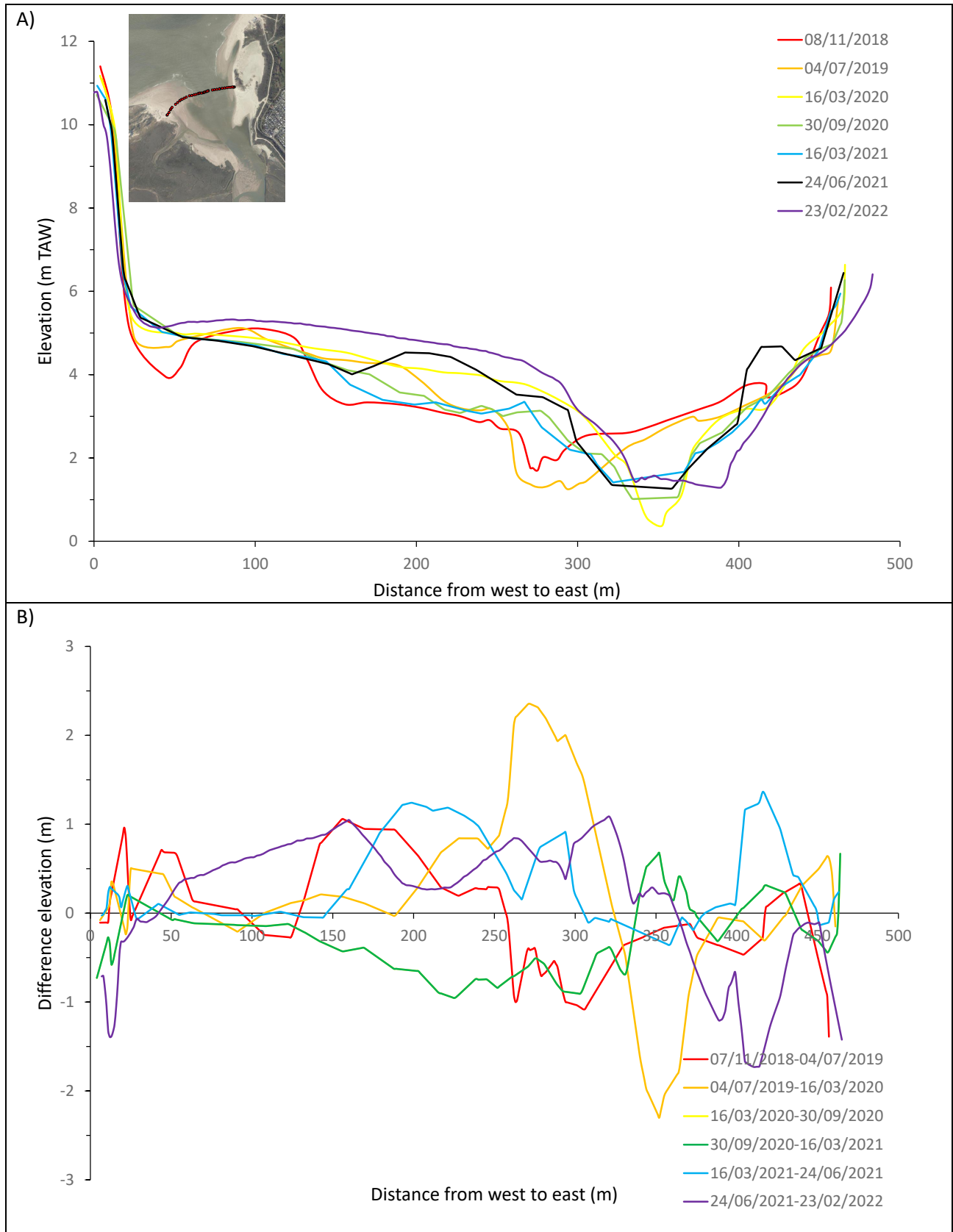


Figure 6 – A) Cross-channel profiles from 11/2018 (pre-opening) to 02/2022; B) difference of consecutive surveys. Insert: location of the profile measurement. Benchmark is located in the west dune.

Table 4 – Definition of morphological indicators

Position western (eastern) edge at spring HW	Distance of the western (eastern) edge of the channel elevation reaching the spring high water level of 4.7 m TAW
Position western (eastern) edge	Distance of the western (eastern) edge of the channel elevation reaching the spring high water level of 3.8 m TAW
Width	Distance of the channel between western and eastern edge
Area	Surface of the channel section between western and eastern edge
Avg depth spring	Average elevation in the channel section
Max depth spring	Maximum elevation in the channel section
Min depth spring	Minimum elevation in the channel section

Table 5 – Summary indicators of the cross-channel marker locations based on the RTK-GPS profiles. Reference spring HW (4.7 m TAW)

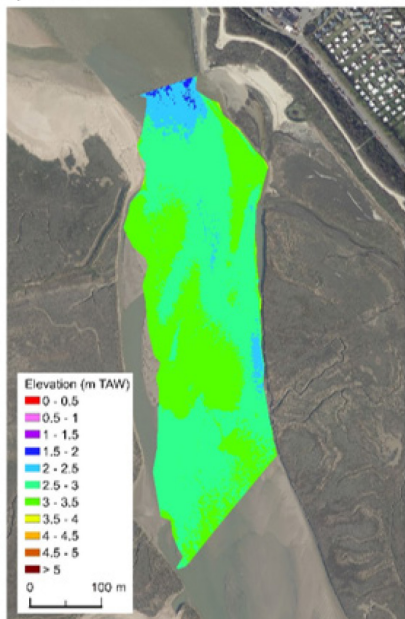
	07/11/2018	04/07/2019	16/03/2020	30/09/2020	16/03/2021	28/04/2021	23/02/2022
Position western edge (m)	126	118	127	108.7	99	95	221
Position eastern edge (m)	448	458	429	455.7	450.5	452.5	459
Width (m)	322	340	302	347	351.5	357.5	238
Area (m ²)	518.5	517.03	364.51	548.27	577.8	431.14	380.9
Avg depth (m TAW)	3.09	3.18	3.34	3.01	3.07	3.5	2.58
Max depth (m TAW)	4.77	4.73	4.7	4.7	4.7	4.76	4.49
Min depth (m TAW)	1.71	1.25	0.37	1.02	1.42	1.26	1.29

Note: just the main channel is considered here, the small secondary channels were not surveyed in detail.

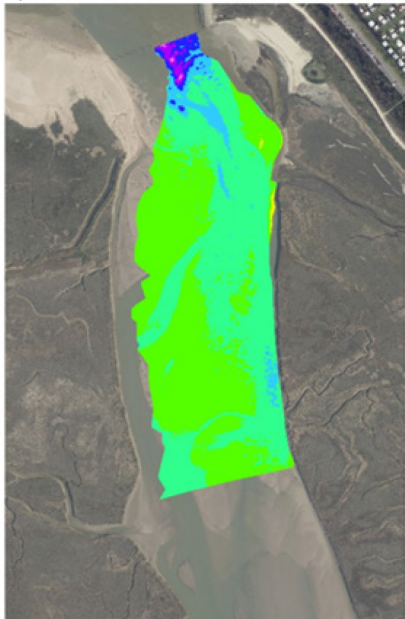
3.3 Inland inlet

Figure 7 presents all the bathymetric DEMs from the Qboat surveys in the inland inlet part from 07/2017 to 09/2021. A clear development of a main channel is visible in the inland inlet from 03/2019 (1 month after the opening) and it has gradually become deeper over the following 2.5 years period. From 10/2020, the morphological changes in the channel have decreased. In 04/2021, the north of the survey area is characterized by a wider and deeper channel compared to the pre-opening surveys, with the bed around 0 m TAW. The channel is clearly asymmetric: the east side of the channel is significantly deeper and wider than the west side except for the area close to the west side bank in the seaward side of the inland inlet. Also, a progressive eastward migration of the channel is observed along with its deepening from the opening of the dyke. Additionally, the inland inlet is characterized by a relatively stable tidal bank with a large sand bar with its crest up to +4 m TAW on the west side as well as smaller features such as bars and mega-ripples along the channel. This large sand bar is enclosed by the main channel and its small meanders.

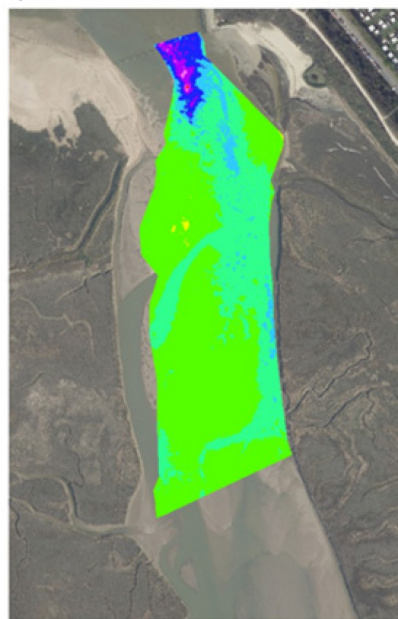
A) 10-11-12/07/2017



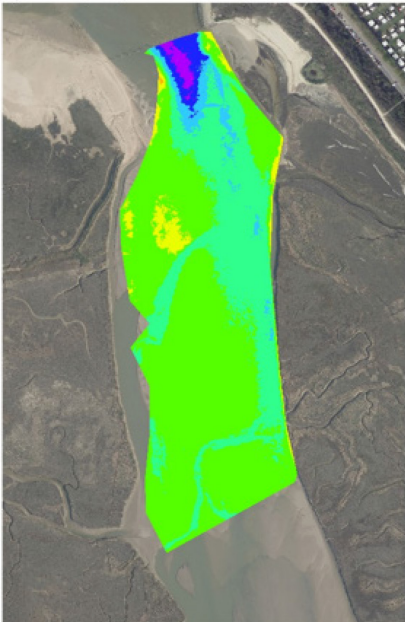
B) 18-19/12/2017



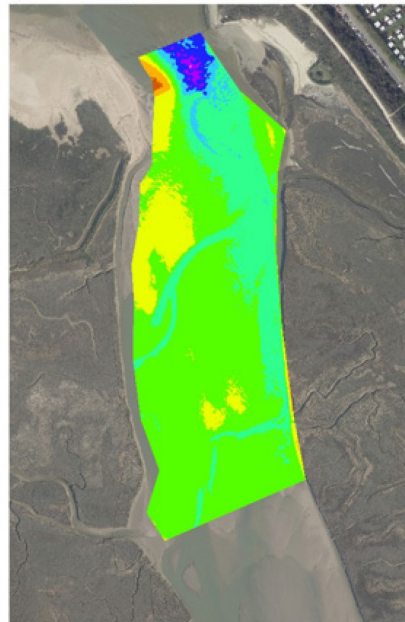
C) 12-13/04/2018



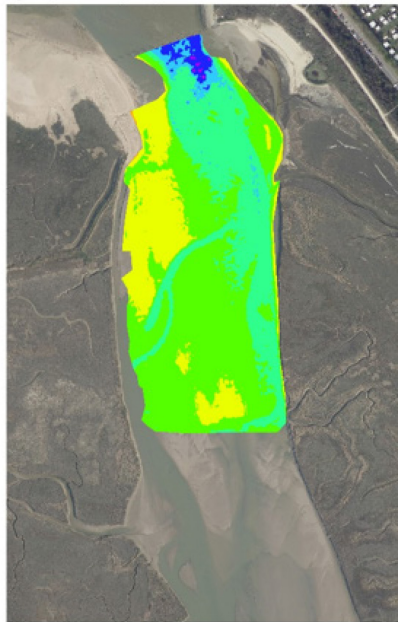
D) 10-16/07/2018



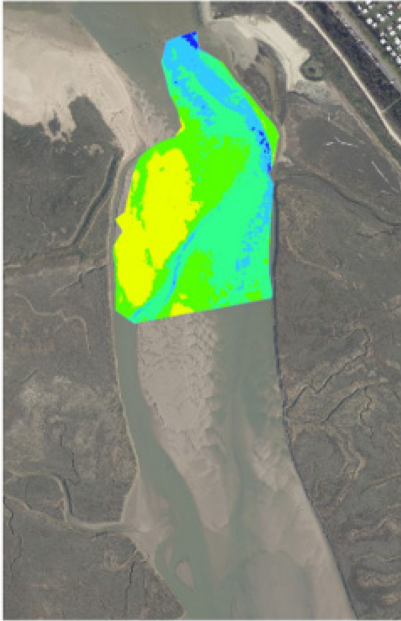
E) 23-24/10/2018



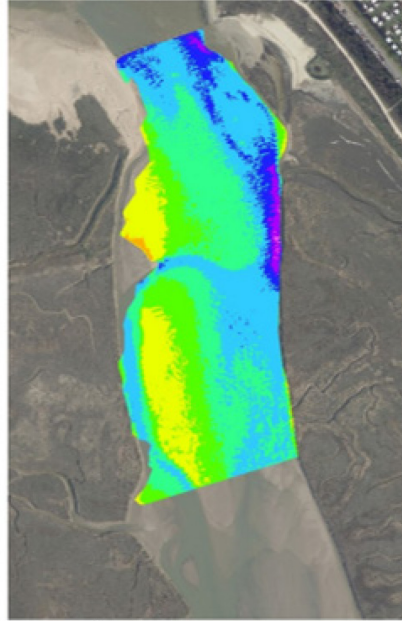
F) 31/01-01/02/2019



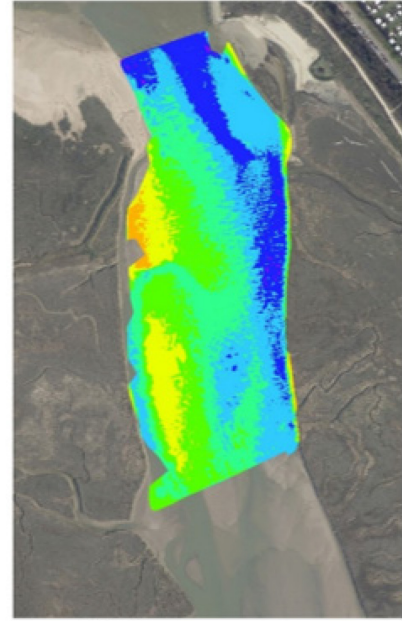
G) 06/03/2019



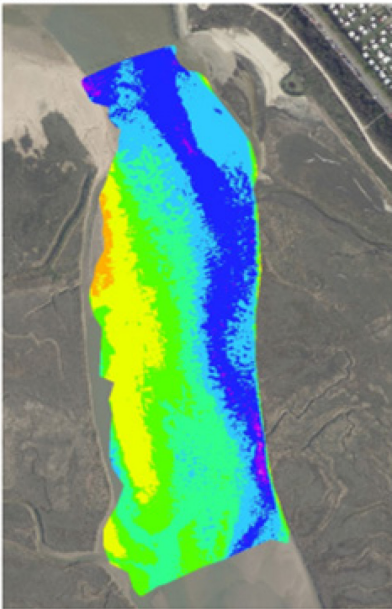
H) 17-18/06/2019



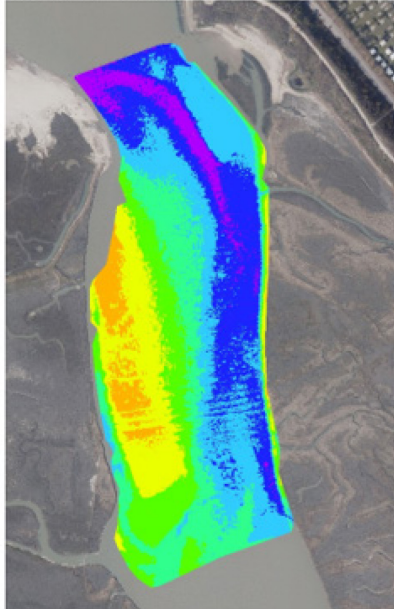
I) 16-17/09/2019



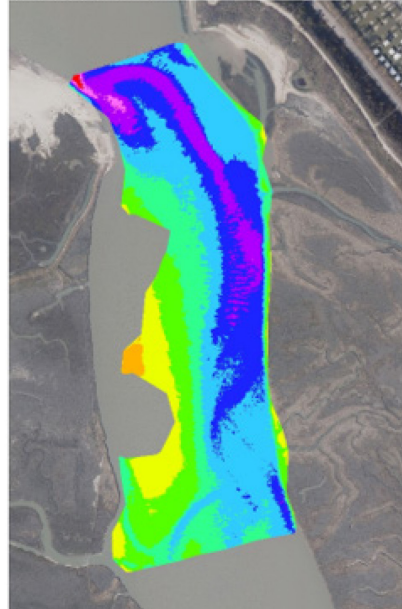
J) 11-12/12/2019



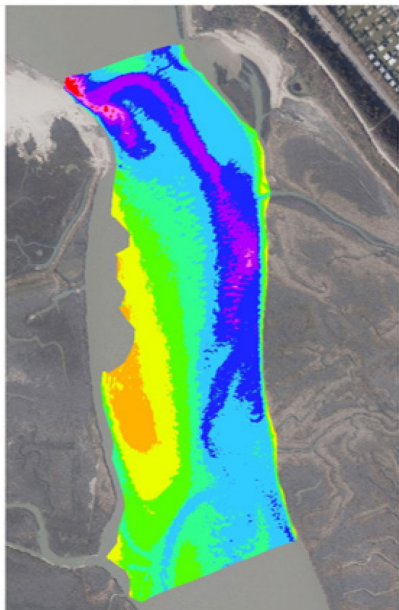
K) 03-04/06/2020



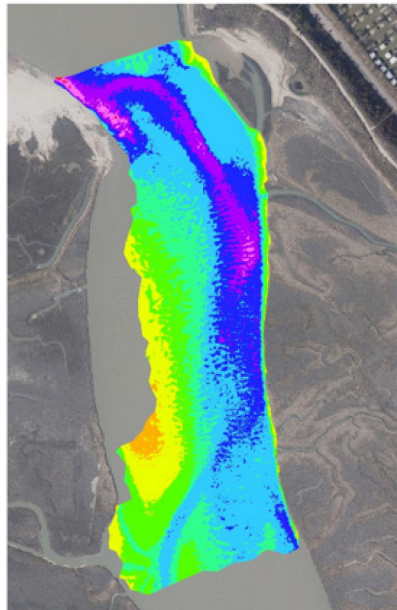
L) 29-30/09/2020



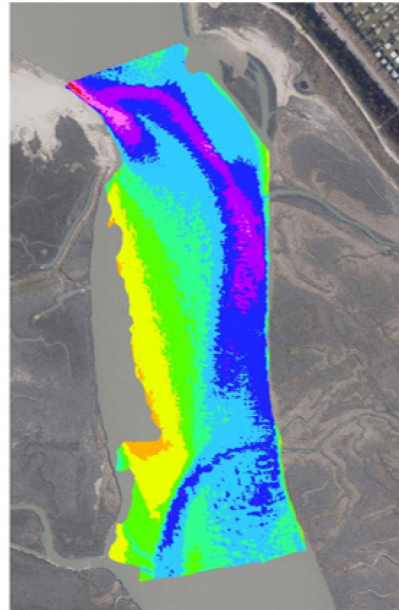
M) 28-29/10/2020



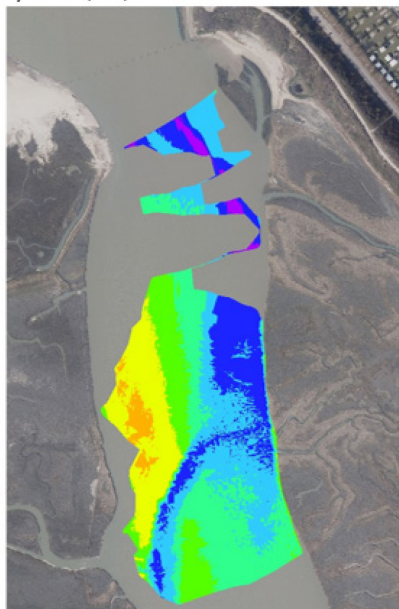
N) 01-02/12/2020



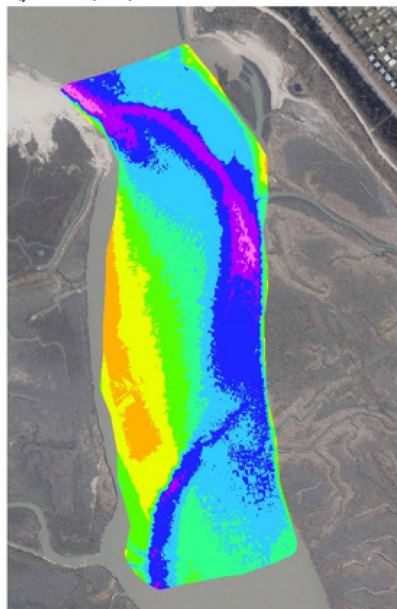
O) 13-14/04/2021



P) 24-25/06/2021



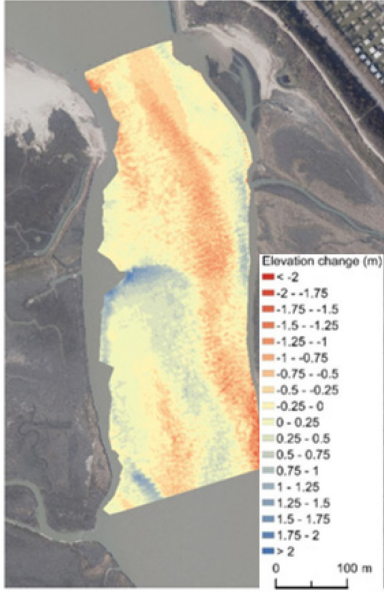
Q) 08-09/09/2021



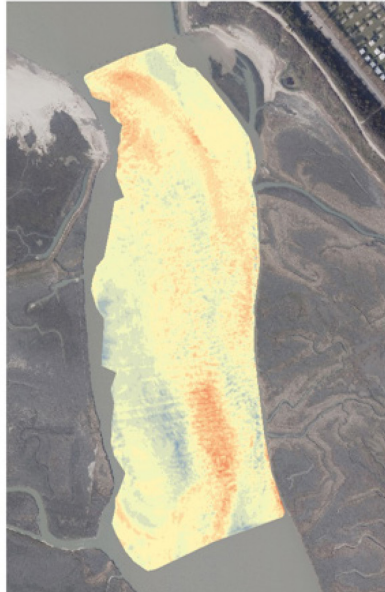
Note: coverage of the surveys varied mainly depending on the meteorological and local topographic conditions during the data acquisition.

Figure 7 – Qboat DEMs of the inland inlet of the Zwin from 2019 to 2021.

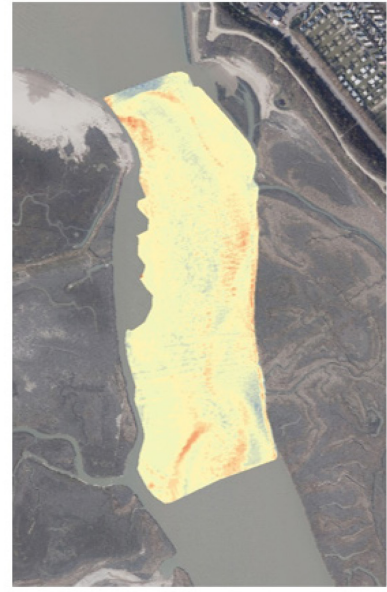
A) 01/2019 – 06/2019



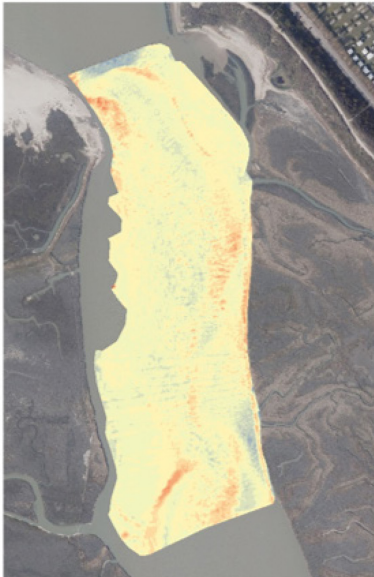
B) 06/2019 – 12/2019



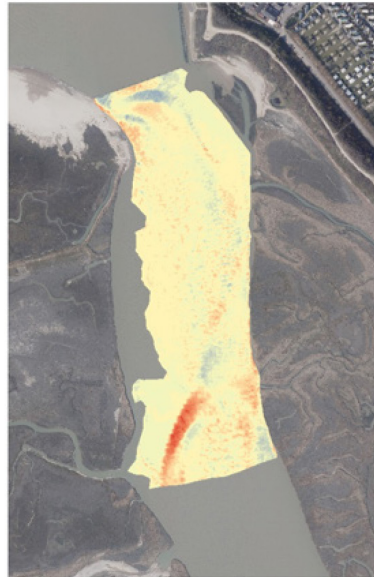
C) 12/2019 – 06/2020



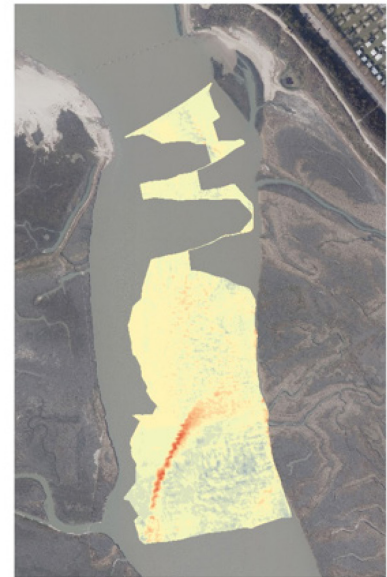
D) 06/2020 – 10/2020



E) 10/2020 – 04/2021



F) 04/2021-06/2021



G) 06/2021-09/2021

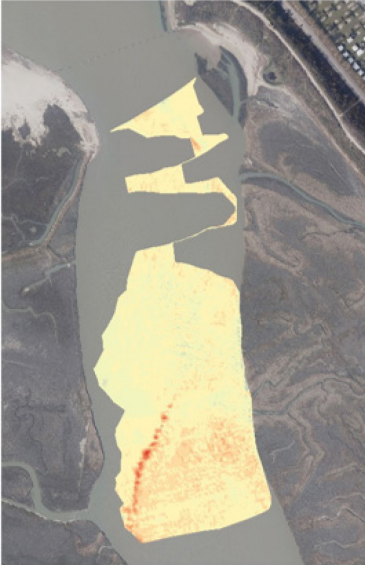
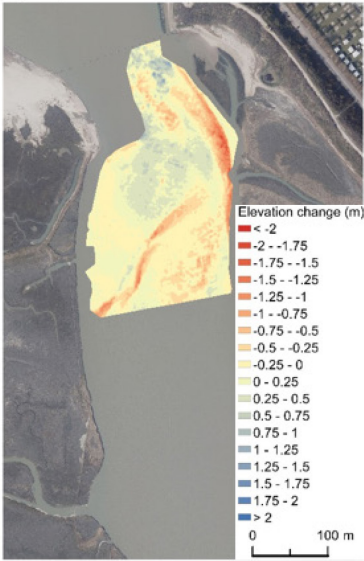


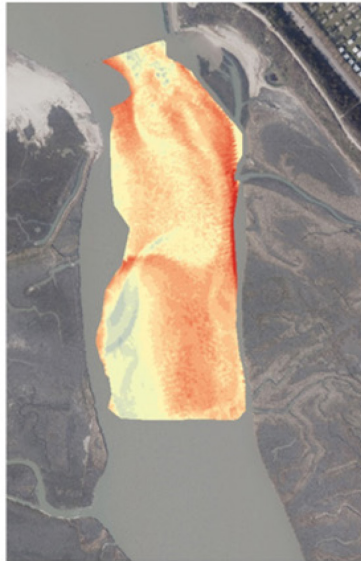
Figure 8 – Qboat DoDs of the inland of the Zwin from 2019 to 2021.

The consecutive DoDs show elevation change between surveys (Figure 8). A high spatial and temporal variability of morphological change in the inland inlet is observed. Generally, erosion occurs in the main channel and along its banks. Also, erosion is generally observed in the seaward part of the inland inlet which is characterized by a narrow width and strong curvature of the channel. This increases hydrodynamics causing significant erosion there. In contrast, the large tidal bank on the west side and located halfway in the area generally experiences positive elevation change with a sand gain. The intensities of change decreased since 12/2019. The comparison between the pre- and post-opening dyke bathymetric surveys clearly shows two opposite morphodynamics trends occurring in the inland inlet namely a sediment gain westward and halfway of the area, while erosion dominates in the rest of the survey area (Figure 9). Over the 2.6 year period (01/2019-09/2021), the inland inlet has become deeper with an average of nearly 0.7 m, which corresponds to a decrease of elevation of 0.32 m/year (Table 6). The deepest part of the channel in 09/2021 was in average -0.6 m lower than before the opening of the dyke.

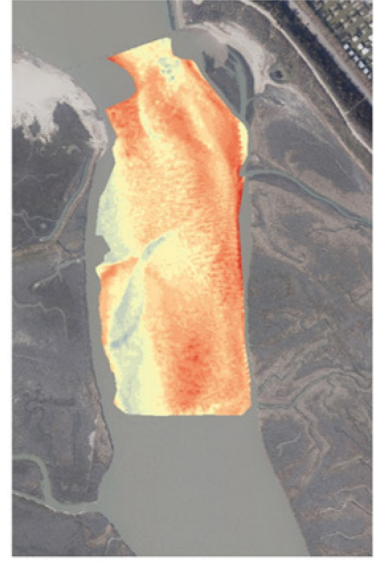
A) 01/2019 – 03/2019



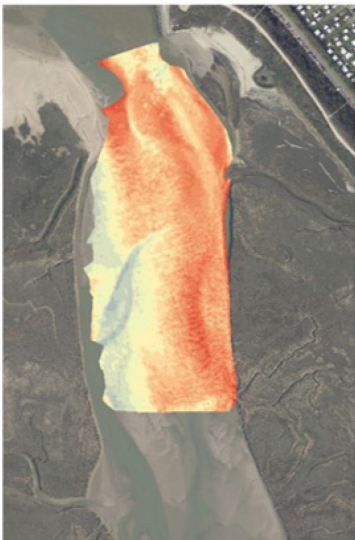
B) 01/2019 – 06/2019



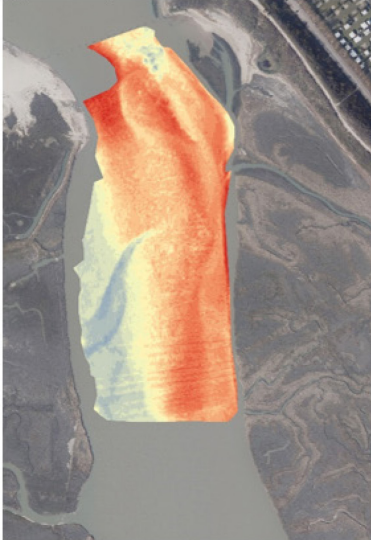
C) 01/2019 – 09/2019



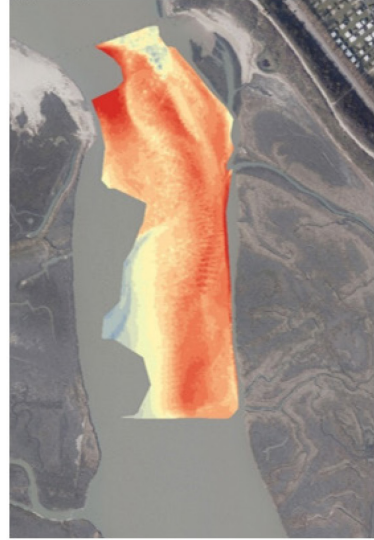
D) 01/2019 – 12/2019



E) 01/2019 – 06/2020



F) 01/2019 – 09/2020



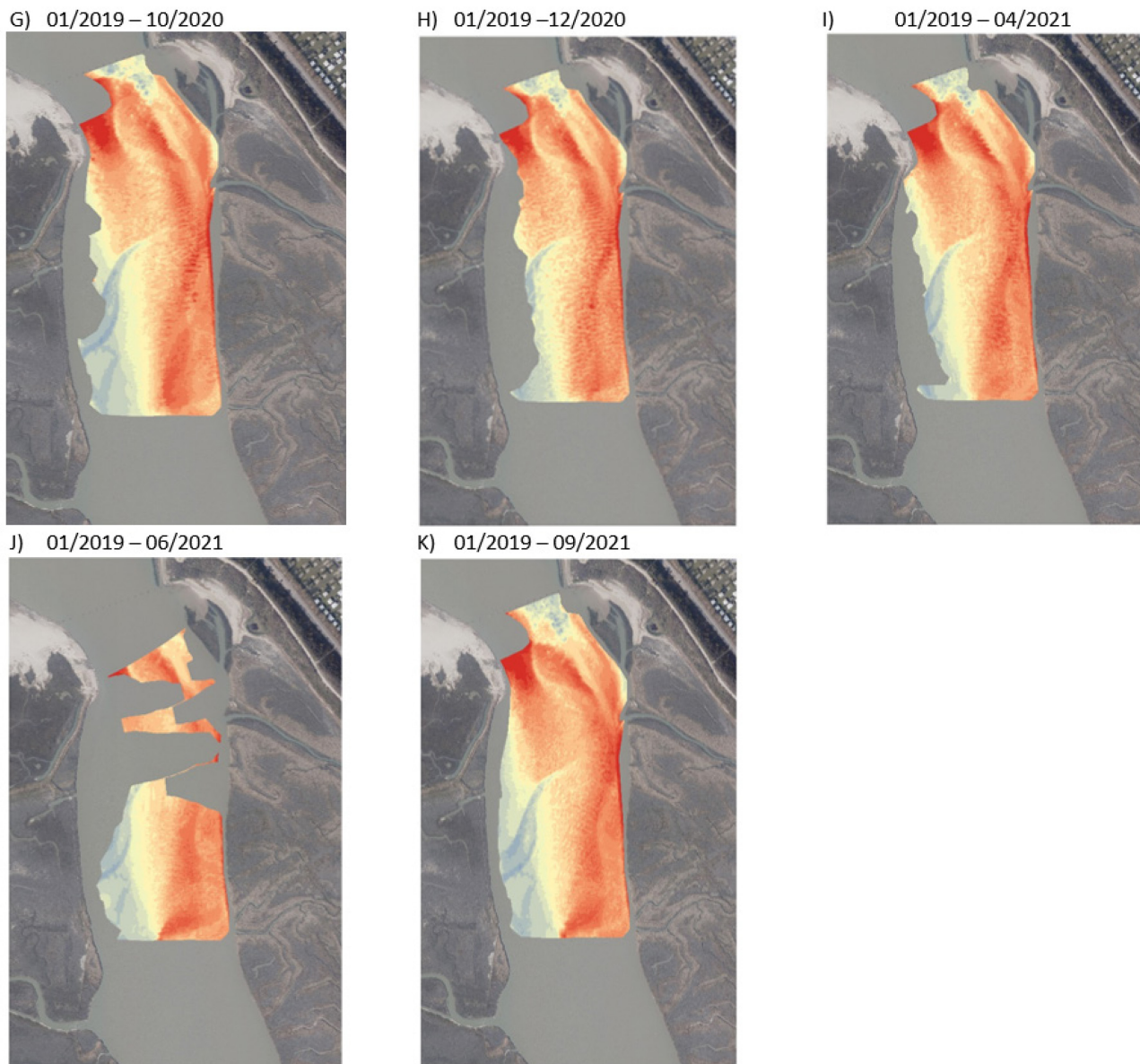
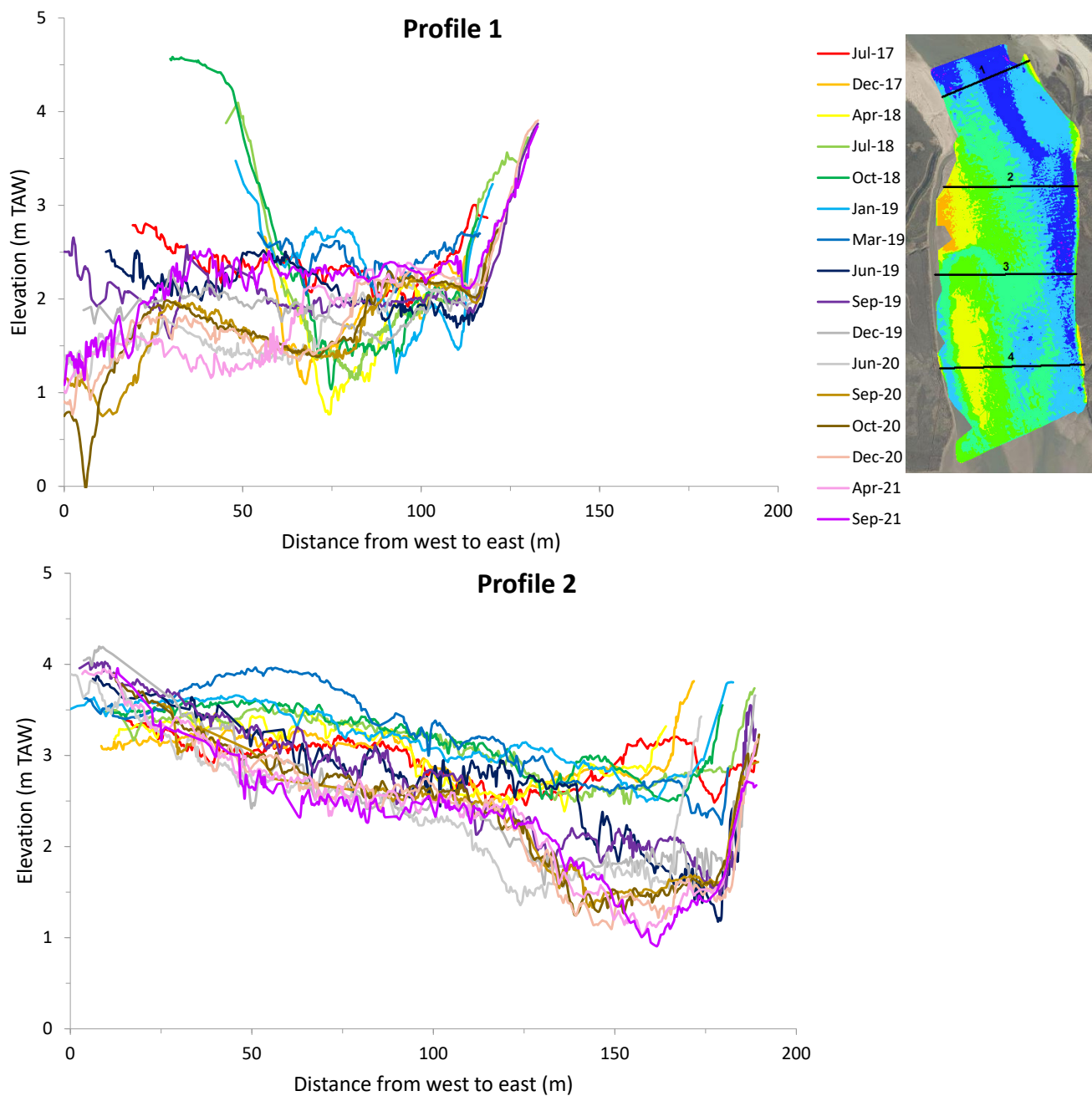


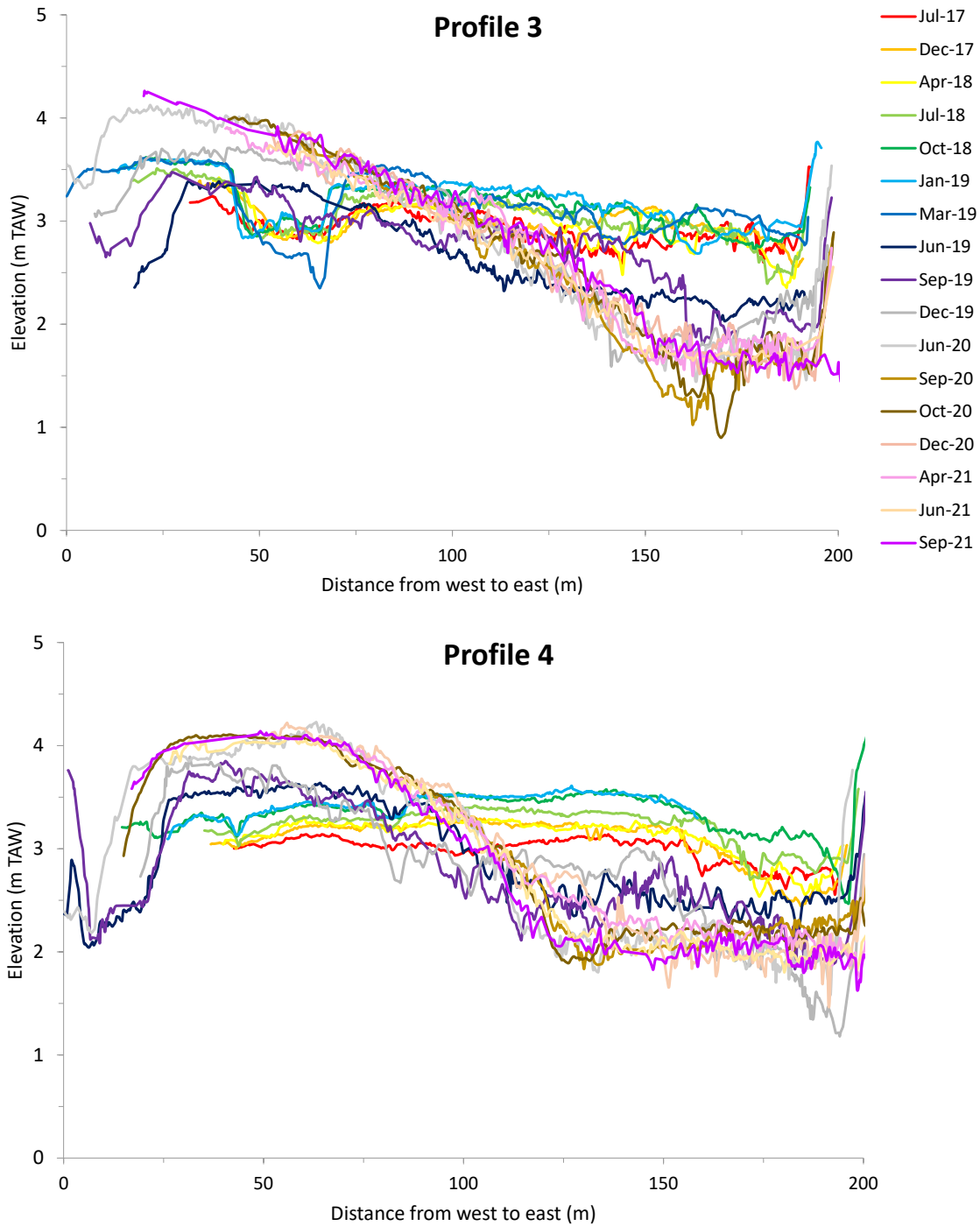
Figure 9 – Qboat DoDs of the inland of the Zwin based on a reference survey on 30/01/2019 (pre-opening dyke survey).

Table 6 – Statistic summary of the Qboat DoDs.

DoD consecutive	Difference of elevation (m)			
	Mean	Max	Min	SD
Survey				
01/2019-03/2019	-0.04	1.50	-2.06	0.347
03/2019-06/2019	-0.43	1.26	-2.43	0.41
06/2019-09/2019	-0.04	1.81	-1.49	0.30
09/2019-12/2020	-0.05	1.53	-1.99	0.33
12/2019-06/2020	-0.01	1.52	-1.71	0.31
06/2020-09/2020	-0.02	1.77	-1.34	0.20
09/2020-10/2020	0.02	1.54	-1.70	0.18
10/2020-12/2020	-0.01	1.77	-1.419	0.20
12/2020-04/2021	-0.05	1.54	-2.19	0.27
04/2021-06/2021	0.07	1.28	-1.96	0.25
06/2021-09/2021	-0.11	1.16	-2.17	0.20
DoD Ref Jan 2019				
01/2019-03/2019	-0.04	1.50	-2.06	0.35
01/2019-06/2019	-0.46	0.98	-3.06	0.47
01/2019-09/2019	-0.49	1.10	-2.42	0.49
01/2019-12/2019	-0.53	1.14	-2.40	0.57
01/2019-06/2020	-0.55	1.386	-2.65	0.72
01/2019-09/2020	-0.76	1.40	-2.84	0.63
01/2019-10/2020	-0.59	1.36	-2.96	0.72
01/2019-12/2020	-0.71	1.21	-3.33	0.65
01/2019-04/2021	-0.67	1.42	-3.16	-0.69
01/2019-06/2021	-0.52	1.30	-2.71	0.71
01/2019-09/2021	-0.58	1.41	-3.02	0.76

The evolution of four extracted profiles from 07/2017 to 09/2021 are shown in Figure 10. Profile 1 located at the seaward side of the inland inlet indicates that the bed elevation of the channel after the opening has progressively become deeper. The lowest elevation just before the opening of the dyke was 1.21 m TAW, while it was 0 m TAW in 10/2020. However, the channel depth remained generally above 1 m TAW. In addition, the main channel is more than two times wider nowadays than before the opening (based on the 2 m contour line) and it has now also larger meanders (Figure 7). At this location the thalweg shifted westwards, while the opposite is true at the other profile locations (probably confined by the stone dyke at the east side here). From 03/2019, the channel migration with sand banks development have been associated with an increase of the bed elevation. In 09/2021, the average of the channel elevation was of 2.2 m TAW. Profile 2, 3 and 4 in the middle and southward part of the inland inlet also show a trend of the channel becoming deeper and wider over time. Another observation is the development of sand banks especially at the western shore of the channel in the central and southern part of the inland inlet. Decimetre-scale mega-ripples, also called submerged dunes, are observed in the channel along the four profiles. These mega-ripples indicate an active sediment transport driven by tidal currents.





Note: Due to limited coverage of the surveys in 06/2021 no profile 1 and 2 could be extracted.

Figure 10 – Extracted profiles from the Qboat DoDs.

4 Forcing factors

4.1 Marine conditions

Water level records with 5 minutes interval were acquired at the Scheur station located offshore around 7 km from the study site (Table 7). Additionally, the wave height, direction and average period were measured continuously at the Zwin buoy located 0.5 km offshore from the study site.

Table 7 – Description of the continuous measurement stations collected from Meetnet Vlaamse Banken.

Parameter	Location	Temporal resolution
Wave: -Significant wave height (Hs, m) -Average wave period (s) -Direction (°)	Zwin [79636E 229580N] from 22/02/2019 0.5 km from the study site Depth of - 2.3 m TAW	30 min
Water level (m TAW)	Scheur 7km from the study site Depth of - 9.7 m TAW	5 min

In total, between 11/2018 and 03/2022, 7 storm surges were recorded at the coast with two events in 2019, one in 2020, two in 2021 and 2022 (Figure 11 and Table 8). The maximum water level during these storm surges ranged from 5.39 m to 5.63 m TAW. The highest water level occurred on 31/01/2022 (Corrie storm) when a surge of 1.29 m was recorded. Significant wave height and 10% highest wave height were 1.85 m and 2.36 m respectively during this event.

Table 8 – Description of the past storm surges over the study period from 11/2018.

Storm surge	Maximum water level (m TAW)	Surge (m)	Average wave height (m)	Wave direction (°)	Wave period (s)
08/01/2019 (peak at 14:25)	5.39	1.09	2.68 [2.96]		5.69
30/09/2019 (peak at 01:00)	5.51	0.41	2.08 [2.65]	309	4.86
10-11/02/2020 (peak on 10/02 at 13:10)	5.61	0.91	1.85 [2.36]	302	4.95
21/10/2021 (peak at 12:55)	5.31	0.66	1.99 [2.01]	322	4.74
07/11/2021 (peak 13:55)	5.46	0.55	1.60 [1.70]	304	4.53
31/01/2022 (peak at 12:35)	5.63	1.29	3.27 [3.35]	314	6.51
21/02/2022 (peak at 3:35)	5.48	0.90	2.16 [2.63]	297	4.87

Surge: difference between the highest measured water level and the astronomical tide.

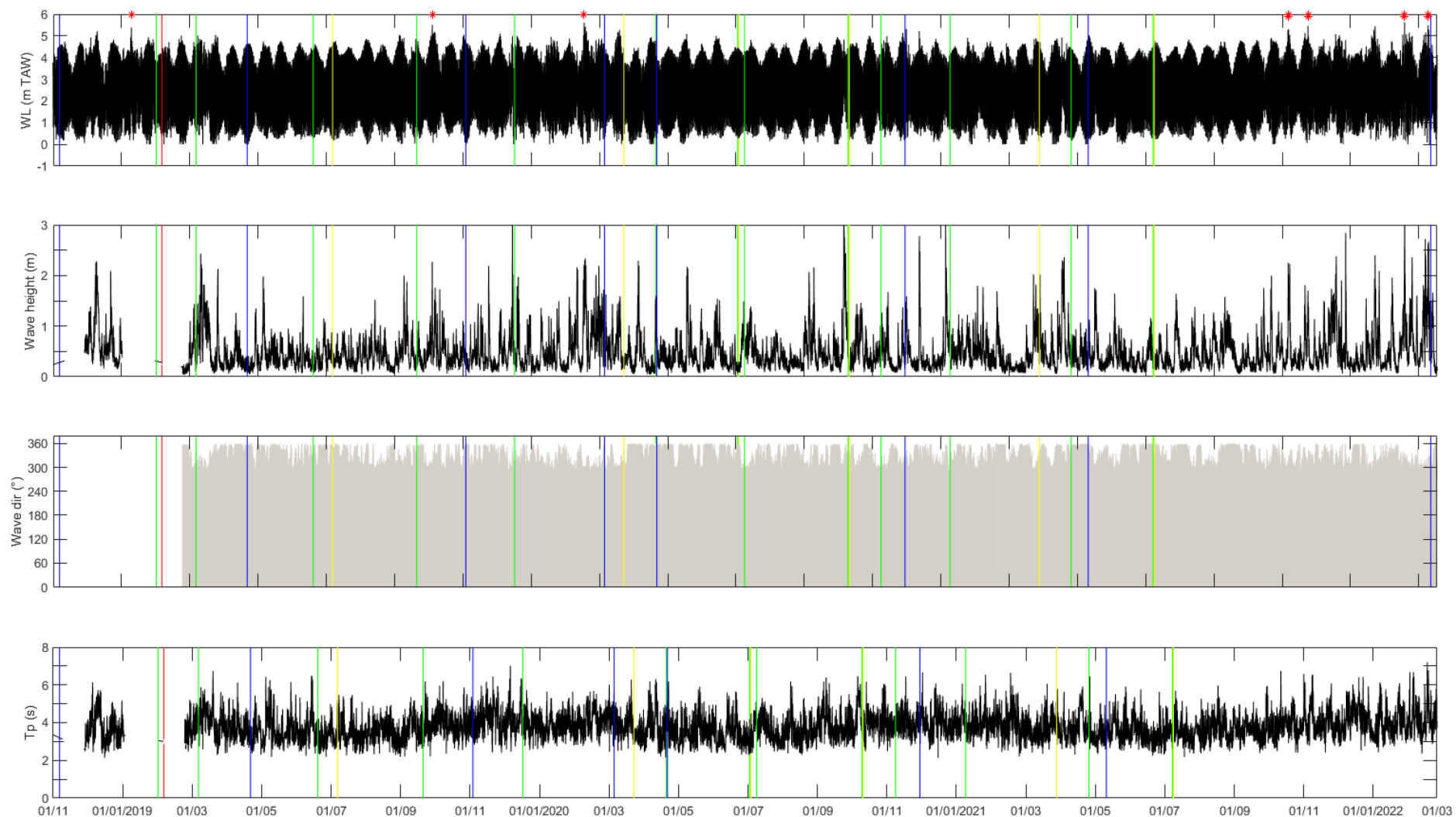


Figure 11 – Time series of water level at Scheur, significant wave height, wave direction and wave period from the Zwin buoy. Blue vertical lines correspond to the LiDAR surveys, green lines to the Qboat surveys, yellow lines to the RTK-GPS profile surveys and red line to the opening of the dyke. Red stars indicate the storm events

Forcing conditions were analysed to get insights about the hydrodynamics driving the morphodynamics of the Zwin inlet before and after the opening of the dyke. Figure 12 presents wave height and direction statistics for the period from 02/2019 to 03/2022. Generally, the waves are coming from the sector 290-340° (WNW-NNW) and the significant wave height is around 0.50 m. The dominant wave direction is 330-320° (NW) which is aligned with the entrance of the Zwin channel. Under energetic conditions, high waves are thus likely to enter in the inlet and then to influence the local morphology. Annual wave regimes from 2019 to 03/2022 were relatively similar (not presented here). The highest wave height was 3.41 m recorded on 25/09/2020 at 19:30. However for 92 % of the time wave height was below 1m.

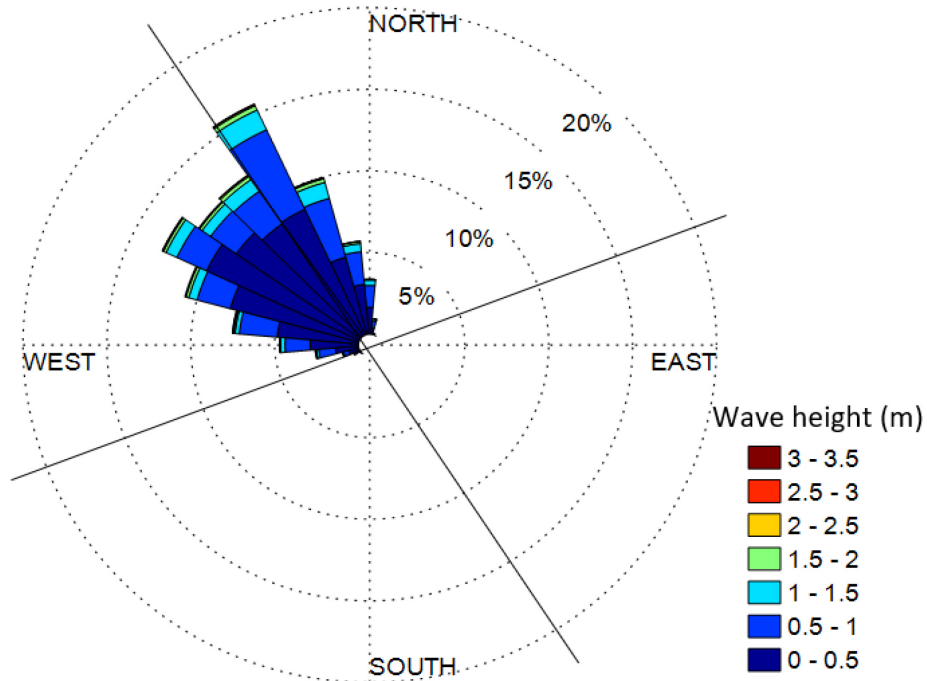


Figure 12 – Wave distribution from the Zwin buoy for the period from 02/2019 to 03/2022. The coastline and the Zwin entrance channel are oriented WSW-ENE (70-250°) and NW-SE (145°-325°) respectively.

5 Ad-hoc hydrodynamics measurements

5.1 Background

Three in-situ ad-hoc measurements were carried out by FHR in different cross-sections of the channel on 04-05/07/2019 (Ad-hoc 1), 5-16/12/2019 (Ad-hoc 2), 29/9-1/10/2020 (Ad-hoc 3). The objectives were to determine the hydrodynamics during spring and calm condition and also to estimate the characteristics of the water discharge across the channel. Meteo- and marine conditions recorded from the continuous offshore stations at Scheur and Zwin are shown in Table 9. Appendix A displays the location of the sensors and the time series of meteo- and marine conditions during the campaigns. Ad-hoc 1 and Ad-hoc 3 were carried out in a cross-section in the entrance inlet; Ad-hoc 2 was carried out at the border of the entrance inlet and the inlet inlet. Ad-hoc 1 and Ad-hoc 3 were characterized by fair weather conditions when the average of wave height was below 0.5 m coming from SW-WNW. While energetic conditions occurred during Ad-hoc 2 when maximum wave height reached nearly 1 m high. Measurements are presented in details in Montreuil et al. (2021a), Montreuil et al. (2021b) and Montreuil et al. (2022).

Table 9 – Summary of meteo-marine conditions recorded from the stations during the ad-hoc measurements.

Parameter	Ad-hoc 1 04-05/07/2019	Ad-hoc 2 5-16/12/2019	Ad-hoc 3 29/9-1/10/2020
Location	Entrance inlet	Border between inland inlet and entrance inlet	Entrance inlet
Duration	22h (2 flood/ebb phases, spring tide)	10 days 17h (21 flood/ebb phases, neap-spring tide)	1 day 19h (4 flood/ebb phases, beginning of the spring tide)
Wind speed Scheur 7 km from the study site measuring at 10 m high	Avg: 3.61 m/s Max: 6.50 m/s	Avg: 10.64 m/s Max: 19.6 m/s	Avg: 5.6 m/s Max: 8.9 m/s
Wind direction Scheur 7 km from the study site	Avg: 193° Max: 360°	Avg: 229° Max: 355°	Avg: 180° Max: 254°
Water level Scheur 7 km from the study site Depth of - 9.7 m TAW	High tide 1: 4.53 m on 4/7 at 13:35 High tide 2: 4.73m on 5/7 at 1:50	Highest high tide: 13/12 12:55 [5 m TAW]	High tide 1: 29/9 13:10 [4.30 m TAW] High tide 2: 30/9 1:30 [4.43 m TAW] High tide 3: 30/9 13:50 [4.29 m TAW] High tide 4: 1/10 2:00 [4.44 m TAW]
Wave Zwin 2 km from the study site Depth of -8 m TAW	Avg: 0.33 m Max: 0.54 m	Avg H: 0.75 m Max H: 3.06 m	Avg Hs: 0.25 m Max H: 0.44 m

During the campaigns, three Aquadopp profilers were used to measure the current velocity and direction in multiple layers through the water column. They measured flow velocities in three directions: eastward, northward and vertical. Wave height, period and direction were measured in the center of the channel. A cross-channel topographic profile was carried out during the campaign using a Real-time kinematic (RTK-GPS) system. Also, sub-layers sediment samples were collected near the three Aquadops. Grain size distributions were determined in the laboratory.

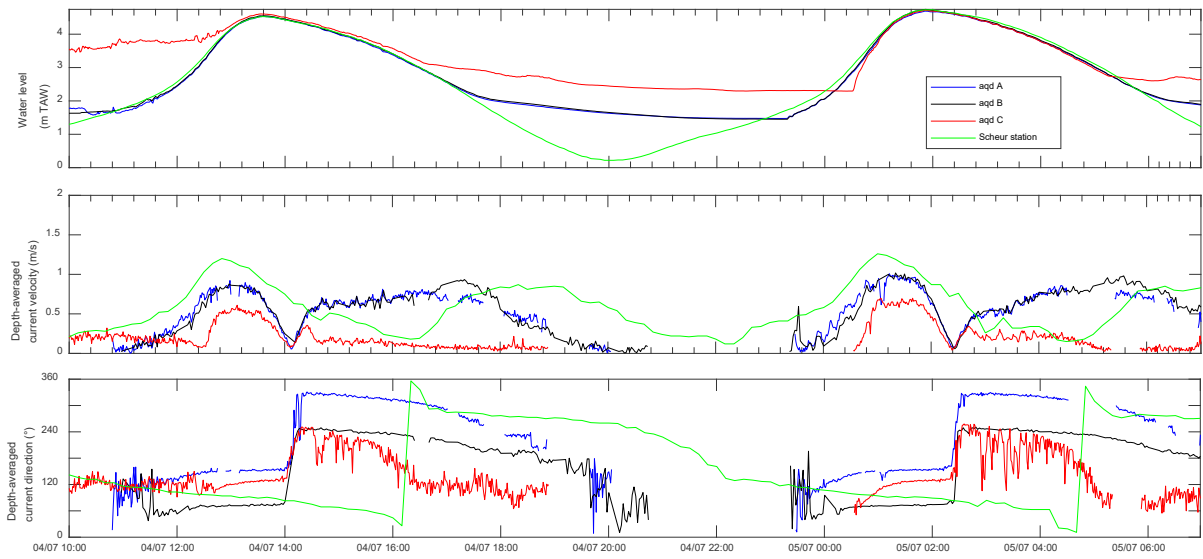
5.2 Results

5.2.1 Hydrodynamics and sediment characteristics

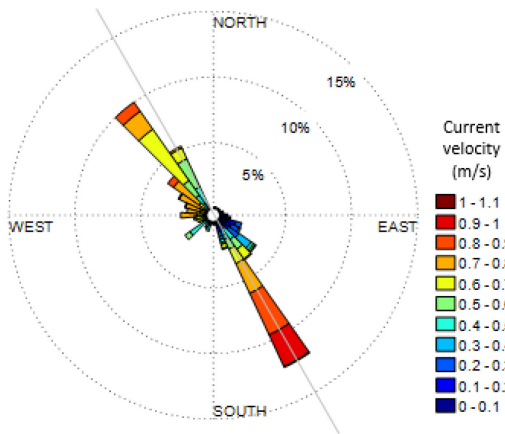
Figure 13 shows time series of water level, depth-averaged of current velocity and direction the current velocity regimes recorded during the campaigns. In the entrance inlet, the flow velocity pattern across the channel is clearly related to the tide, and is characterised by an asymmetry. A current velocity peak occurs 30 minutes before high tide, followed by a sudden drop around 30 minutes after high tide. Then the current velocity re-increases during most of the ebb phase to gradually decrease at the end of it. The flood phase is dominated by a current directed to 135-140°. This is followed by a sharp reverse of direction to 330-350° when the velocity drastically drops starting around 30 minutes after high tide. This current direction dominates during the ebb phase. The ebb phase last about two times the duration of the flood phase. The center of the channel is ebb-dominated, with flow direction centred around 340° (NNW). To a lower degree, an ebb dominated regime also characterizes the east side of the channel. In contrast, the current regime measured at the west bank of the channel is characterized by a dominance of SSE currents centred around 140°-160° with lower velocity than the center of the channel. This indicates that the current inflow is faster than the outflow, reflecting a flood-dominance there. In general, there is an offset between the flow and channel direction of 20°. The deviation in flood direction can be understood as the channel is much wider during high water, while local topography might explain the deviation during lowering tide. Although it is a rough estimation, the flow is thus aligned with the channel orientation.

Regarding the inland inlet, hydrodynamics in the centre (Aqd B) and east (Aqd C) of the channel are relatively similar with a slight dominance of NW (ebb) currents (310°) characterized by an average of 0.4-0.5 m/s and maximum speed up to 1.4 m/s. This indicates that the current outflow is faster than the inflow. Thus, a similar ebb-dominance to the one in the entrance of the inlet is observed. The inflow is the strongest and directed SE (150°) at the west side of the channel. This flood-dominated process occurs probably caused by the presence of the sand bank and the steep west bank. These features might diffract currents (i.e. secondary diffracting effect). The morphological shape of the sand bank morphology and its orientation of 175° (ebb-dominated) reflects this process as well. In addition, a comparison of hydrodynamics state for 6 hours indicates that the current velocity in the inland inlet ranges from 0.06 to 0.91 m/s under calm condition while it could be up to two times higher under energetic condition. In general, the strongest current velocity occurred 2 hours before high tide while it is the lowest at high tide under both conditions. After high tide, the currents velocity progressively increases. Also, results suggest that the tidal reverse under energetic conditions occur around 20 min after high tide, while it takes more time, around 30 min, under calm conditions.

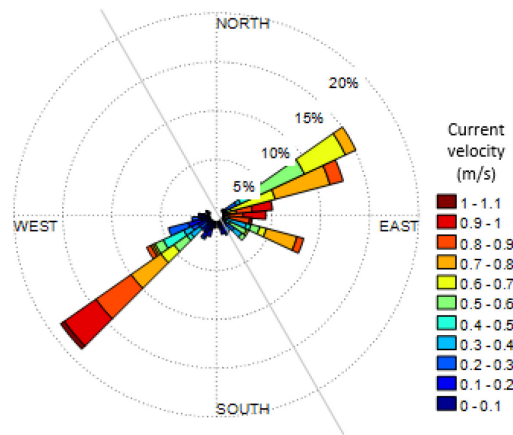
Ad-hoc 1



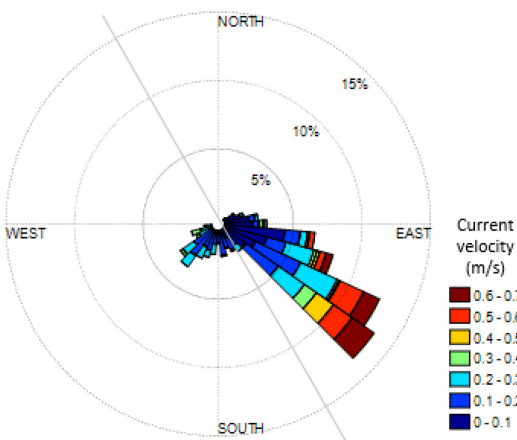
A) Aqd A



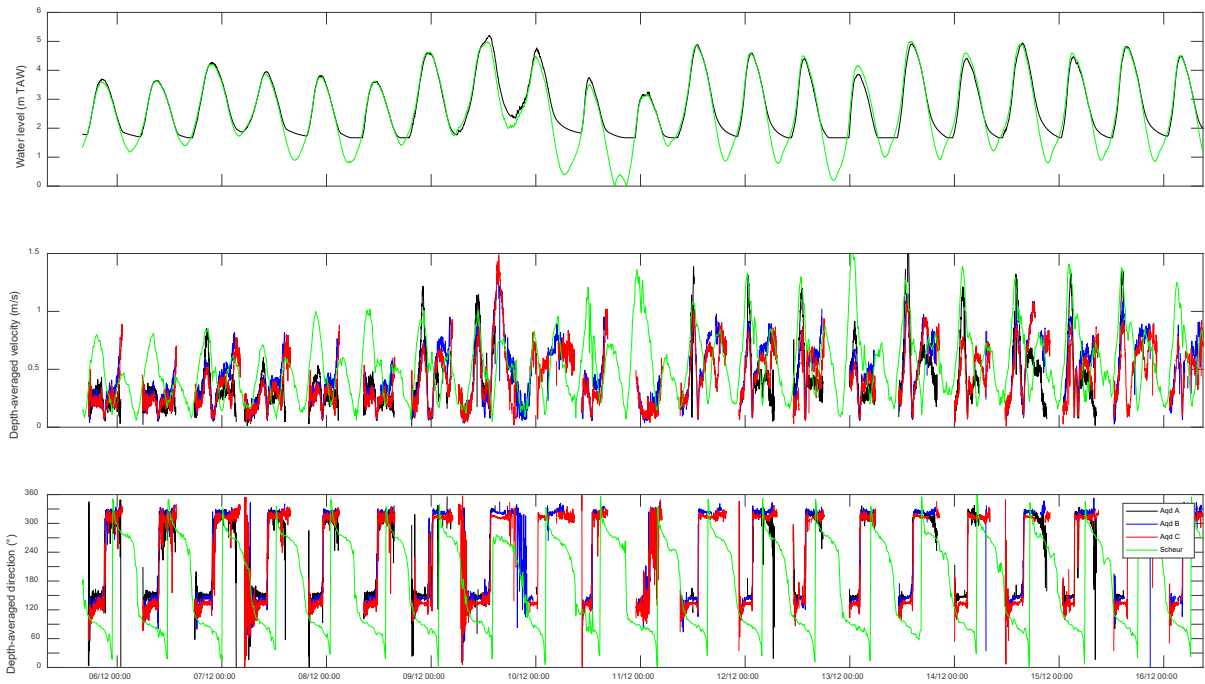
B) Aqd B



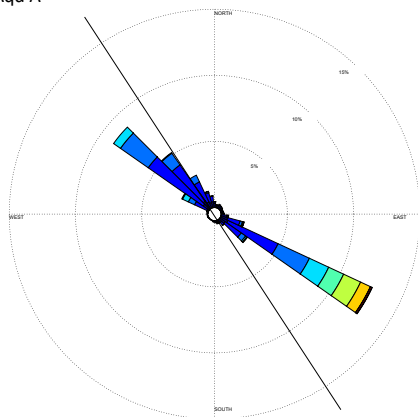
C) Aqd C



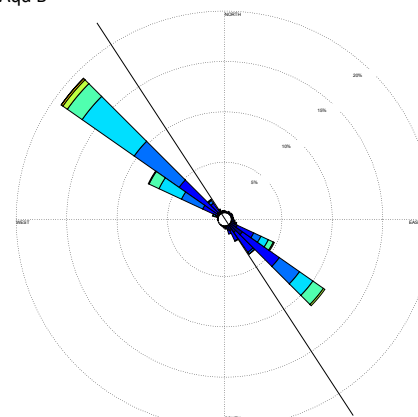
Ad-hoc 2



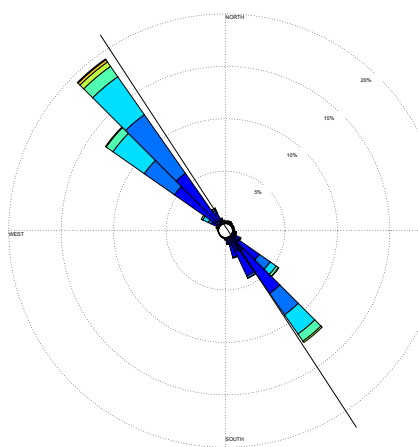
Aqd A



Aqd B



Aqd C



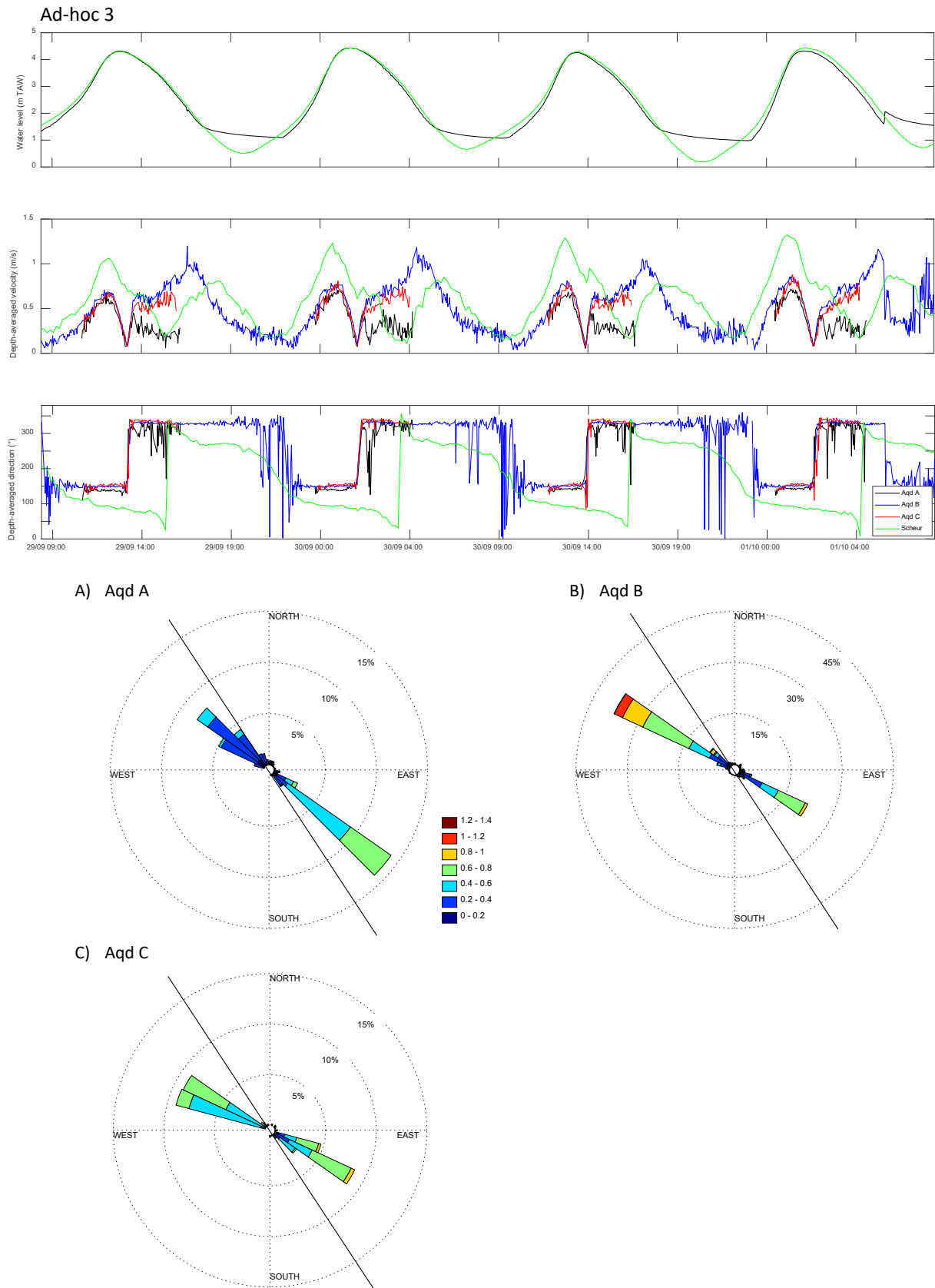
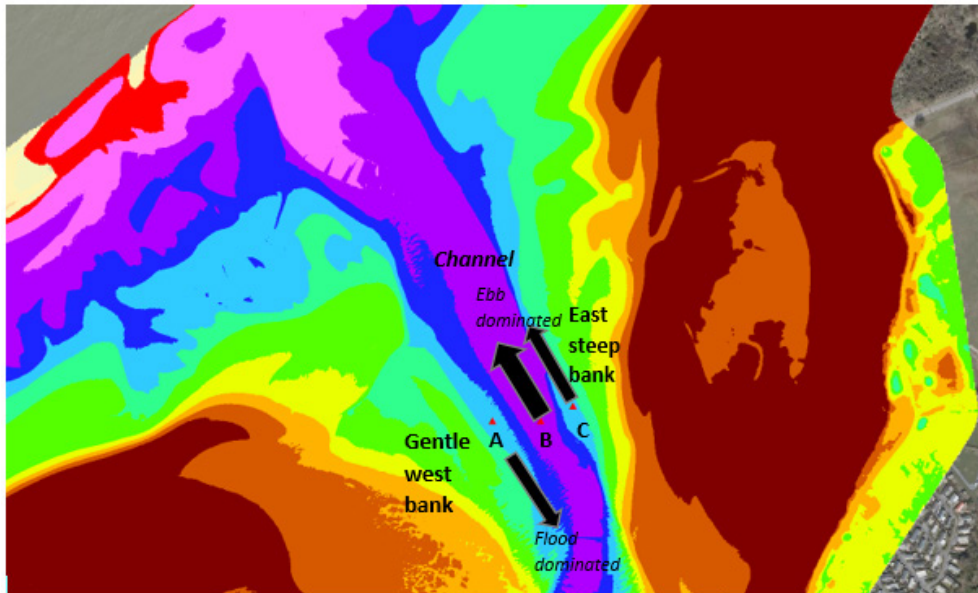


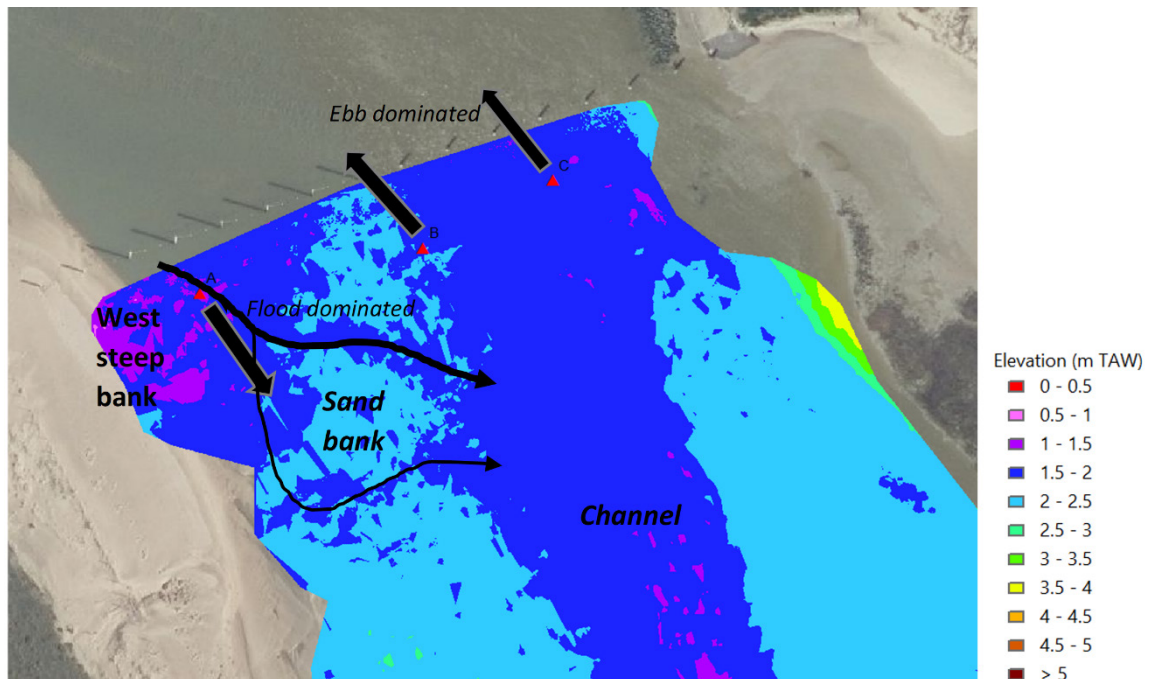
Figure 13 – Time series of water level, depth-averaged current and direction for the Aquadopps and Scheur station, Roses of current velocity (m/s) from the 3 Aquadopps indicating the current direction going to. Black line corresponds to the main channel orientation (145°-325°) for the ad-hoc campaigns.

A sketch of the hydrodynamic processes related to the topography in the entrance and inland inlet is displayed in Figure 14. There is an important inter-relationship between hydro- and topographic processes. The general morphological evolution (DoDs) shows also an important role of external processes (supply of sand over the beach both from the west at the west bank of the entrance channel and from the north at the east bank).

A) Entrance inlet



B) Inland inlet



Note: Inland inlet is located south of the entrance inlet, just at its southward border.

Figure 14 – Sketches of processes in the entrance and inland inlet based on the ad-hoc campaigns.

The particle size at the 3 Aquadopp locations is presented in Table 10. The sediments consist of coarse sand with a D_{50} of 586 μm (Ad-hoc 1) and 433 μm (Ad-hoc 3) in the center of the channel and typically around 600 μm for the banks of the channel (Aqd A and Aqd C). These are nearly two times larger than the sediment in the protected reserve of the inland inlet. These coarser sediments are probably transported by local advection processes from waves or/and currents. We can hypothesize that they come from coastal nourishments which is supported by large quantity of shell fragments in the samples.

Table 10 – Statistic summary of the grain size for the three sediment samples collected near the Aquadopps during the ad-hoc measurements.

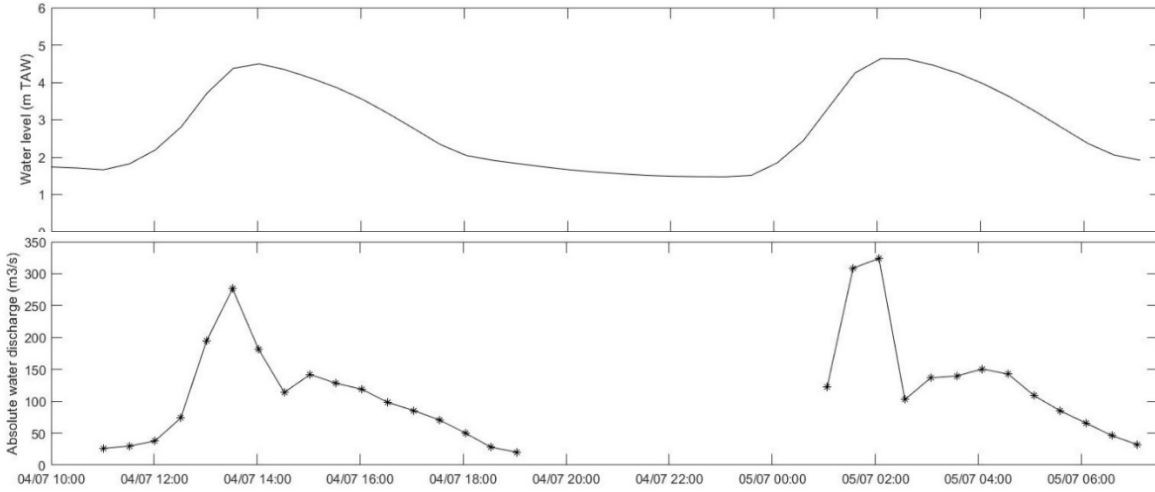
	Grain size (D_{50} μm)		
	Ad-hoc 1 04-05/07/2019	Ad-hoc 2 5-16/12/2019	Ad-hoc 3 29/9-1/10/2020
Aqd A	586	335	619
Aqd B	619	369	433
Aqd C	639	367	690

5.2.2 Water discharge

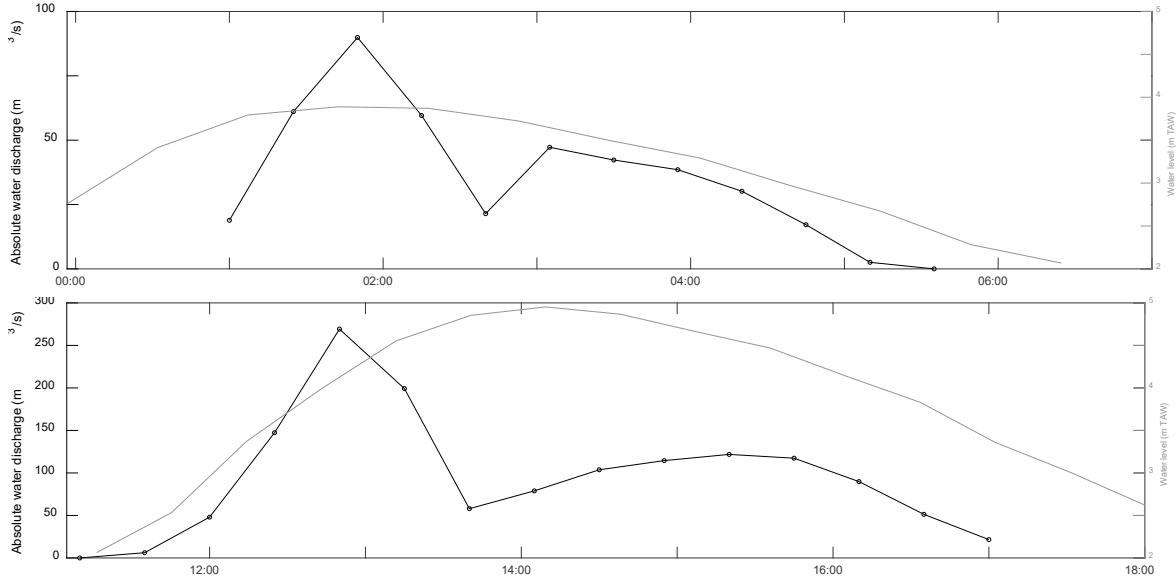
Water discharge was estimated across the channel (Figure 15). Appendix B reports the methodology and a statistical summary of the records.

The peak of estimated water discharge ranges from 325 to 400 m^3/s just before high tide in the entrance inlet (during flood). In 10/2020 (AD-Hoc 3), The average total volume of water that flowed in with the flood and ebb currents is of 1 888 000 m^3 and 1 500 000 m^3 respectively. It can be expected that the ebb draining continues for some time after the last measurement in each tidal cycle, which should result in a balance between flood and ebb discharge. As expected, the discharge peak occurred during the flood phase when sediments were likely to be flushed inside the Zwin. The peak flood discharge before high tide was ca. two times greater than the peak discharge during ebb. The peak value of water discharge (394 m^3/s) in the entrance inlet is greater than the maximum of 196 m^3/s measured in the inland inlet. Ad-hoc 3 campaign measurements indicates water discharge was ca. 30 % greater than in July 2019 (Ad-hoc 1) under similar hydrodynamic conditions. This is probably related to the changes in morphology of the inlet.

Ad-hoc 1



Ad-hoc 2



Ad-hoc 3

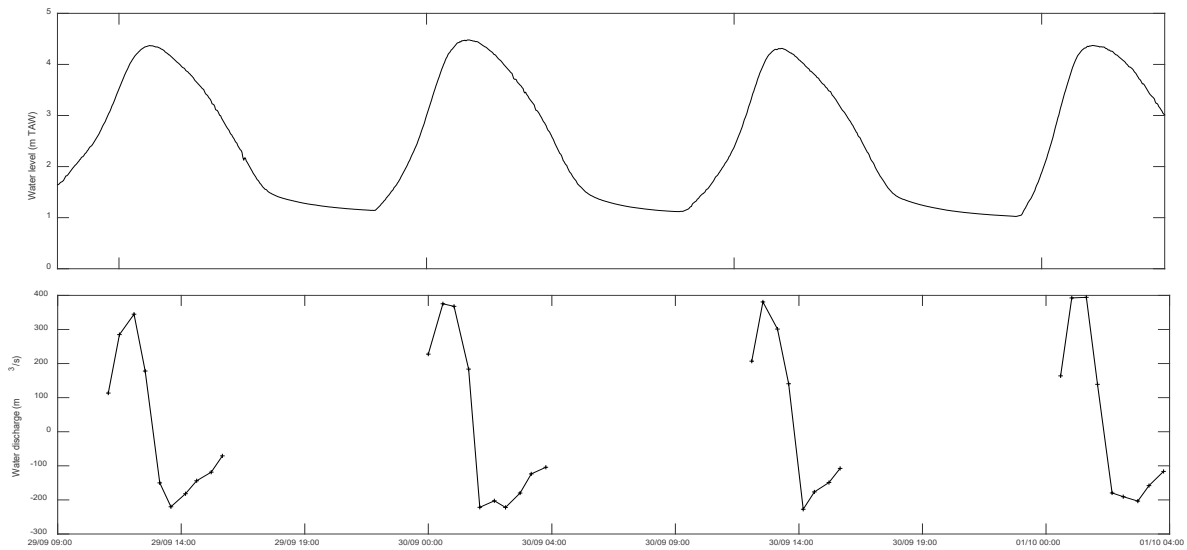


Figure 15 – Time series of 30 minutes averaged water level and estimated water discharge across the channel.

At the border of the entrance inlet and the inland inlet, the total volume of water that flowed in the Zwin was estimated to 429 m³/s (maximum discharge of 89.9 m³/s) under calm condition and to 1373 m³/s (maximum discharge of 269.2 m³/s) under energetic condition. Thus as expected, the water discharge under energetic condition was much greater up to three times than under calm condition. Similar pattern of water discharge is observed under calm and energetic condition with a peak occurring 1 – 1.5 hours before high tide and one hour after the maximum current velocity records. After the flood peak, a drop takes place at high tide, and then the water discharge re-increases slightly to progressively decrease under the ebb phase. Additionally, flood discharge peaks (on average 200 m³/s) at this location are two times lower of those of measured in the entrance inlet (ca. 400 m³/s). The flood stage lasts longer at this location compared to the location in the entrance inlet.

5.2.3 Inland inlet before and after the opening of the dyke

Aqua Vision carried out a survey in the inland inlet with a controlled Q-boat 1800RP system before the opening on 23/10/2018 and 1.8 years after on 29-30/09/2020 (Aqua Vision, 2019, 2020). Bathymetry and flow rates were measured, stored simultaneously and then processed with ViSea Data Acquisition and survey toolbox software. The results allowed to determine the water discharge. The water discharge from the Qboat survey was determined at a specific location from the bathymetry and water velocity data through the water column. The velocity is measured in the middle of the profile while the top and bottom are extrapolated. The average duration of the measurements at each specific location ranged from 1 to 3 minutes.

Time series of water level and water discharge are presented in Figure 16.

Before the opening of the dyke, the maximum of flood discharge was of 100 m³/s. The total volume of water that flowed in with the flood was calculated at 464,731 m³. The ebb flow started 15 min after high tide. The water flows out of the area at a rate of 25 m³/s. The ebb phase lasts longer than the flood phase resulting in a tidal asymmetry as previous observed. It causes the flow velocities during flood phase to be greater than during ebb phase. Such a regime usually results in sedimentation of the inlet system. Sedimentation occurs there where the flow is less concentrated and decreases rapidly over a short distance.

The maximum flood discharge of nearly 200 m³/s was reached 1.8 year after the opening. This is two times higher than the pre-opening campaign. In general, the ebb flow discharge starts about 45 minutes after high water and rapidly rose to a maximum of about 100 m³/s. During the measurement, tidal asymmetry was also observed with a flow velocity greater during flood phase than during ebb phase.

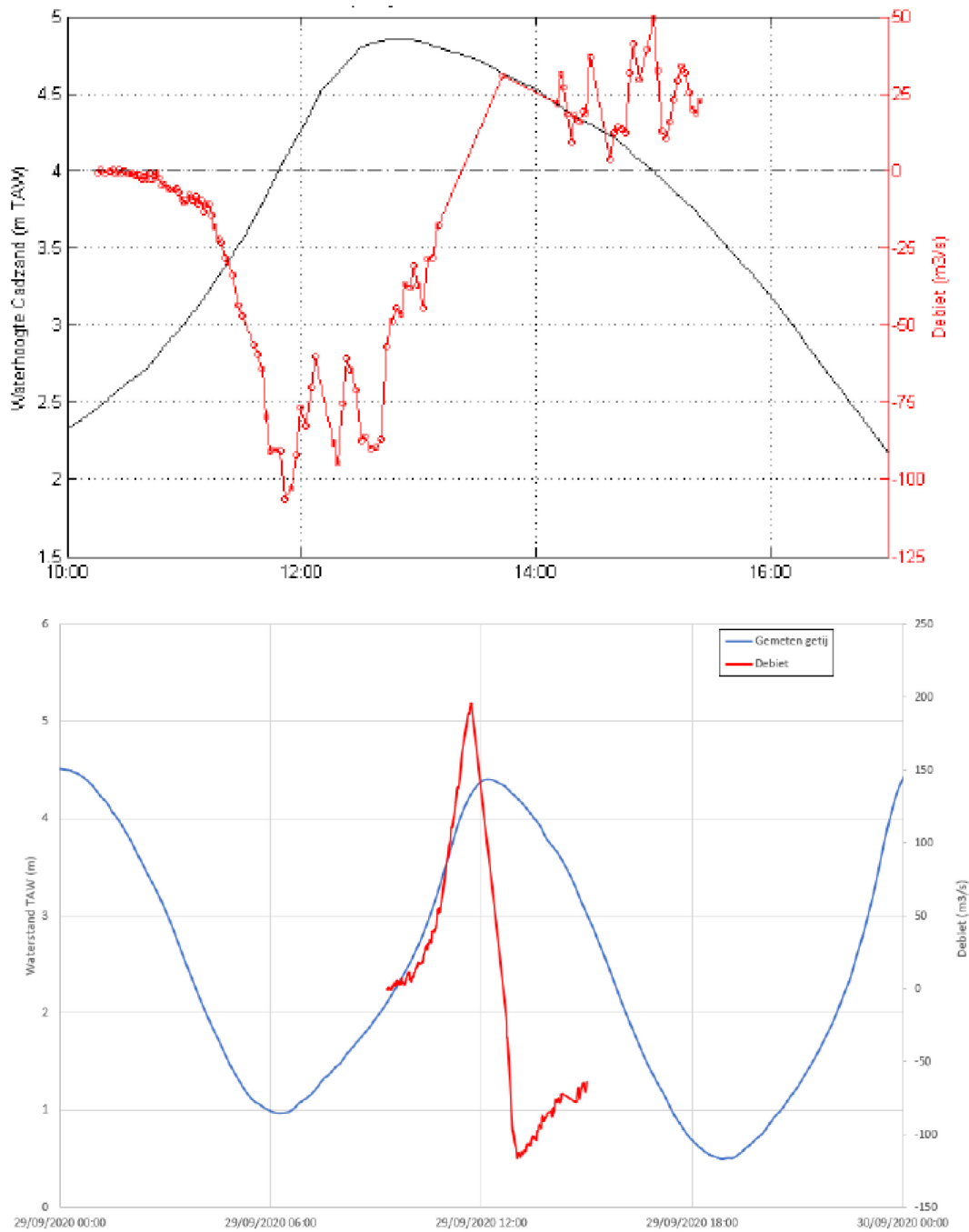


Figure 16 – Time series of water level and water discharge before (23/10/2018) and 1.8 years after the opening of the dyke (29/9/2020) (Aqua Vision, 2020). Note that the vertical discharge axis in the first subplot has reversed sign.

6 Tidal prism and stability of a tidal inlet

6.1 Context

Several authors (van de Kreeke & Haring, 1980; Stive et al., 2009; Tung et al., 2011) discuss a stability condition for lagoons and inlets first put forward in the early 20th century for the US coasts. The stability condition is also found to apply to tidal inlets, both those with a river mouth (estuary) and those without (lagoons). It puts forward that the cross-sectional area, A , of a tidal inlet channel in equilibrium is in a given fixed relationship to the volume of water (i.e. the tidal prism, P) that flows with each tidal cycle through it. It is thought that a part of the coastal longitudinal transport (the part that operates in the elevation range of the tidal channel mouth) tends to choke and fill the channel. The ebb currents that flow out of the inlet, if sufficiently strong, clear this sand and keep the channel open. A dynamic equilibrium relationship between A and P is assumed to exist at the narrowest part (throat) of the tidal channel through the action of the current strength in the channel that is controlled by P and in turns controls A . For a given area, the transport capacity in the channel due to the ebb current equals the relevant part of the coastal longitudinal transport, and the inlet channel is in dynamic equilibrium. Both the cross-sectional area and the tidal prism are usually taken at mean spring tide level. The relationship has the following shape

$$A = cP^q$$

where c and q are empirical coefficients.

The equilibrium is called dynamic because at an event time scale morphological changes can occur, but over a time scale of months an average state can be observed.

Van de Kreeke (2004) and Stive et al. (2009) argue that theoretically the A-P relationship is only valid for sets of inlets that have the same values of littoral drift (M_{tot}), grain diameter (d_{50}), grain density (ρ_s) and tidal period (T). This condition is named phenomenological similarity, meaning that sets of phenomenologically similar inlets would go with a given c and q .

Van de Kreeke (2004) reported values of c in the range of 10^{-5} and 10^{-4} and q between 0.85 and 1.05 for natural systems of inlets.

Stive et al. (2009) summarize some best-fit results for US entrances: $c = 1.08 \cdot 10^{-4}$ or $6.25 \cdot 10^{-5}$; for the Wadden Sea: c from 5.65 to $7.75 \cdot 10^{-5}$; for the Zeeland entrances: $c = 8.2 \cdot 10^{-5}$. In all cases $q = 1$.

Tung et al. (2011) report values, obtained by numerical experiments, of $c = 5 \cdot 10^{-6}$ and $q = 1.17$ for small inlets not too dissimilar from the Zwin inlet characterized by tidal amplitudes between 0.5 and 1.0 m and basin surface areas between 1500 and 3000 ha.

The regular surveys from Coastal Division cover the Zwin area. They are available as 2 m-cell rasters (Table 11). These allow to establish the relationship A-P for a sequence of moments in time. In this section, we look at the relationship and its evolution over the first two years after the expansion of the Zwin area. As a reference level more or less representing maximum spring high water in the calculation of the tidal prism and cross-sectional area, the value of +5 m TAW is taken (mean spring high water is +4.59 m TAW at Zeebrugge and +4.79 m TAW at Vlissingen).

Table 11 – Overview of Lidar surveys used for the A-P analysis.

Survey	Date of Lidar flight	Name of DEM raster
Spring 2018	17/04/2018	Strand2018_1
Autumn 2018	6/11/2018	Strand2018_2
4 February 2019: opening of dyke and expansion of intertidal area		
Spring 2019	20/04/2019	Strand2019_1
Autumn 2019	29/10/2019	Strand2019_2
After storms Ciara on 9 February and Dennis on 16 2020	28/02/2020	Strand2020_0
Spring 2020	10/04/2020	Strand2020_1
Autumn 2020	18/11/2020	Strand2020_2
Spring 2021	28/04/2021	Strand2021_1
February 2022	23/02/2022	Strand2022_0

6.2 Evolution of the tidal prism before and after the expansion

6.2.1 Method

The tidal prism of the Zwin inlet can be calculated from the Lidar DEMs. The Lidar survey flights are performed at low water. Most of the intertidal area is then emerged. However, some small areas and part of the tidal channel remain flooded and Lidar system does not penetrate water surfaces. The DEMs interpolate between the shores of the ponded areas and the water surface appears to be a flat land surface. The real bed of flooded areas is thus not shown in the DEMs. The impact this has on the tidal prism is discussed below.

The number of cells inside zones that have an elevation value defined by elevation classes can in ArcMap be determined using the Spatial Analyst Tool "Zonal Histogram". The tool output is a table of numbers of cells per zone and elevation class. From this table, the tidal prism at the time of the survey can be derived with reference to a selected water level.

6.2.2 Definition of partial areas

Firstly, the area must be determined in which the tidal prism is to be calculated. This depends on the choice of the section through the inlet channel and on the actual morphology of the intertidal basin, which changes in time. Here, a number of partial areas has been defined based on the Spring 2021 morphology. They correspond to parts of the intertidal basin that are successively flooded during rising tide. The seawater enters through the gap in the dunes in coastal sections 255 and 256 and first floods the lowest parts of area 1 (Figure 17). Areas 2, 3, 4 and 5 are subsequently flooded. The borders of the partial areas and the order of flooding have been verified and confirmed by the field manager of the area.

The flooding penetrates the successive areas through the sections shown in red. When the tidal level is high enough to flood the marsh, flooding also occurs directly from area 1 to 5, etc. This is however seldomly the case. Zone 5 is regulated by an adjustable weir situated at the red line at the border of zones 4 and 5. This keeps the water level in zone higher in the breeding season, from April to August, at +4.2 to 4.3 m TAW. In the other months, the minimum water level is +3.4 m TAW. For the calculation of the tidal prism contribution from zone 5, this means that the volume below +3.4 m is never added, and the volume below +4.2 m is not added if the survey is during the breeding season.

The outer contours of the intertidal area are the dunes and the encircling embankment. The partial areas are furthermore based on some narrow passages in the channel system (indicated in with red lines at the borders of the partial areas in Figure 17). The small zone 6 used to be part of the Zwin intertidal area, but due to changes in the morphology at the border of zones 1 and 6, it is no longer flooded by water flowing in through the tidal channel. There is a new entrance in the north, though this only functions at water levels exceeding +5 m TAW.

From Figure 17, it follows that the tidal prism for the red section at the north side of zone 1 is obtained by adding the tidal prism contributions of zones 1, 2, 3, 4 and 5. For the section at the border of zones 1 and 2 (this is the border between the entrance inlet and the inland inlet), at about the location of the pile row and the ad hoc measurement campaigns, the tidal prism is obtained by adding the contributions from zones 2, 3, 4 and 5.

For the surveys predating the opening of the International Dike on 4 February 2019, the contribution of zone 3 must be excluded as this area was then no part of the intertidal area served by the Zwin channel.

The contours of the zones are contained in the shapefile ZwinTidalPrismArea.shp. Figure 18 presents the principle of the tidal prism calculation.

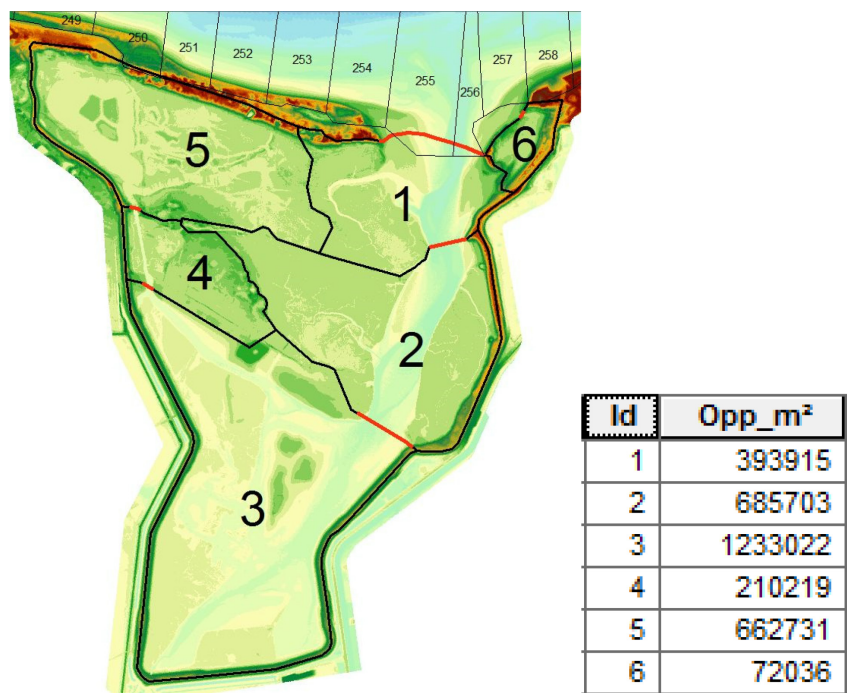
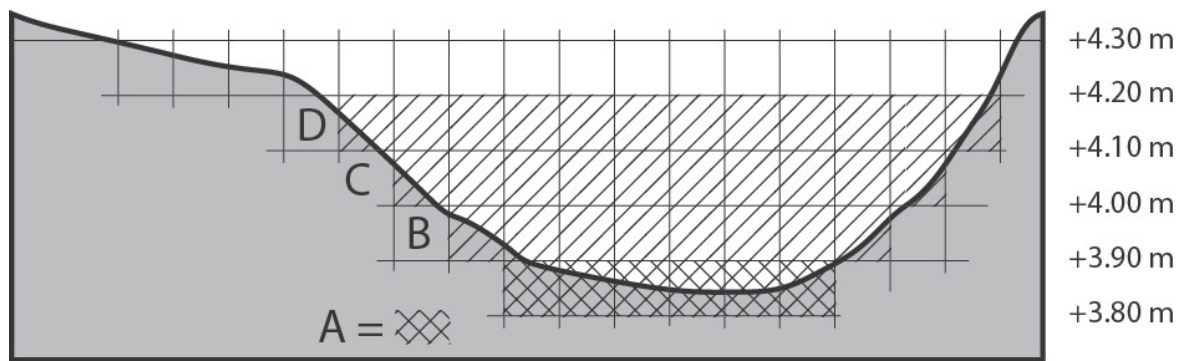


Figure 17 – Definition of partial areas that contribute to the tidal prism of the Zwin channel.

The map is tilted by 30° (Lambert 72 North is in upper right). Background is elevation map of Spring 2021 survey, coloured in 0.5 m steps. Near the borders, the encircling embankment is visible in dark green and orange (depending the elevation of its crest). The intertidal marsh is about 2.5 km long in N-S direction and about 2 km at its widest E-W section. Partial areas have black outlines and are numbered 1-6. Opp_m² is the surface area per partial area in m². The sections through which the partial areas communicate are shown in red. Polygons at the north with narrow black outline are the beach sections used for monitoring the beach morphology, with their number. Note that the border between zone 1 and zone 2 is at the border between the entrance inlet and the inland inlet.



volume in lowest bin "+3.80 to +3.90 m" = $A/2$
 number of cells in this bin x cell area x bin height / 2
 B, C, D... = number of cells for overlying bins
 tidal storage below +4.20 m (total hatched volume) =
 $A/2 +$
 $A + B/2 +$
 $A + B + C/2 +$
 $A + B + C + D/2$

Figure 18 – Principle of calculating the tidal prism in a zone, here shown on an arbitrary cross section.

The contributions of all partial areas are added so that the tidal prism for the section in the entrance of the inlet and for the section at the boundary of zones 1 and 2 is obtained, for the water levels between +3 and +6 m TAW, in 0.1 m steps. This allows to evaluate, per survey, the growth of the tidal prism with water level.

6.3 Results

The results of the tidal prism calculations are shown in Table 12, Table 13, Figure 19 and Figure 20.

Table 12 – Tidal prism for the section in the north of zone 1 as a function of water level.
The volumes are graphically depicted in Figure 19.

Elevation [m TAW]	Tidal prism below elevation [m ³]								
	17/04/2018	6/11/2018	20/04/2019	29/10/2019	28/02/2020	10/04/2020	18/11/2020	28/04/2021	23/02/2022
	2018_1	2018_2	2019_1	2019_2	2020_0	2020_1	2020_2	2021_1	2022_0
3.0	26309	28457	62503	110632	124674	144766	138372	158522	139744
3.1	35767	38301	91054	138966	156319	180735	168636	190120	166857
3.2	48228	50599	136430	180824	198845	225535	207454	228427	199016
3.3	64648	66186	192800	233008	248941	277314	254456	273965	236564
3.4	84767	85571	256621	291732	305257	335291	308835	326868	281035
3.5	107570	108155	325829	356128	367150	398737	369829	386560	333537
3.6	132168	132806	398994	426140	434038	467072	436578	452694	393730
3.7	157953	159010	475777	501078	505767	540150	509781	524460	460829
3.8	184630	190117	556676	580174	583162	618014	591728	601477	535090
3.9	212263	226487	641983	667991	669651	700780	681753	683703	618698
4.0	240937	265058	732722	766282	765837	789564	778630	771823	711574
4.1	270486	305457	831954	874123	871101	888044	884880	869027	813509
4.2	300923	347581	944031	996033	989888	1000144	1004658	979391	928532
4.3	332514	391644	1084495	1130649	1122266	1131005	1137456	1101692	1057469
4.4	366463	438517	1228809	1272250	1263063	1272347	1278399	1235245	1196273
4.5	412550	491819	1385017	1420994	1413227	1426149	1428631	1386915	1344769
4.6	480163	561539	1563361	1586671	1584396	1603092	1598793	1562940	1512120
4.7	571762	655325	1767963	1779041	1783606	1807416	1795088	1765430	1704451
4.8	687706	771872	1995099	1997395	2007731	2034785	2015807	1992271	1920538
4.9	822776	905950	2238893	2236200	2250555	2279785	2256942	2237718	2157399
5.0	969493	1051211	2493998	2489412	2505383	2536623	2511811	2495286	2408900
5.1	1123187	1203459	2757619	2752191	2768774	2802158	2775626	2761071	2669733
5.2	1282328	1360814	3028541	3022500	3039297	3074680	3046539	3033515	2937961
5.3	1445669	1522282	3304940	3298449	3315472	3351992	3322742	3310623	3212040
5.4	1612146	1687285	3584814	3577983	3595486	3632512	3602337	3590878	3490042
5.5	1781212	1855233	3867494	3860374	3878320	3915752	3884752	3873871	3771243
5.6	1952354	2025558	4152543	4145185	4163379	4201183	4169503	4159093	4055108
5.7	2125211	2197836	4439456	4431902	4450258	4488378	4456089	4446043	4341050
5.8	2299556	2371709	4727886	4720189	4738704	4777099	4744247	4734513	4628660
5.9	2475154	2546898	5017549	5009760	5028442	5067062	5033721	5024253	4917691
6.0	2651735	2723131	5308166	5300292	5319156	5357950	5324195	5314954	

Table 13 – Tidal prism for the section at the boundary of zones 1 and 2 as a function of water level. Results at water level +5 m in bold as this is used in the analysis below. The volumes are graphically depicted in Figure 20.

Elevation [m TAW]	Tidal prism below elevation [m ³]								23/02/ 2022
	17/04/ 2018	6/11/ 2018	20/04/ 2019	29/10/ 2019	28/02/ 2020	10/04/ 2020	18/11/ 2020	28/04/ 2021	
	2018_1	2018_2	2019_1	2019_2	2020_0	2020_1	2020_2	2021_1	2022_0
3.0	6124	7311	26761	58687	78516	93545	83905	98239	88546
3.1	9911	11603	50084	81438	105228	124327	108416	123762	110218
3.2	16106	17771	89778	117504	142595	163692	141166	155727	136691
3.3	25704	26577	139956	163659	187297	209770	181759	194631	168280
3.4	38492	38513	197045	216066	237942	261772	229395	240564	206489
3.5	53487	53135	259019	273811	293845	318929	283328	292922	252416
3.6	69760	69418	324554	336773	354425	380607	342673	351297	305702
3.7	86617	86857	393232	404198	419442	446560	408091	414837	365485
3.8	103771	108564	465270	475272	489524	516583	481702	483052	431970
3.9	121153	134751	540827	554325	567962	590660	562740	555813	507367
4.0	138755	162396	620951	642833	655223	669902	649940	633809	591551
4.1	156586	191185	708711	739893	750635	757974	745779	720250	684232
4.2	174750	221123	808524	850156	858732	858870	854490	819250	789365
4.3	193547	252494	935956	972341	979656	977803	975580	929534	907585
4.4	214092	286172	1066444	1100720	1108218	1106379	1104104	1050231	1034679
4.5	245035	325203	1206994	1235074	1244451	1245225	1240736	1187208	1169999
4.6	294358	377588	1366095	1383362	1398052	1403138	1394075	1344981	1320870
4.7	364082	450002	1547483	1553942	1575301	1584304	1569181	1525211	1492606
4.8	454434	541629	1747577	1746851	1773205	1784817	1765105	1726172	1684591
4.9	560231	647106	1960905	1956750	1986003	1999441	1977513	1941786	1893573
5.0	674841	760687	2183256	2177751	2208249	2223353	2200158	2166464	2113880
5.1	794722	879392	2412705	2406336	2437455	2454476	2429981	2398008	2341591
5.2	919023	1002111	2648565	2641534	2672893	2691834	2666033	2635508	2575662
5.3	1046923	1128262	2889358	2881922	2913541	2933601	2906865	2877224	2814940
5.4	1177609	1257502	3133305	3125632	3157763	3178340	3150802	3121812	3057708
5.5	1310681	1389432	3379859	3372019	3404635	3425638	3397363	3368957	3303396
5.6	1445679	1523580	3628630	3620679	3653603	3674988	3646118	3618193	3551562
5.7	1582270	1659557	3879151	3871114	3904272	3925963	3896590	3869044	3801656
5.8	1720234	1797020	4131106	4123016	4156405	4178343	4148525	4121309	4053290
5.9	1859340	1935702	4384214	4376114	4409740	4431865	4401676	4374750	4306226
6.0	1999335	2075346	4638208	4630095	4663965	4686227	4655739	4629064	4560185

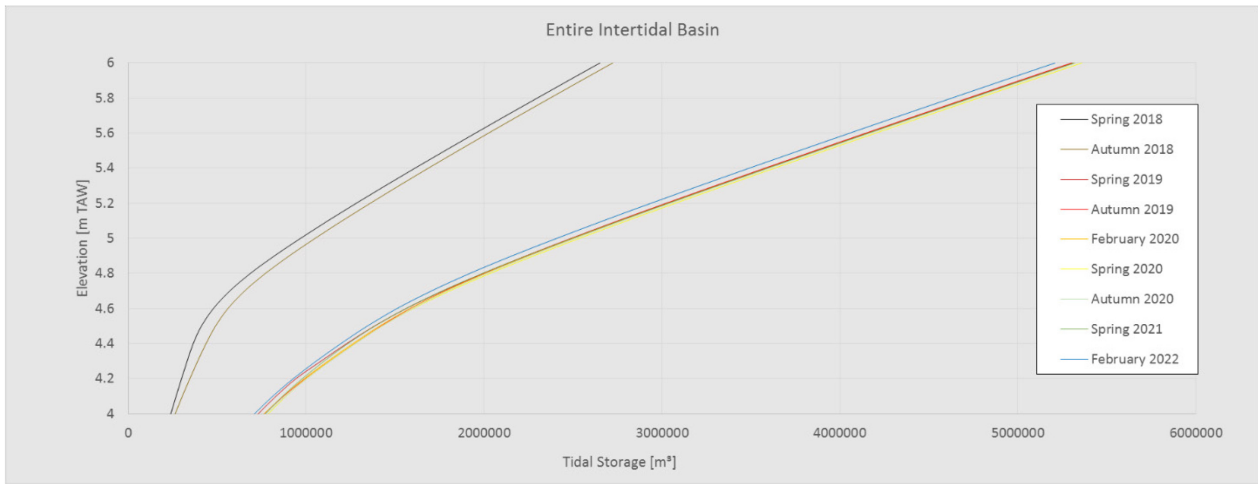


Figure 19 – Evolution of the tidal prism at the entrance of the Zwin channel (at north border of zone 1) as a function of water level, and through time.

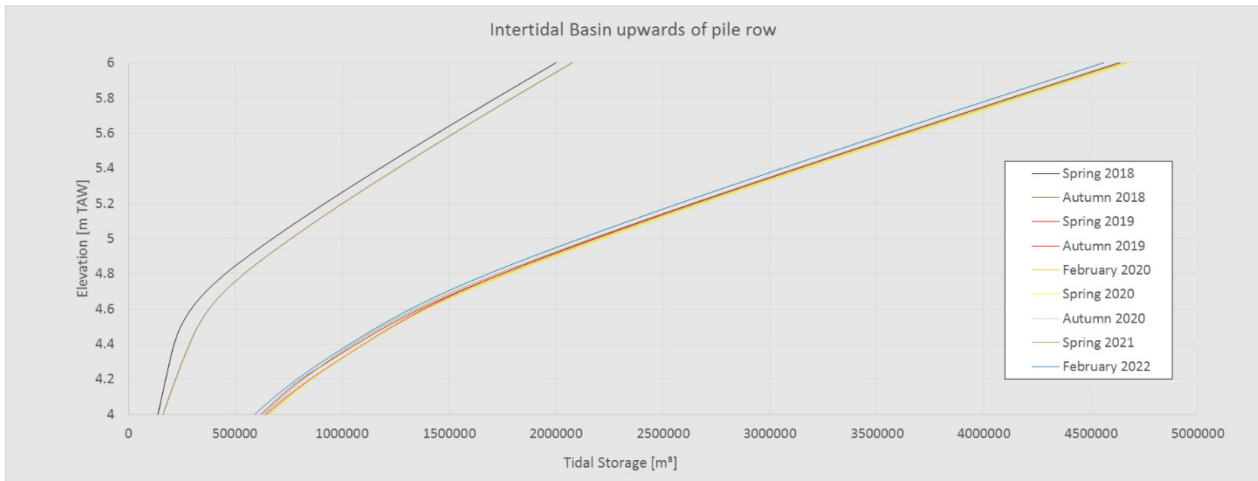


Figure 20 – Evolution of the tidal prism at the pile row in the Zwin channel (at boundary of zones 1 and 2) as a function of water level, and through time.

For both considered sections, the tidal prism rises slowly with elevation until about the level +4.7 m TAW, above which the flooding of the tidal flats and marshes allows a fast increase in tidal prism. From about the level +5.2 m TAW, the contribution of higher elevation classes remains equal, i.e. there is no extra area to flood and the contribution is equal to the rise of water level.

It can be seen that the tidal prism at water level +5 m TAW multiplied by about 2.5 when the intertidal area was expanded on 4 February 2019. The proportional increase of the lower elevation classes was even bigger.

The tidal prism didn't change much in the first three years after the expansion. The maximum tidal prism was found at the Spring 2020 survey, though the deviation from the other post-expansion surveys is less than 1 %.

6.3.1 Discussion

The error on the determination of the tidal prism contains three contributions.

The first is the absolute error on elevation in Lidar surveys. Averaged over sufficiently large areas, this is estimated to be at most 5 cm. The most recent quality reports on the Lidar surveys report an error of 3 cm. A realistic estimation of this contribution is then $3 \text{ cm} \times 2.8 \times 10^6 \text{ m}^2$ (area of zones 2, 3, 4, 5) $\cong 84,000 \text{ m}^3$ or about 4% of the tidal prism for the section at the boundary of zones 1 and 2 at water level +5 m TAW.

The second contribution is uncertainty of the elevation measurement in vegetated areas. It was noted the ground surface elevations in vegetated areas of the tidal marsh may differ up to 5 cm between spring and autumn surveys (vegetation is better developed in the autumn). On the other hand, only about 1/3 of the area of zones 2, 3, 4 and 5 is vegetated. This results in an error contribution of $5 \text{ cm} \times 2.8 \times 10^6 \text{ m}^2 \times 1/3 = 45,000 \text{ m}^3$ or about 2% of the tidal prism for the section at the boundary of zones 1 and 2 at water level +5 m TAW.

The third contribution is the volume ponded at each survey. Table 14 shows the altitudes of the lowest point present in each Lidar survey at three locations.

Table 14 – Altitudes in m TAW of lowest land surface point at some locations of the main tidal channel.

Survey	At border 1-2	In centre of zone 2	In centre of zone 3
Spring 2017	2.7	10.73 (dike)	2.5
Autumn 2017	2.75	10.66 (dike)	2.62
Spring 2018	2.55	10.55 (dike)	2.6
Autumn 2018	2.55	2.7	2.55
Spring 2019	2.55	2.85	3.06
Autumn 2019	1.95	2.56	2.81
February 2020	1.85	2.4	2.65
Spring 2020	1.6	2.33	2.61
Autumn 2020	1.65	2.44	2.71
Spring 2021	1.55	2.33	2.59
February 2022	1.71	2.15	2.69

Comparison of Lidar and Qboat surveys performed at nearly the same time allows to estimate that the average depth of the water left in the bed of the main channel is at most 0.5 m for the Autumn 2018 survey and less than 0.25 m for Spring 2019 and Spring 2021 (Figure 21). The ponded depth likely decreases more upstream, but can be deeper as a relic of the Zwin expansion works in zone 3, the newly expanded intertidal area. Therefore, an estimated value of 0.25 m can be assumed to apply over the entire length of the tidal channel. An estimation of the maximum ponded length of the intertidal channel is 1500 m and of the width 100 m. This yields a ponded volume of $0.25 \times 1500 \times 100 = 37\,500 \text{ m}^3$. This volume that is missed out in the calculation of the tidal prism is thus of the same order of magnitude as contribution 2 above. However, most of this ponded volume probably never participates in the tidal prism, as this would require that it is allowed to completely evacuate at the lowest point of the water level in the tidal cycle. The various thresholds (sand banks) present in the tidal channel probably prevent this to happen. Therefore, the third contribution to the error on tidal prism is thought to be almost zero.

If we assume the possible error on tidal prism to be on the order of 155 000 m³ (contribution 1 + 2), than all curves since Spring 2019 in Figure 19 and Figure 20 are within the variation band and it must be concluded that during the first two years after the expansion of the tidal area, there is no change in tidal prism. However, the change shows some logic, as is explained below in section 6.4. Therefore, the error on tidal prism may here be overestimated.

6.4 Evolution of the Cross-Sectional Area A of the Tidal Channel

6.4.1 Data and method

As the narrowest section in the tidal channel, the section at the boundary of zone 1 and 2 is chosen (Figure 17). An alternative could have been the section at the entrance (north side) of zone 1. The section at the boundary of zones 1 and 2 was preferred, as there discharge and flow measurements are available from the ad hoc measurement campaigns.

The cross-sectional area was calculated from the Lidar DEMs of Table 11. The impact of the fact that the surveys contain water ponded in the channel was evaluated using profiles derived at the same location from DEMs with 1 m-cells made from the Qboat surveys near the Autumn 2018 Lidar survey (Qboat: 23 and 24 October 2018), the Spring 2019 Lidar survey (Qboat: 6 and 7 March 2019) and the Spring 2021 Lidar survey (Qboat: 13 April 2021).

The cross profile was determined using ArcMap's tool "Interpolate Shape" which interpolates elevation points at a specified sampling distance (here 2 m was used) along the profile line. This is exported using the tool "Feature ClassZ to ASCII" and imported in the Excel file ZwinZonalVolumes.xlsx, tab sheet "ProfilesBoundary1_2". The calculation of the cross-sectional area below the water level +5 m TAW is the summation of all profile points lower than +5 m, subtracted from +5, times the points' separation (2 m). The cross-sectional area of the profiles derived from the Qboat surveys was determined from the artificial bottom level (because of the ponded water) of the Lidar-survey derived profiles. It represents the part of the complete cross-section below the water surface missed out in the profiles from the Lidar Surveys. This was used to correct the cross-sectional areas derived from the Lidar DEMs. The Qboat cross section was added to it. For the surveys where no Qboat DEM was available, a reasonable estimation of the area below the water surface was used.

6.4.2 Results

The cross-sectional areas are listed in Table 15.

Table 15 – Cross-sectional areas for the profile across the tidal channel at the boundary of zone 1 and 2, with respect to water level +5 m TAW.

Survey date	Lidar DEM	Cross-sectional area [m ²] below +5 m TAW	Qboat, below level [m TAW]:	Qboat area [m ²]	Cross-sectional area from Lidar survey corrected with Qboat area
17 April 2018	2018_1	226.8	(est.)	40	266.8
6 November 2018	2018_2	224.9	2.56	40.0	264.9
20 April 2019	2019_1	326.3	2.34	9.2	335.6
29 October 2019	2019_2	405.1	(est.)	15	420.1
28 February 2020	2020_0	425.5	(est.)	15	440.5

10 April 2020	2020_1	440.4	(est.)	15	455.4
18 November 2020	2020_2	435.6	(est.)	15	450.6
28 April 2021	2021_1	421.4	1.6	19.1	440.5
23 February 2022	2022_0	426.2	(est.)	15	441.2

Figure 21 displays the profiles graphically.

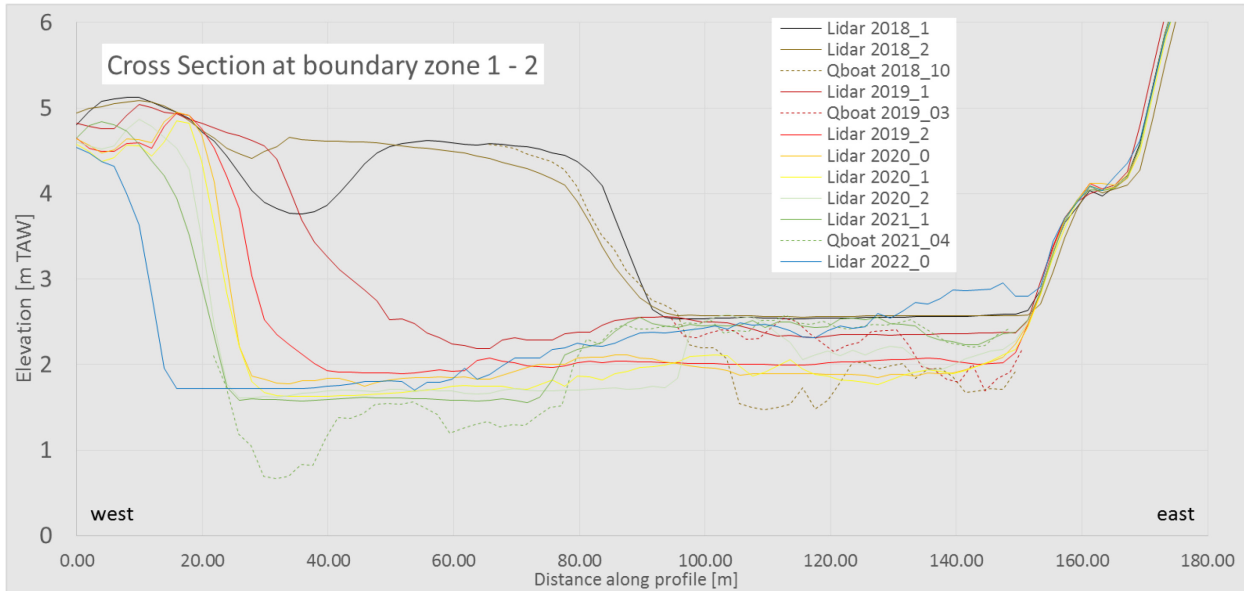


Figure 21 – Cross-sectional profiles, based on Lidar surveys, of the main tidal channel at the boundary of zones 1 and 2. For three surveys, the bed profile from the Qboat surveys has been added (for dates, see Table 11). Elevation in m TAW.

The part missed out due to ponded water in the channel for the survey before the expansion of the intertidal area was considerable (40 m² versus an emerged part of about 225 m²). The ponded part was much smaller for the Spring 2019 and Spring 2021 surveys. It can be put forward that the expansion of the intertidal area had as an immediate result a better flushing of the tidal channel with lower thresholds. This effect apparently held on during the first two years after the expansion of the intertidal area.

The wet section increased considerably after the expansion of the intertidal area. In preparation for the intertidal area expansion important excavation works have been carried out. The channel and the dunes west of the channel mouth were excavated between the survey flights of 10 April 2016 and 17 January 2017. The channel was widened and deepened over a length of about 1.6 km and a width of about 250 m. This work involved the estimated removal of about 311 400 m³ on Belgian territory and about 115 000 m³ on Dutch territory. Also the area of the cross section of Figure 21 was then involved. The channel was drastically narrowed by natural processes between early 2017 and Spring 2019. This was a very local, strong development right at the location of the profile. A sandbank, attached to the western shore of the channel, and fed by the flood current, migrated into the profile and filled its west bank. The Spring and Autumn 2018 profiles in Figure 21 reflect this situation.

After the expansion of the Zwin, the sand bank at the western bank was quickly removed. From Spring 2019 to February 2022, the channel bed deepened in a consistent, gradual way by about 1 to 2 m in the western half while it filled by almost 1 m in its eastern half. The evolution reflects the influence of the basalt revetment at the Dutch side. The profile sits at the tip of this revetment (Figure 17). The channel is not allowed free movement to the east. Just north of the profile, a channel bend develops cutting in the west bank. This is connected to the deepening western half of the bed in the profile. The bank there is also shifting westwards.

The (corrected) cross-sectional area increased strongly after the expansion of the intertidal basin in February 2019 (Figure 22). It increased from about 265 m² to 455 m² between Autumn 2018 and Spring 2020. The rate of increase slowed down from survey to survey. There was a slight decrease to about 450 m² in Autumn 2020 and further down to 440 m² in the latest surveys.

Over this two-year period, morphological features in the bed of the main tidal channel are observed to migrate landwards through the channel over a cumulated distance of 100 to 150 m.

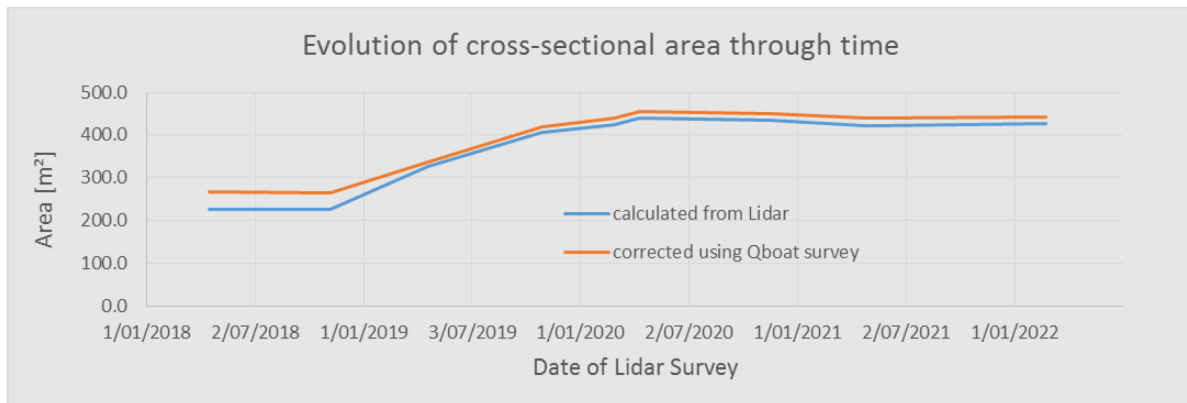


Figure 22 – Evolution of cross-sectional area of profile at boundary of zones 1 and 2 through time.

The increase of cross-sectional area between Autumn 2018 and Spring 2020 likely reflects the adaptation of the channel at the site of the cross profile in response to the opening of the International Dike on 4 February 2019 and the increase of intertidal basin area realized then. The slight decrease after Spring 2020 might reflect a response on incipient decreasing tidal prism. The above observations on the tidal prism do not contain an indication for a decreasing tidal prism, but this is related to uncertainties as discussed before (cf. section 3.1). However, the landward migration of large bed features in the main channel is a clear indication that this process is going on. The number of surveys after the tipping point in the curve of the cross-sectional area is however insufficient at this time to be sure the turnaround has already set in.

6.5 Relation A/P

6.5.1 Method

Both tidal prism and cross-sectional area at the border of zones 1 and 2 increased significantly at the moment of expansion of the intertidal area on 4/02/2019 (first observation Spring 2019). The tidal prism almost quadrupled and then stayed constant over the first two years after the expansion. The cross-sectional area first increased by about 25% at the Spring 2019 survey, by about 60% at the Autumn 2019 survey and by 70% at the Spring 2020 survey. Afterwards, it decreased to about 66% at the Spring 2021 survey. Though the change in tidal prism after the expansion of the intertidal area remains below the estimated accuracy, it shows a consistency: first a small increase till Spring 2020 followed by a small decrease (arrow 2 in Figure 23). Table 16 presents the cross-sectional area between A/P.

Table 16 – Cross-sectional area A and tidal prism P for the successive available surveys at the border of zone 1 and 2.

	17/04/2018	6/11/2018	20/04/2019	29/10/2019	28/02/2020	10/04/2020	18/11/2020	28/04/2021	23/02/2022
Lidar Survey	2018_1	2018_2	2019_1	2019_2	2020_0	2020_1	2020_2	2021_1	2022_0
Tidal prism P at level +5 m from Lidar	674841	760687	2183256	2177751	2208249	2223353	2200158	2166464	2113880
Cross-section area [m ²] from Lidar	226.8	224.9	326.3	405.1	425.5	440.4	435.6	421.4	426.2
Qboat, below level:	(est.)	2.56	2.34	(est.)	(est.)	(est.)	(est.)	1.6	(est.)
Cross-section area [m ²] from Qboat	40.0	40.0	9.2	15	15	15	15	19.1	15.0
Corrected cross section area A [m²]	266.8	264.9	335.6	420.1	440.5	455.4	450.6	440.5	441.2
Ratio of section on 2018_2 base			1.27	1.59	1.66	1.72	1.70	1.66	1.67

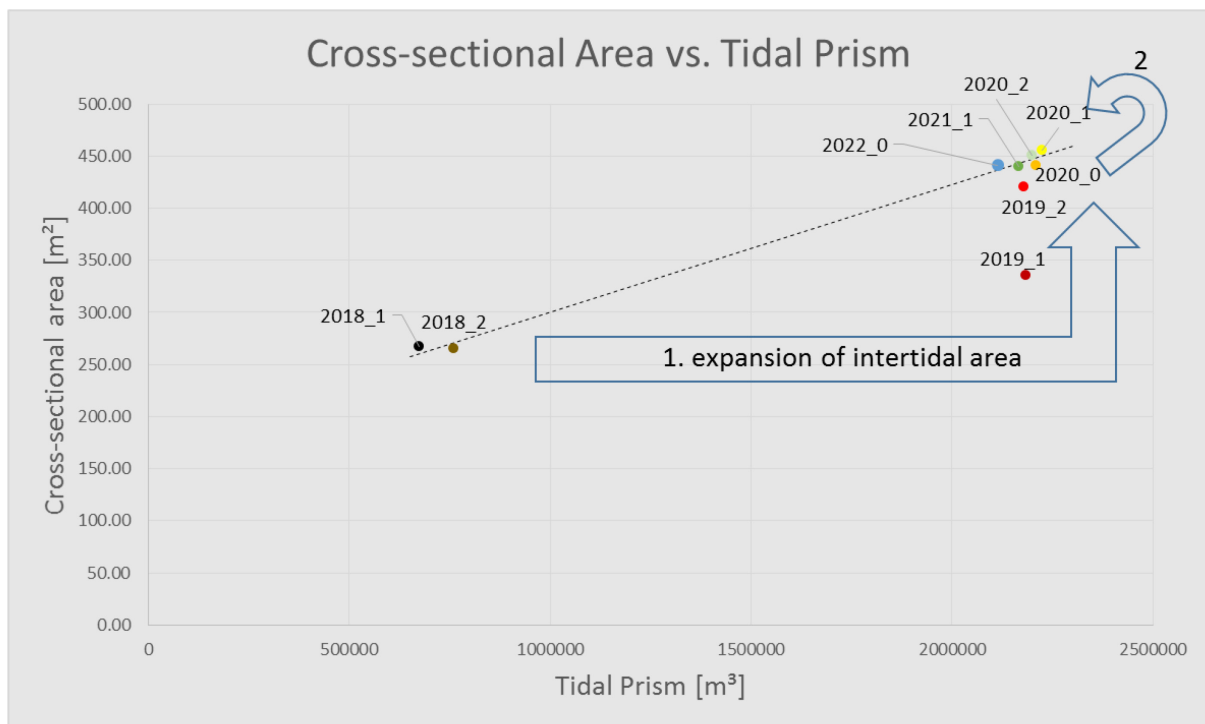


Figure 23 – Cross-sectional area A versus tidal prism P for the successive available surveys at the border of zone 1 and 2.

After the significant expansion of the Zwin area, the channel responds by increasing its cross section. This takes about one year and can be thought to be completed by Spring 2020. As observed above, the morphological change in the intertidal basin upwards of the considered cross-section is small, but sandbanks all over the about 2 km long main channel are seen to migrate inland. This means that at least the storage inside the lowest part of the main channel is decreasing. As the bedforms migrate landwards, they show there is a net import of sand into the area. This implies the accommodation of the lowest part of the main channel is decreasing.

The number of observations is too small, and the observations are too clustered, to try to fit an exponential relationship. The linear relationship shown in Figure 23 was established excluding the two points of 2019. It is thought that over 2019, the channel was not in equilibrium and the section gradually evolved toward equilibrium. An exponential relationship using seven available points

$$A = 0.527 P^{0.46}$$

can be fitted with $r^2 = 0.993$.

A more supported relationship might be possible to derive after more time has elapsed and more observations become available.

6.5.2 Discussion

The A-P relationship and coefficients for inlet channel stability cited in the literature are not confirmed for the Zwin inlet. It is remarked here that in general, the relationship A-P remains a model that needs further verification. An aspect that may be overlooked so far is the effect of sediment entering the inlet, though it is indirectly accounted for by the change in the tidal prism. The equilibrium condition for the inlet channel only considers the balance between choking of the channel by longshore coastal transport and the clearing effect of the ebb discharge in the channel. In the case of the Zwin inlet, it is clearly observed that sediment is also evacuated from the channel entrance by the flood currents, and imported into the tidal marsh. This is a condition that probably arises in nearly all inlets, as they all tend to attract sediment from the marine environment.

The changes in time of the A-P relationship observed for the Zwin inlet nevertheless show a consistent and well interpretable pattern (cf. the change from label 1 to label 2 in Figure 23).

So far, it is concluded that the expansion of the intertidal area in early 2019 meant a very significant increase of tidal prism, which almost quadrupled. The response at the border of the entrance inlet and the inland inlet was quick and strong. A recent sandbank was quickly cleared during the first year after the expansion. As a result of this, the channel cross-sectional area attained a new equilibrium around 450 m² at the Spring 2020 survey. This section was only reduced by about 10 m² at the Spring 2021 and February 2022 surveys. It can be expected that sanding up will first affect the inland most sections of the main channel. This will in the years to come have a limited effect on the tidal prism at spring high water. It is not even clear at this point whether the turnaround of the channel evolution towards smaller cross sections at the boundary of zones 1 and 2 has even started yet. Continued monitoring of the topobathymetry in the following years will allow to observe if and at what speed the expected evolution to sanding up and tidal prism reduction occurs.

7 Discussion

The Zwin inlet can be classified as a secondary tidal inlet system according to Lincoln and FitzGerald (1988). It is characterized by a main channel, sandy bedforms or banks and bars as well as secondary channels, as a three-dimensional complex dynamic system. Their presence and movements reflect active sediment transport in the system. Our work highlights the need to consider the inlet as an integrated 3D system, particularly in areas with a complex morphological configuration and bathymetry. The monitoring programme uses LiDAR and Qboat bathymetric surveys, as well as discharge measurements in selected cross-sections. The topobathymetric monitoring provide valuable 3D information on morphological evolution which cannot easily be obtained using traditional local survey methods such as GPS-profiles.

After ca. 3 years after the dyke opening on 04/02/2019, significant morphological changes have occurred in the entrance inlet. There, spatial and temporal morphological changes are observed with alternating accretion and erosion zones either arranged parallel to the coast or situated near the edge of the salt marsh and dune line. This footprint is typical of migration of three dimensional patterns with a complex interplay between sandy bedforms near and inside the inlet channel. Based on the topographic cross-shore profiles, the channel is now nearly 0.4 m deeper in its centre, up to 40 m wider and its thalweg moved eastward compared to the pre-opening period. In the entrance inlet, the average channel migration rate to the east is 4 m/year. The combination of wave-induced and tidal currents are the main forcing factors driving morphological changes of the entrance inlet. Short-term dynamics in the middle of the entrance inlet unit were studied during an ad-hoc campaigns. A regime of ebb-dominance is found in the center of the channel, and to a lower degree at its east side, while the west side of the channel is flood-dominated. Generally, the ebb phase lasts about two times the duration of the flood phase. Although there is a high spatial and temporal variability of the mobility of the sandy bedforms, the sediment volume shows no clear trend in the entrance inlet since the opening of the dyke. This might be due to a balance between wave related sediment input from the Belgian and Dutch coast as observed by the formation of sand spits on both sides and the tidally driven material exported from the entrance inlet. Since there is no developed ebb delta at the entrance of the Zwin inlet, this suggests that the exported sand is carried away further offshore or moved into the inland part of the inlet (e.g. saltmarsh or tidal accretion in the south, i.e. the previous Leopold polder). This must be further examined in the coming years.

Sediment movement to the inland part of the Zwin is expected at a slow rate in accordance with the inlet evolution theory. The curvature of the coastline strip (51), forming a bay with respect to the surrounding beaches, plays an important local role (Houthuys et al., 2021). Following nourishment in 05-06/2019 in Cadzand, there is also a significant transport of sand toward the Zwin around the high water line at the Dutch side (i.e. between the border and the small harbour in Cadzand; actually belonging to the municipality of Sluis). During flood phase, the local current at the Dutch side is, inferred from the morphological evolution (sand spit shape and growth), directed to the south toward the intertidal area of the Zwin. The flooding of the Zwin intertidal area demands a large amount of water which is drawn at rising tide into the Zwin channel toward the south until the inlet is full. Sand nourishments at Knokke and Cadzand may increase the supply of sand at the Zwin entrance. Part of the 02-03/2019 artificial sand supply in Knokke is transported by the coastal drift toward the east, such as can be inferred from the evolution of spits around the high-water mark near the entrance of the Zwin channel. The morphodynamics of the entrance inlet is thus governed by an interplay of coastal processes (i.e. combined wave and tidal hydrodynamics and sediment supply) near and in the channel, and the increased tidal prism of the inlet system resulting in increased discharges through the Zwin channel, as well as an increased cross-sectional area.

The governing coastal drift results in the existing, long-term trend of the Zwin channel shifting to the east. The significant erosion in the south-east part of the entrance inlet is an expression of these dynamics. However, a local phenomenon of sand supply from the north, along the Dutch coast, also drives the growth of a spit at the east side of the channel entrance. The combined dynamics of spits and secondary meanders have cut off an area along the Dutch basalt dyke near Zwinhoeve which currently functions as a backwater pond. Suspended sediment is deposited there which is a local phenomenon called pond effect.

Important morphological changes shaping the inland inlet have also occurred after the opening of the dyke. Two opposite morphodynamic trends occur in the inland inlet, with a sediment gain at the western side, while erosion dominates in the middle and east of the inland inlet where a net eastward shifting of the channel has occurred (Figure 24). About 71% of the area defined as inland inlet experiences erosion. It has been subject to a decrease of sediment volume equivalent to an averaged reduction in bed height by 0.44 m over the monitoring period. The change is not spread evenly over the area. Like observed in the entrance inlet, the channel has become deeper, exceeding 1.36 m at some locations. An increase of its width and migration toward the east characterize its behaviour and evolution. The erosion rate of the east side of the inland inlet was high in the first year after the opening of the dyke, but it has decreased over the last years (04/2020-2022). Since then, the channel has migrated back and forth, with a limited overall change. As expected, the morphological changes inside the inland inlet were the largest just after the intervention work and diminished until a dynamic equilibrium appears to have been reached. The narrow width of the inland channel in combination with high discharges, increased since the opening of the dyke, is likely to accelerate the peak velocity of tidal currents which in turn induce erosion. Thus, the combination of hydro- and morphodynamics results in the large scale dynamics of the channel including its migration toward the east. In longitudinal direction along the channel, areas of erosion alternate along the banks. This shows a tendency of the channel to meandering. Free meandering is hindered by the basalt dyke. The possible morphological role of meandering should be further investigated in the coming years. The west side of the inland inlet is accreting with the development of sand banks. Their development since 2019 indicates they were likely supplied by sediment from the entrance inlet. There is thus a strong interaction between the entrance and inland inlet units. The development of sand banks and other local topographic features such as meanders and small bars (hydraulic dunes) shifting through tides reflect an active and ongoing local bed transport. These secondary features are the local expression of processes that over longer periods influence the overall channel behaviour. Further monitoring will allow to track their role in the overall evolution. Bowman (1993) reported that the interactions between topography and tidal hydraulics explain the spatial complex of the channel and bedforms in the Zwin as well as their textural trends ranging from coarse sediment grain sizes and shell deposits in the throat to fine sediment in the inland inlet. The net input is mainly caused by the tidal asymmetry. The alongshore coastal sand transport also pushes the long-term trend of the entrance channel's shift to the east. This rate was on average 23 m/year before human interventions in 1980's (Trouw et al., 2015).

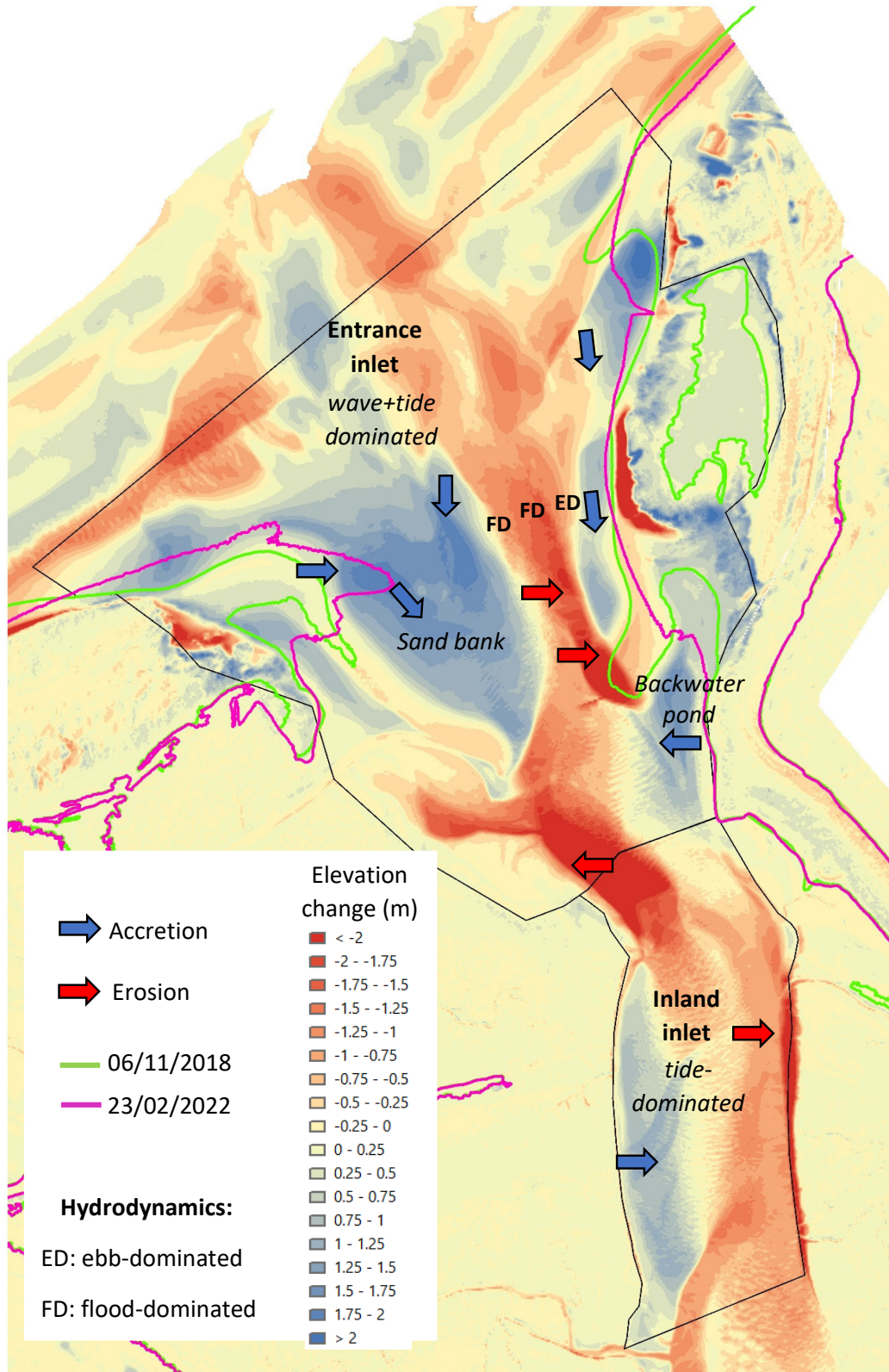


Figure 24 – Summary sketch of the morphological changes and hydrodynamics under calm weather conditions on the Zwin inlet. Arrows indicate the direction of movement of morphology based on successive DEMs. Contour lines correspond to 5 m TAW.

As expected after the expansion of the intertidal surface area from 150 to over 333 ha, the entire inlet has changed, responding to both hydrodynamic and morphological feedbacks. Under the increase of the tidal prism, the access channel adjusted by becoming wider and deeper in order to be able to drain larger volumes of water. The results show that the intertidal water volume that enters into the Zwin during a tidal cycle strongly depends on the tidal amplitude. Based on the tidal prism and cross-sectional area analysis, it is concluded that the expansion of the intertidal area in early 2019 meant a very significant increase of tidal prism, which almost quadrupled. The response in the entrance channel was quick and strong. A recent sandbank was quickly cleared during the first year after the expansion. As a result of this, the channel cross-sectional area attained a new equilibrium around 450 m² in 04/2020. Both tidal prism and cross-sectional area at the border of zones 1 and 2 increased significantly at the moment of expansion of the intertidal area on 04/02/2019 (first observation Spring 2019). The tidal prism almost quadrupled and then stayed constant over the first two years after the expansion. The cross-sectional area first increased by about 25% at the Spring 2019 survey to 70 % at the Spring 2020 survey. Afterwards, it decreased to about 66% at the Spring 2021 survey. Therefore, the response in the entrance channel was quick and strong after the opening of the dyke. It can be expected that sanding up will first affect the inland most sections of the main channel. This will have a limited effect on the tidal prism at spring high water in the future. Just a small part of the intertidal and salt marsh area remains dry under high water level. An increase of the high water level by a storm surge leads to an increase of the tidal prism of the order of the basin area times the surge height (van der Vegt and Hoekstra, 2012). Future monitoring of the inlet and calculation of the tidal prism of the entire floodable area through time will allow to better evaluate and predict the inlet evolution. Sediment will continue to be imported as long as it is available such as in all tidal inlets (FitzGerald, 1996). This will inevitably lead to the decrease of the tidal prism. At present, the tidal channel functions well such as shown above. The continued monitoring programme will allow to estimate time scales of the expected sanding up and will help to increase our knowledge of the system, thus contributing to steer future interventions.

8 Conclusions

The Zwin inlet is a complex three dimensional morphological system, characterized by a main channel, sandy bedforms or banks and bars as well as secondary channels. Their presence and movements reflect active sediment transport in the system. The inlet is controlled by waves and tidal currents, water levels, tidal prism and sediment supply. In 2019, the intertidal area of about 150 ha was doubled to about 333 ha by de-poldering the Willem-Leopold polder. The actual expansion took place on 04/02/2019 when a large breach was dug in the old International Dyke, separating the existing intertidal area from the newly floodable area. The present study reports the morpho- and hydrodynamics of the entrance and inland parts of the tidal channel that connects the intertidal marsh to the sea from before the dyke opening to more than 3 years after.

After the opening of the dyke, significant morphological changes have occurred in the channel of the entrance inlet unit which became nearly 0.4 m deeper in its centre and up to 40 m wider, while its thalweg moved eastward. Although there is a high spatial and temporal variability of the morphological change, the sediment volume is relatively stable in the entrance inlet unit since the opening of the dyke. This is probably due to a balance between sediment input from the Belgian and Dutch coast as observed by the formation of sand spits on both sides and the material exported more inland from the entrance area. Short-term dynamics in the middle of the entrance inlet unit were studied during three ad-hoc campaigns under different marine conditions. In general, a regime of ebb-dominance is found in the center of the channel with a velocity exceeding 0.6 m/s, and to a lower degree at its east side. In contrast, the west side of the channel is flood-dominated. The ebb phase lasts about two times the duration of the flood phase. Therefore, the morphodynamics of the entrance inlet reflects an interplay of coastal processes (i.e. wave and tide hydrodynamics and sediment supply), which tend to feed in sand, and tidal currents near and in the channel, which allow to keep the channel open.

Overall erosion of the inland inlet area occurred. The inland inlet unit experienced important morphological changes with its deepening and eastward channel migration after the dyke-opening. It has thus been subject to a decrease of sediment volume equivalent to a reduction in bed height by 0.58 m over the monitoring period. The change is not spread evenly over the area. In the first year after the opening of the dyke, the erosion rate of the east side of the inland inlet was high but it has decreased over the last year (04/2020-02/2022). During that last year, the channel has migrated back and forth, with a limited overall change. The combination of hydro- and morphodynamics thus resulted in a quasi-equilibrium over the third year of monitoring.

As expected after the expansion of the intertidal surface area from 150 to over 333 ha, the entire inlet has changed, responding to both hydrodynamic and morphological feedbacks. Induced by the increase of the tidal storage area of the inlet, the access channel adjusted by becoming wider and deeper in order to be able to import and drain larger volumes of water at each tidal cycle. Both tidal prism and cross-sectional area at the border of zones 1 and 2 increased significantly at the moment of expansion of the intertidal area on 04/02/2019. The tidal prism almost quadrupled and then stayed constant over the first two years after the expansion. The cross-sectional area first increased by about 25% in 02/2019 survey to 70 % in 04/2020. Afterwards, it decreased to about 66% in 04/2021. Therefore, the response in the entrance channel was quick and strong after the opening of the dyke. An inter-relationship of process-response occurs in this complex dynamic system between channel, sandbanks and other morphological features. For example, a sandbank was quickly cleared during the first year after the expansion. As a result of this, the channel cross-sectional area attained a new equilibrium around 450 m² at the Spring 2020 survey. This section was only reduced by about 10 m² at the Spring 2021 and February 2022 surveys. Thus, the tidal channel currently functions well. The continued monitoring programme will allow to estimate the time scales of the expected sanding up and will help to increase our knowledge of the system, thus also allowing to steer future interventions.

9 References

- Aqua Vision (2018) Het Zwin Bathymetrie en stromingsmetingen oktober 2018, 25p.
- Aqua Vision (2019) Het Zwin Bathymetrie en stromingsmetingen juni 2019, 25p.
- Aqua Vision (2020a) Het Zwin Bathymetrie en stromingsmetingen september 2020, 23p.
- Aqua Vision (2020b) Het Zwin Bathymetrie en stromingsmetingen oktober 2020, 23p.
- Bowman, D. (1993) Morphodynamics of the stagnating Zwin inlet, The Netherlands, *Sedimentary Geology*, 84, 219-239.
- FitzGerald, D. (1996) Understanding Physical Processes at Tidal Inlets: Based on Contributions by Panel on Scoping Field and Laboratory Investigations in Coastal Inlet Research. *Journal of Coastal Research*, 23, 47-71.
- Houthuys, R., Trouw, K., De Maerschack, B., Verwaest, T., Mostaert, F. (2013). *Inschatting van de morfologische impact van strandsuppleties te Knokke op het Zwin en de Baai van Heist. Versie 4.0. WL Rapporten, 12_107. Waterbouwkundig Laboratorium & IMDC: Antwerpen, België.*
- Houthuys, R., Verwaest, T., Dan, S., Mostaert, F. (2021) *Morfologische evolutie van de Vlaamse kust tot 2019: Evolutie van de Vlaamse kust tot 2019. Versie 2.0. WL Rapporten, 18_142_1. Waterbouwkundig Laboratorium: Antwerpen.*
- INBO report (2021) Sam Provoost, Alexander Van Braeckel, Wouter Van Gompel. *Monitoring hydrologie Zwin Rapportage 2021.*
- Montreuil, A-L., Dan, S., Verwaest, T., Mostaert, F. (2021a) *Monitoring the morphodynamics of the Zwin inlet: interim report: 1 year after the works. Version 0.1. FHR Reports, 16_089_3. Flanders Hydraulics Research: Antwerp.*
- Montreuil, A-L., Dan, S., Verwaest, T., Mostaert, F. (2021b) *Monitoring the morphodynamics of the Zwin inlet: interim report: 2 years after the works. Version 0.1. FHR Reports, 16_089_2. Flanders Hydraulics Research: Antwerp.*
- Montreuil, A-L., Dan, S., Verwaest, T., Mostaert, F. (2022) *Monitoring the morphodynamics of the Zwin inlet: interim report: 3 years after the works. Version 0.1. FHR Reports, 16_089_3. Flanders Hydraulics Research: Antwerp.*
- Nortek, 2017. *The Comprehensive manual*, 153pp.
- O'Brien, M.P. (1969) *Equilibrium flow areas of inlets on sandy coasts. Journal of Waterway Port Coast Ocean Engineering* 95 (1) 43-52.
- Stive, M. J. F., J. Van de Kreeke, N. T. Lam, T. T. Tung, Ranasinghi, R. (2009). *Empirical relationships between inlet cross-section and tidal prism: a review. Proceedings of Coastal Dynamics 2009, Tokyo, Japan, 1-10*
- Stroomatlas (1992) *Noordzee Vlaamse Banken, Dienst der kusthavens hydrograpij Oostende*, 29p.

Tung, T.T., van de Kreeke, J. & Stive, M.J.F., 2011. Dynamic equilibrium and morphological stability of idealized tidal inlets using process-based modelling. The Proceedings of the Coastal Sediments 2011, Miami, Florida, USA, 2 May – 6 May 2011, Edited By: Julie D Rosati (University of South Florida, USA), Ping Wang (University of South Florida, USA) and Tiffany M Roberts (University of South Florida, USA), pp. 406-418

Trouw, K., Zimmermann, N., Wang, Li., De Maerschalck, B., Delgado, R., Verwaest, T., Mostaert, F. (2015).

Scientific support regarding hydrodynamics and sand transport in the coastal zone: Literature and data review coastal zone Zeebrugge - Zwin. Version 4_0. WL Rapporten, 12_107. Flanders Hydraulics Research. Antwerp, Belgium.

Van de Kreeke, J. and Haring, J. 1980. Stability of Estuary Mouths in the Rhine-Meuse Delta. Proceedings International Conference on Coastal Engineering, ASCE Press, NY, 2627-2639.

Van de Kreeke, J. (2004). "Equilibrium and cross-sectional stability of tidal inlets: application to the Frisian Inlet before and after basin reduction," Coastal Engineering ,51 (5-6), 337–350.

Van der Vegt, M., Hoekstra, P. (2012) Morphodynamics of a storm-dominated, shallow tidal inlets: the Slufter, the Netherlands. Netherlands Journal of Geosciences, 991-3, 325-339.

ZTAR Newsletter (2017) Het Zwin revived! Zwin tidal area restoration. 1-16.

Appendix A: Ad-hoc campaigns

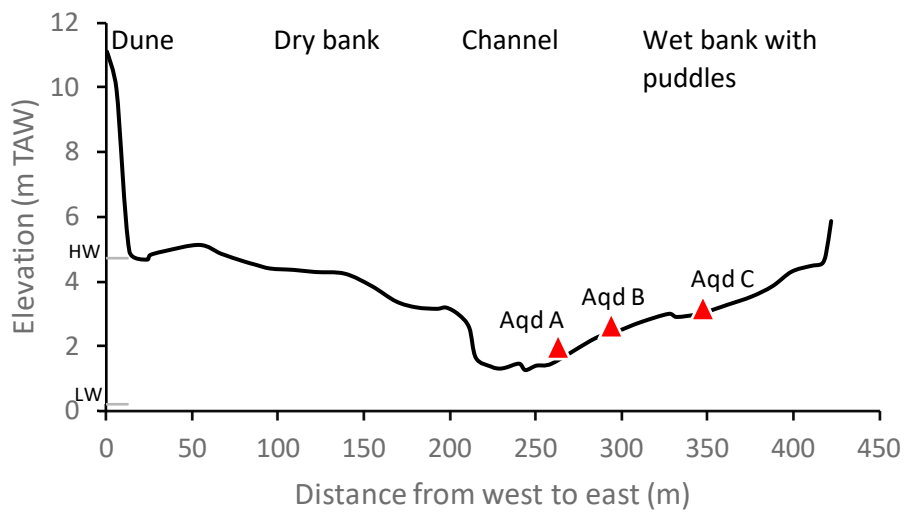


Figure 25 – Ad-hoc 1 – entrance inlet.

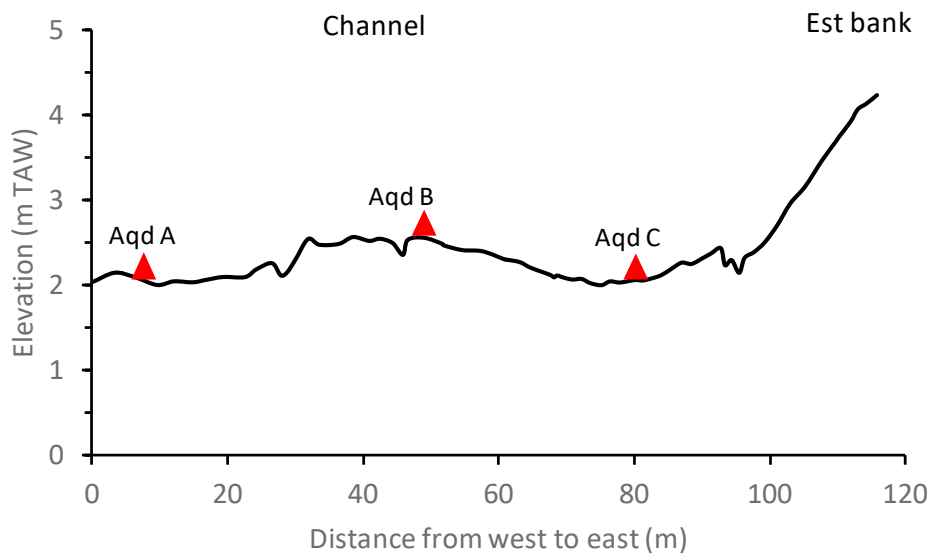
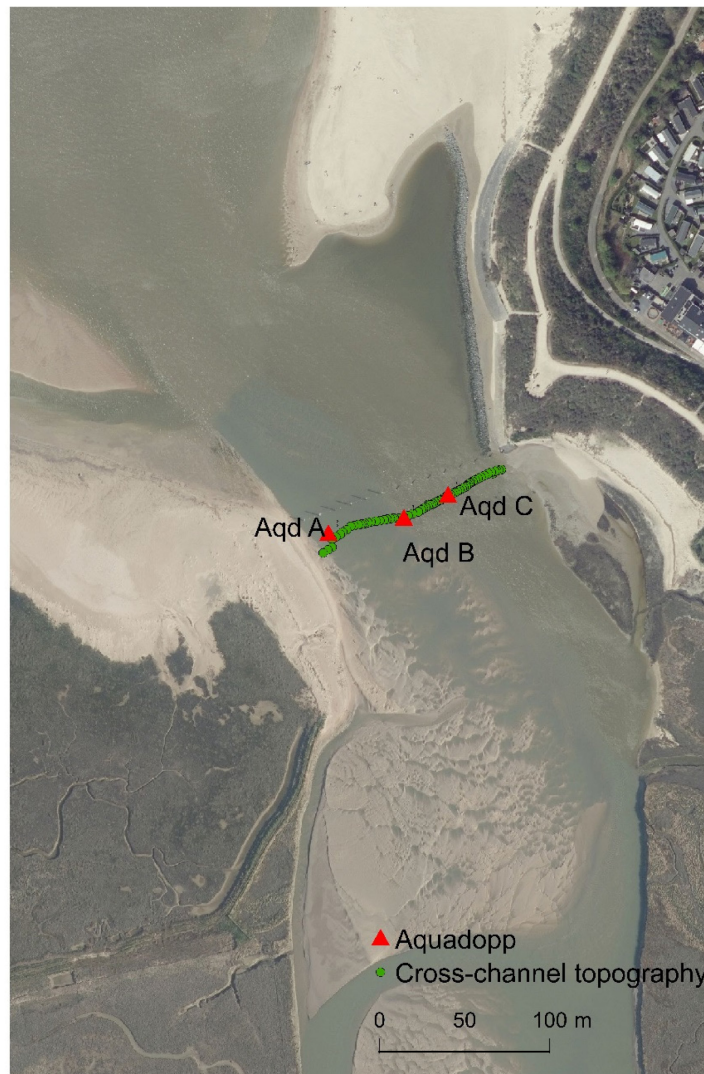


Figure 26 – Ad-hoc 2 – border between entrance inlet and inland inlet.

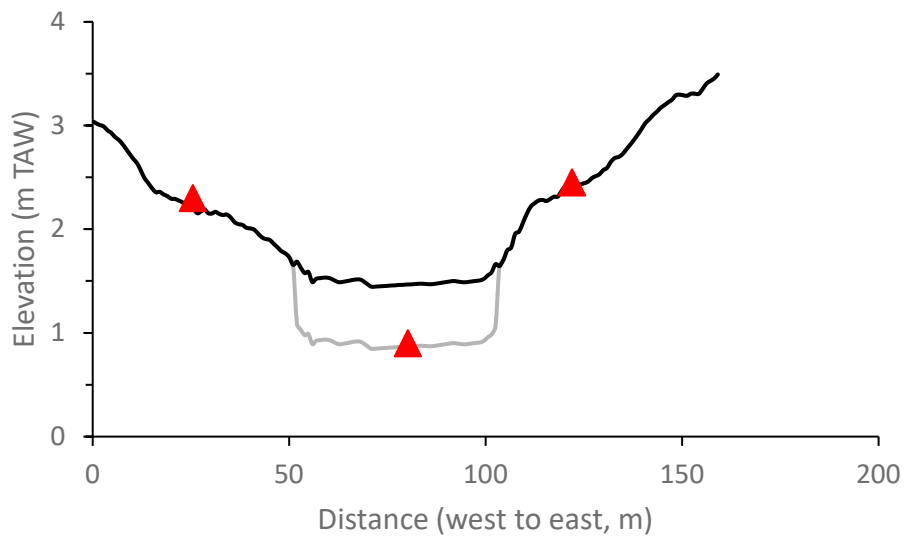


Figure 27 – Ad-hoc 3– entrance inlet.

Cross-channel topographic profile extracted from the LiDAR survey on 18/11/2020 with the position of the Aquadopp sensors. Black line corresponds to the probable water surface at the time of the LiDAR flight. Grey line is corrected position calculated as an average shift in depth of 0.6 m (based on Qboat depth measurement on 30/09/2020).

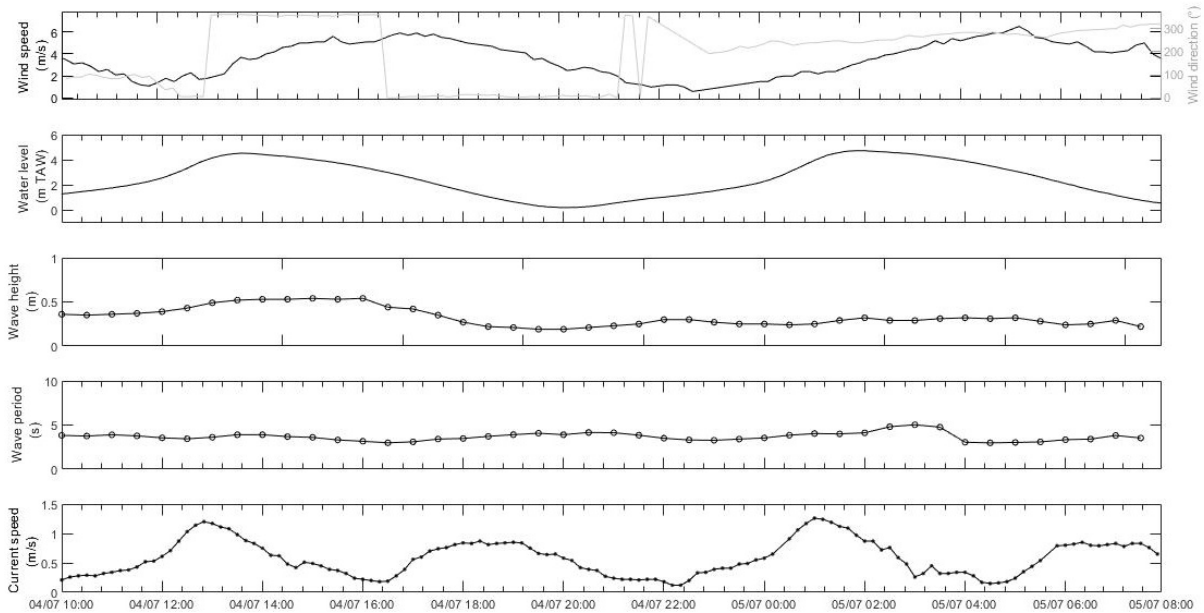


Figure 28 – Ad-hoc 1 – meteo-marine parameters.

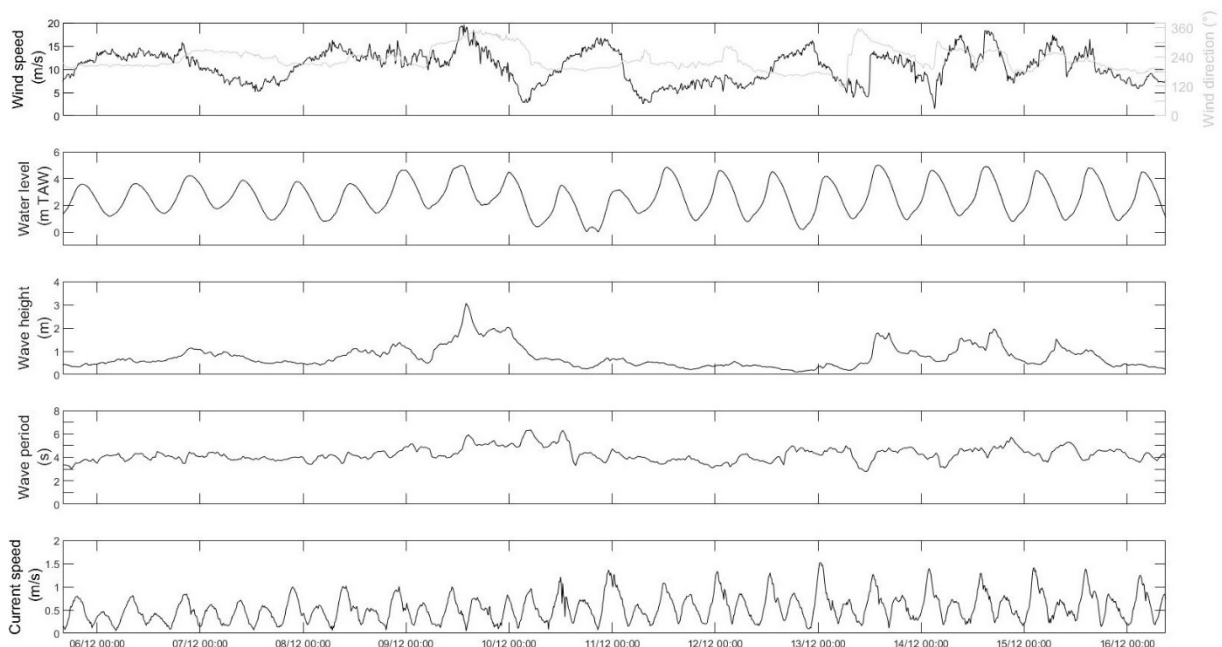


Figure 29 – Ad-hoc 2 – meteo-marine parameters.

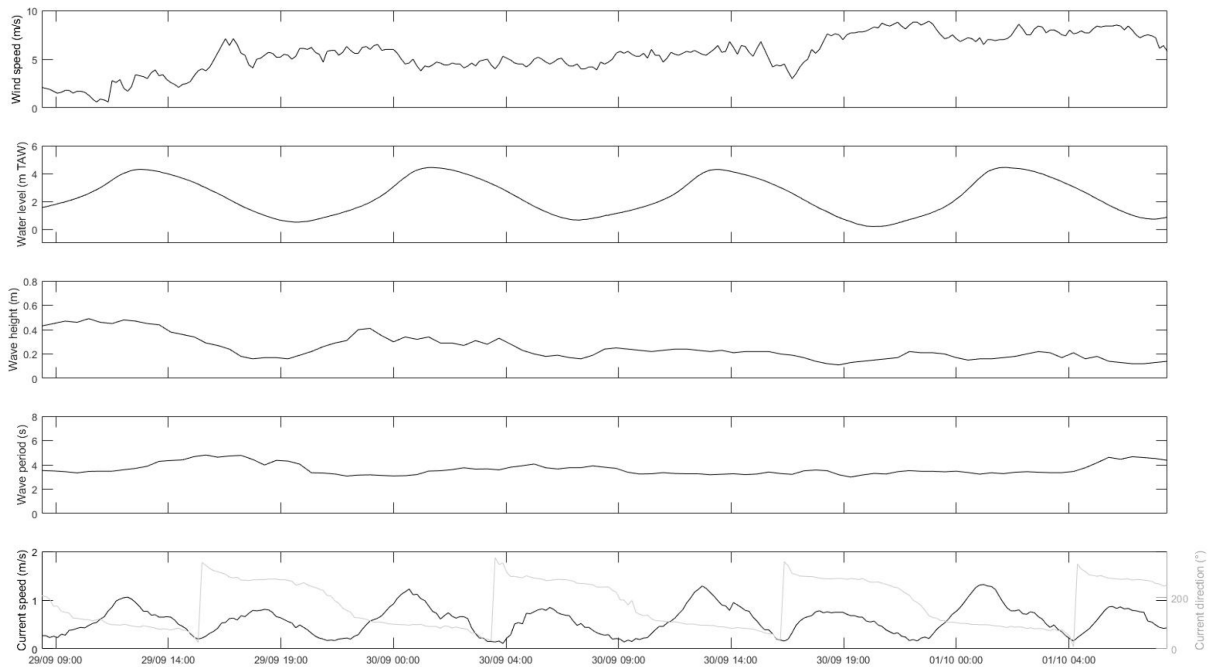


Figure 30 – Ad-hoc 3 – meteo-marine parameters.

Appendix B: Estimation of water discharge

Water discharge was estimated by dividing the cross-channel topographic profile in 4 sections to calculate the water area (A_{water}) (Figure 31). For this, the estimated geometric area (A_{geo}) was subtracted from the core area (A_{core}) for each section. Then, the water discharge per section was calculated by multiplying A_{water} and the depth-averaged velocity current measured by the Aquadopps for the respectively section. Finally, the water discharge of the four sections was summed. Cross-channel topographic profile was interpolated with a distance interval of 0.1 m to extract representative water level. Also, the depth-averaged velocity current and water level was averaged every 30 min for the campaign period. It was assumed that the current velocity measured by the Aquadopps at a specific location is representative of the velocity for the entire section while it is likely to be lower near the embankment of the channel.

Table 17 – Summary statistics of water discharge across the channel, water level, current velocity and direction measured in the deep channel during the three ad-hoc campaigns.

	Water level (m TAW)	Avg. current velocity in the deep channel (m/s)	Avg. current direction in the deep channel (°)	Absolute water discharge (m ³ /s)
Ad-hoc 1				
3h before 1st HW	1.69	0.07	88.94	25.99
2h before 1st HW	2.01	0.17	120.83	33.78
1h before 1st HW	3.26	0.66	145.99	134.54
HW on 4/7	4.37	0.82	151.97	276.46
1h after 1st HW	4.42	0.40	209.38	147.99
2h after 1st HW	3.99	0.62	323.26	135.16
3h after 1st HW	3.35	0.72	312.60	108.57
Ad-hoc 2				
1h before 1st HW	3.80	0.84	148.50	215.97
HW on 5/7	4.64	0.84	153.38	323.80
1h after 1st HW	4.54	0.35	253.64	119.67
2h after 1st HW	4.09	0.60	324.11	145.12
3h after 1st HW	3.40	0.76	314.24	125.66
Ad-hoc 3				
-1h30 HW	3.36	0.65	149.15	178.01
- 1h HW	4.14	0.72	150.56	356.49
HW	4.33	0.30	176.16	160.39
+1h HW	3.96	0.59	331.75	-197.45
+2h HW	3.34	0.70	329.09	-194.83

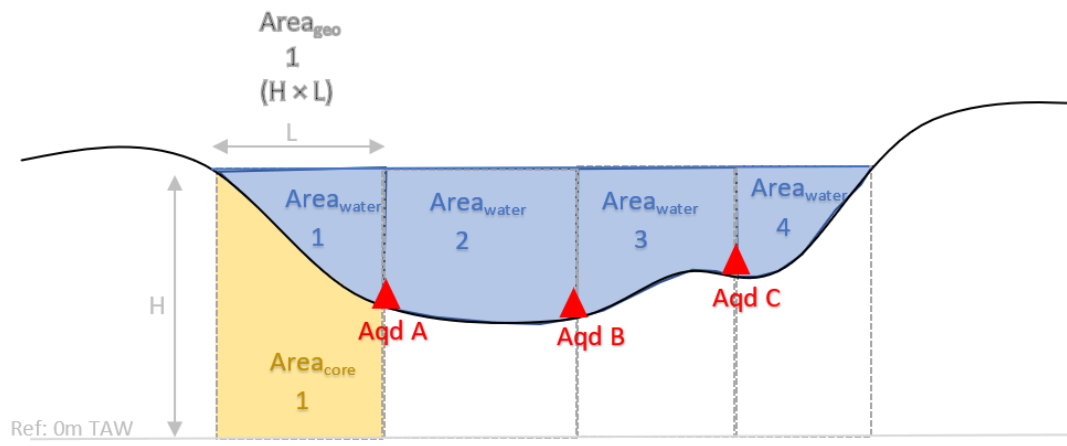


Figure 31 – Method of estimating water discharge.

DEPARTMENT **MOBILITY & PUBLIC WORKS**
Flanders hydraulics

Berchemlei 115, 2140 Antwerp

T +32 (0)3 224 60 35

F +32 (0)3 224 60 36

waterbouwkundiglabo@vlaanderen.be

www.flandershydraulics.be